Diesel Engine Performance Using Oxygenated Fuels

by
Cornelius Janse Blom

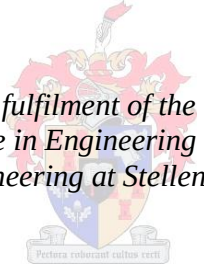

Thesis presented in partial fulfilment of the requirements for the degree of Master of Science in Engineering (Mechatronic) in the Faculty of Engineering at Stellenbosch University

Supervisor: Mr. RW Haines

March 2015

DECLARATION

By submitting this thesis electronically, I declare that the entirety of the work contained therein is my own, original work, that I am the sole author thereof (save to the extent explicitly otherwise stated), that reproduction and publication thereof by Stellenbosch University will not infringe any third party rights and that I have not previously in its entirety or in part submitted it for obtaining any qualification.

March 2015

ABSTRACT

With worldwide emissions standards becoming more stringent over the last decade, the South African market seems set to follow suit. Older technology engines are however unable to attain these stringent standards and will require cleaner burning fuels. Biofuels like biodiesel and bioethanol-diesel blends are an attractive option as a result of their inherently oxygenated nature and renewable, low carbon footprint. Oxygenated fuels have been found to lower particulate and soot emissions without any significant increase in NO_x, thus alleviating the usual particulate-NO_x trade-off.

In this study an existing diesel engine test facility has been upgraded to include emission equipment, and a low cost pressure indicating system. Fuel-to-fuel comparative testing was done with pump diesel and splash blended fuels consisting of pump diesel blended with varying amounts of ethanol and also biodiesel without including any cetane enhancing or blend stability additives. Emission analysis of the blended fuels showed a marked reduction in soot emission with little to no increase in NO_x emission for all oxygenated fuels. This type of soot reduction without NO_x increase is difficult to obtain through any other method. Blend stability was however a problem with the 15% ethanol-diesel blends.

OPSOMMING

Met wêreldwye uitlaatgas standaarde wat al hoe strenger geword het oor die laaste dekade, lyk dit asof dit net ‘n kwessie van tyd is voor Suid-Afrika dieselfde roete volg. Ouer tegnologie binnebrandenjins kan egter nie hierdie streng standaarde handhaaf nie en sal dus vereis dat die brandstof skoner brand. Biobrandstowwe, soos biodiesel en bio-etanol-diesel mengsels, blyk ‘n aantreklike opsie te wees vanweë hul natuurlike inhoud van suurstof en as hernubare hulpbron. Wanneer suurstof houdende brandstowwe soos hierdie verbrand word, word daar gevind dat daar ‘n daadwerklike afname in rook uitlaat is sonder enige merkbare toename in NO_x uitlaatgasse. Dit is teenstrydig met die gewoonlike wisselwerking wat daar tussen hierdie twee uitlaatgas produkte is.

In hierdie studie word die bestaande diesel enjin toetssel opgegradeer om uitlaatgas analiese toerusting asook ‘n lae-koste silinderdruk meettoestel te bevat. Brandstof-tot-brandstof vergelykings toetse word gedoen met gewone diesel asook toets diesel wat gemengde konsentrasies biodiesel of bio-etanol bevat. Die toets diesel bevat egter geen aanvullings om mengselstabiliteit of cetaan te verbeter nie. Toetsresultate toon dat daar merkbare vermindering in rook uitlaat is met min tot geen toename in NO_x. Hierdie tipe van resultaat met produkte van ontbranding is moeilik om op enige ander manier te bewerkstellig. Daar word ook gevind dat diesel met 15 % bio-etanol nie ‘n stabiele mengsel is nie en dat fase skeiding plaasvind.

Opgedra aan my ouers, sonder julle was dit nie moontlik nie.

Tanya, jou motivering het my deur gedra.

ACKNOWLEDGEMENTS

The author thanks Mr. Richard Haines for his incredible guidance and insight throughout the project. His efforts and knowledge of the field is instrumental in keeping this research alive.

To all the workshop and facility personnel of the Mechanical and Mechatronic Department a big thank you for all your support and advice.

TABLE OF CONTENTS

LIST OF FIGURES

LIST OF TABLES

NOMENCLATURE

A	Surface area inside cylinder
ATDC	After top dead centre
B	Cylinder bore
BMEP	Brake mean effective pressure
BSFC	Brake specific fuel consumption
BTDC	Before top dead centre
BTF	Biofuels testing facility
C	Capacity ratio
CA	Crank angle
CAT	Catalytic converter
CCI	Cetane index
CFR	Cooperative fuel research committee
CN	Cetane number
CO	Carbon monoxide
CO_2	Carbon dioxide
CV-joint	Constant velocity joint
CVCA	Constant volume combustion apparatus
C_c	Heat capacity of hot fluid
C_E	Voltage to pressure scaling factor
C_h	Heat capacity of cold fluid
C_p	Specific heat
c_v	Constant volume specific heat
DCN	Derived cetane number
DI	Direct injection
DOE	Department of Energy
DPF	Diesel particulate filter
E	Signal from pressure transducer
EGR	Exhaust gas recirculation
E_{IBDC}	Signal from pressure transducer at IBDC

FGT	Fixed geometry turbocharger
FMEP	Friction mean effective pressure
FSN	Filter smoke number
HC	Hydro carbons
HHV	Higher heating value
IBDC	Inlet bottom dead centre
ID	Inside diameter
IDI	Indirect injection
IND	Ignition delay
IMEP	Indicated mean effective pressure
k_g	Thermal conductivity
LHV	Lower heating value
m	mass
MAF	Mass airflow
MBT	Minimum ignition advance for best torque
N	Engine speed
n	Polytropic constant
NTU	Number of transfer units
n_r	Number of crank revolutions per power stroke
NO_x	Nitrogen oxides
OD	Outside diameter
OEM	Original equipment manufacturer
p	Pressure
PID	Partial integral differential
PM	Particulate matter
P_i	Indicated power
p_m	Pressure from a motored pressure trace
p_{max}	Peak pressure
p_{IBDC}	Pressure at IBDC
p_r	Pressure at a known state (ex. IBDC)
Q_w	Heat transfer

Q_{max}	Maximum possible heat transfer
R	Long fuel hydrocarbon chains
Re	Reynolds number
ROHR	Rate of heat release
r_v	Compression ratio
SAPIA	South African Petroleum Industry Association
SFC	Specific fuel consumption
SI	Spark ignition
Strk	Stroke
STTD	Short term thermal drift
TDC	Top dead centre
TDI	Turbocharged direct injection
$t_{10,50,90}$	10,50,90 % recovery temperature, corrected for barometric press.
T_g	Instantaneous bulk gas temperature
T_r	Temperature at a known state (ex. IBDC)
T_w	Mean wall temperature of the cylinder
U	Overall heat transfer coefficient
u_p	Mean piston speed
V	Volume
VGT	Variable geometry turbine
V_d	Displacement volume
V_r	Volume at a known state (ex. IBDC)
V_s	Swept volume of cylinder
W_p	Pump work
$W_{i,g}$	Gross indicated work
$W_{i,n}$	Net indicated work
σ	Stephan-Boltzmann constant
γ	Specific heat ratio
ε	Effectiveness
ρ	Density
υ	Kinematic viscosity

1. INTRODUCTION

World emissions standards have become more stringent over the past decade. From the inception of the Euro 1 standard in 1992, to the current Euro 6 standard, allowable carbon monoxide (CO) emissions for diesel engine passenger vehicles have reduced by 81.6 %; allowable hydrocarbon (HC) + nitrogen oxides (NO_x) reduced by 82.5 %; and particulate mass have been reduced by 96.4 %. Particulate mass measurement has become difficult to measure and the Euro 5 and 6 standards now also include legislation governing the maximum particle number emitted from these vehicles. The progression can be seen in Figure 1 and Figure 2. To implement this measurement, particle counters had to be included in legislation as compulsory test equipment (DieselNet, 2013).

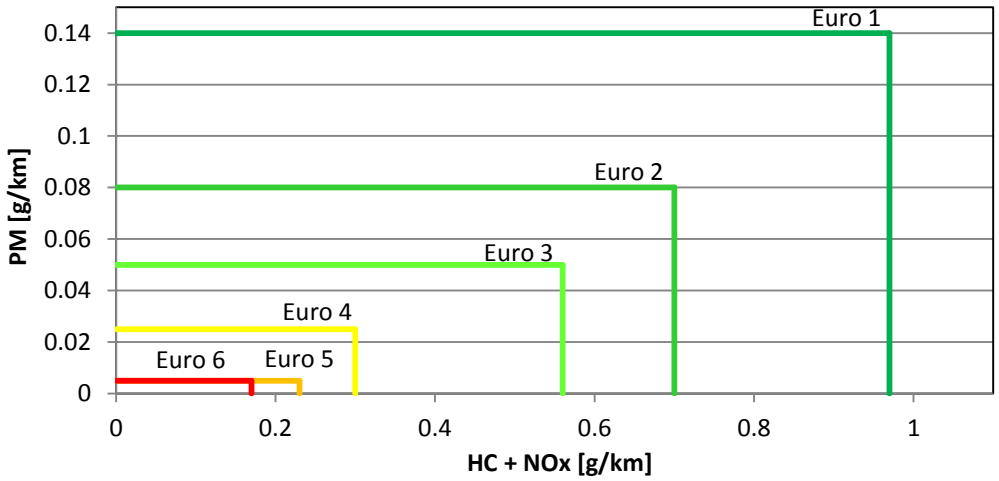

Figure 1: Graphical representation of European emissions regulation development for HC + NO_x and PM in passenger vehicles (DieselNet, 2013).

A similar progression has also taken place in both the light commercial and heavy-duty (HD) truck and bus emission standards. In HD diesel applications the reduction from Euro I to the current Euro VI has been 66 % for CO; 88 % for unburned HC; 95 % for NO_x and 98 % for particulate mass from 0.621 g/km to 0.01 g/km (DieselNet, 2012).

Progression of this magnitude is due to major advancements in diesel engine technology but also largely to the progression in producing cleaner fuels. The biggest reduction has been that of sulphur which, under the current EU regulations, is governed to a maximum of 10 ppm. The current regulation, EN 590:2009, has also made allowance for 7 % v/v of fatty acid methyl ester (FAME) biodiesel content. This allowance is expected to rise in future (DieselNet, 2010).

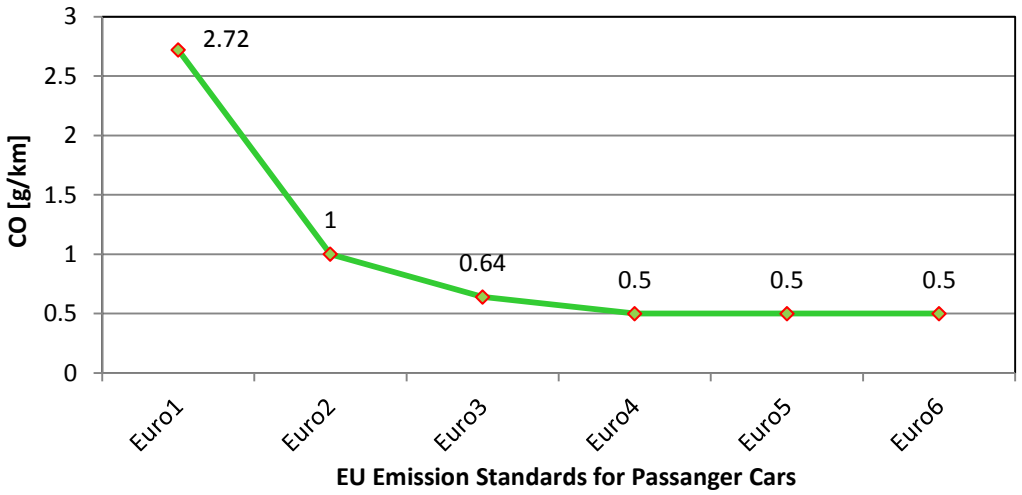

Figure 2: European emissions standards development for CO (DieselNet, 2013).

The South African regulation for diesel emissions is adopted from the European standards and currently corresponds to the Euro 2 specifications. Euro 5 emissions specifications are planned to roll out in 2017 according to the latest communications from the Department of Energy (DOE). This roll out will however require major upgrades to the countries refineries and fuel logistics infrastructure, posing the risk of high energy price increases to offset the large investment cost. The DOE also plans to introduce *Mandatory Blending Regulations* for biofuels by October 2015. This is still subject to the finalization of the Biofuels Pricing Framework (Martins, 2013).

It is clear therefore that the pressure to reduce automotive tailpipe emissions is also slowly mounting in the South African market. South Africa is however faced with some challenges in this regard. One of these is that a large percentage of the South African vehicle *parc* still consists of vehicles with older technology engines. This is mainly due to vehicle turn around not being as quick as in developed markets. Figure 3 shows an example of the distribution compiled by the South African Petroleum Industry Association (SAPIA). The only solution for these vehicles would be to use fuels that burn cleaner and have a smaller carbon footprint.

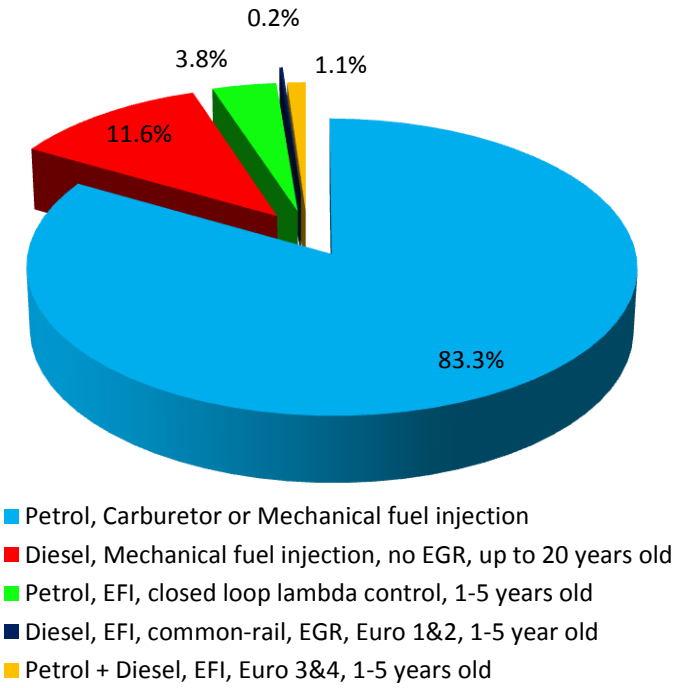

Figure 3: South African vehicle parc technology distribution as compiled in 2008 (SAPIA, 2008).

Renewable biofuels are an attractive solution mainly because of their low carbon footprint and their inherently oxygenated nature. Oxygenates have been found to have positive effects on the emissions from combustion when blended with pump fuel. It could therefore serve as a form of additive to improve the tailpipe emissions from older technology engines.

Another limitation in the South African fuel industry is the logistics surrounding introduction of new fuels. New fuels would require additional storage at bulk holding sites, additional tanks at service stations, additional freight tankers and additional change-overs in the fuel pipelines which would increase the chances of cross contaminated fuel. It would therefore be advantageous, especially with the possible compulsory biofuel blending strategy from the DOE, to have these fuels splash blended during the final freight process or at the service stations. This will require fuels that are inherently stable when blended.

This project aims to test the effects of oxygenated fuels on the performance and exhaust emissions of a turbocharged, intercooled, high injection pressure diesel engine.

2. LITERATURE SURVEY

2.1. Diesel Engine Technology

2.1.1. The Reciprocating Internal Combustion Engine

The internal combustion engine transforms chemical energy into mechanical energy. The energy originates from the exothermic chemical reaction during the oxidation of the fuel used in the engine. For the internal combustion engine, the combustion takes place internally in a closed system and the fuel and air needed for combustion as well as the products of combustion are the working fluid of the thermodynamic process. In a reciprocating engine, the energy is transferred directly toward the reciprocating components of the engine from the working fluid (Heywood, 1988).

Different derivatives of the internal combustion engine have been developed over its more than two and a half century history. Two variants have however proceeded to develop into the most popular engine derivatives of today: The four stroke Otto cycle, spark ignition engine as well as the compression ignition engine developed by Rudolf Diesel. The fuel for this engine is also named after its inventor (Stone, 1999).

The spark ignition (SI) engine and specifically the Otto four stroke cycle, was developed by Nicolaus Otto. It uses four strokes of the piston to complete the cycle. The intake stroke fills the cylinder with fuel and air mixture. The compression stroke then compresses the fuel-air mixture to a higher pressure for the start of ignition. During the expansion stroke, combustion of the fuel-air mixture continues and the resulting pressure rise drives the reciprocating piston. As the name “spark ignition” suggests, ignition is achieved by means of a spark. Finally, the exhaust stroke purges the products of combustion before a fresh fuel-air mixture is induced into the combustion chamber.

The first working compression ignition (CI) engine was built by Rudolf Diesel in 1893 in conjunction with Maschinenfabrik Augsburg A.G, the company that would later become M.A.N. The engine utilizes the same four strokes as with the Otto cycle, but Diesel believed that using Carnot’s thermodynamic principle would improve efficiency. The principle states that maximum efficiency could be achieved if heat was added at a constant high temperature and removed at a constant low temperature. Fuel is therefore not compressed with the air, but added just before combustion is required. The added fuel is thus ignited purely by the high temperature and pressure at the end of the compression stroke. He later abandoned isothermal combustion in favour of isobaric combustion (Andersson, n.d.). When running at the same compression ratio the Otto cycle is actually more efficient than the Diesel cycle (Ferguson & Kirkpatrick, 2000). The diesel engine can however run at far higher compression ratios as it is not knock limited. This coupled with the excess air available during combustion and the un-throttled air intake system during part load makes for a practically more fuel efficient engine (Andersson, n.d.).

The following sections discusses in more detail, the operation of the CI engine.

2.1.2. Compression Ignition

The compression ignition or diesel engine is widely used as power source in the industrial, automotive and marine sectors. This is mainly due to its very good thermal efficiency (Owen & Coley, 1990) (Xing-cai et al., 2004). A diesel engine is typically 25 % more fuel efficient than an SI engine with the same configuration and size, used in the same vehicle. The efficiency can be, in part, attributed to the high energy density of diesel fuel, but also to a fundamentally more efficient combustion process (Andersson, n.d.).

Combustion

As previously stated, the four stroke CI cycle is very similar to the four stroke SI cycle. Fuel is injected just before the piston reaches top dead centre (TDC) and the injection event can continue during the expansion stroke. The air and fuel mixture is therefore not homogeneous. In the past some CI engines had a separate chamber linked to the combustion chamber where injection took place. These were known as *Indirect Injection* (IDI) diesel engines.

In most modern CI engines, however, the fuel is injected directly into the combustion chamber. This is known as a *Direct Injection* (DI) diesel engine. The fuel is injected and atomized in the form of a fine mist which then vaporises and disperses in the combustion chamber as a result of the high temperature of the compressed air inside the chamber. The pressure and temperature in the combustion chamber is higher than that needed for spontaneous combustion of the fuel. The fuel therefore starts to combust after a short period of delay, aptly called the *ignition delay* period (Heywood, 1988). Unlike the SI engine, ignition in the CI engine starts at multiple points within the combustion chamber. These points have all reached the conditions where ignition and combustion can be sustained (Khair & Jääskeläinen, 2011). The next phase is known as the *premixed combustion/burn* phase. This phase is characterised by the rapid combustion of fuel that has mixed with air to within the flammability limits as can be seen in Figure 4. This is followed by the *main mixing-controlled combustion/burn* phase. During this phase the burn rate is determined by the rate that fuel becomes available for combustion. It is mainly controlled by the fuel-vapour air mixing process. The combustion process ends with the *late combustion/mixing-controlled burn* phase. Heat release in this phase may come from products of combustion undergoing further oxidation or unburned fuel that become ready for combustion through further mixing. Combustion during this phase is usually more complete (Heywood, 1988).

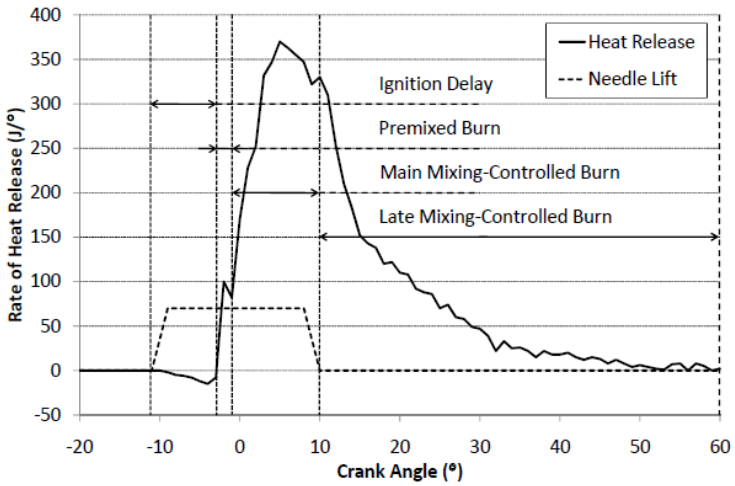

Figure 4: A rate of heat release (ROHR) diagram showing phases of diesel combustion (Andersson, n.d.).

Diesel engine technology has, however, not remained unchanged. Constant development has ensured that diesel engines have become more powerful, more fuel efficient, smaller, lighter and, crucially, cleaner. The following sections will touch on some of the more important advances in diesel engine technology.

Turbocharging

Diesel engines have no throttling device and the mass of air that flows into the cylinder during the intake stroke is purely determined by how restrictive the air intake system is. Supercharging increases the amount of air that gets delivered to the cylinders by means of a driven compressor that raises the density of the air. Increased air density means that more fuel can be injected, and thus more power developed, per stroke. The engine can therefore develop more power with a smaller swept volume (Challen & Baranescu, 1984).

There are two main methods of driving the compressor. The first being a mechanical drive connected to the drive shaft. This is normally referred to as *supercharging*. The second, and more common method in diesel engines, is to drive the compressor by means of a shaft connected to a turbine. The turbine is in turn driven by the hot exhaust gasses escaping from the cylinders. This method is called *turbocharging*. Turbocharging recovers some of the enthalpy in the exhaust gas that would otherwise be lost although it does increase the back pressure which again is detrimental to engine performance. The net effect is however found to be more efficient than constant mechanical load from a supercharger in most operating conditions.

One of the big disadvantages of turbocharging is the inertia of the turbocharger rotor resulting in a lag between exhaust energy increase and the required boost pressure increase when the load is applied. This is commonly referred to as *turbo lag*. The available boost pressure at low engine speeds is also limited as a result of lower energy available in the exhaust system. The opposite is true for high engine

speeds where the amount of available energy in the turbine will cause the turbocharger to over-boost. To prevent this, a *waste-gate* or bypass valve is used to regulate the boost pressure (Hawley et al., 1999).

A turbocharger fitted with a variable geometry turbine (VGT) is capable of optimally functioning at a far wider range of engine speeds and load conditions. This is achieved by varying the angle of the spindle of vanes surrounding and leading to the turbine. Varying the geometry of these vanes alters the angle of air flow to the turbine and the effective inflow cross sectional area of the turbine. The VGT is therefore capable of delivering the optimal boost pressure for the operating condition. The added control also increases the response time of the turbocharger under transient conditions, lessening the effect of turbo lag (Hawley et al., 1999).

Charge Air Cooling

As previously stated, turbocharging can increase the power output of an engine by increasing the mass of intake air in the cylinder, allowing for increase fuel delivery. The process of pressurisation however, increases the temperature of the charge. The increase in charge air temperature means that its density is reduced and that some of the effect of the charging process is lost (Challen & Baranescu, 1984).

Charge air cooling restores part of this loss in density. In automotive applications the charge is usually cooled in either an air-to-air or air-to-liquid heat exchanger. The efficiency of these intercoolers is very important, as a very restrictive intercooler would again result in a loss of charge air pressure.

Analysis of test results from an engine with charge air cooling showed a decrease in not only inlet manifold temperature, but also a decrease in temperature in the entire cycle. The heat transfer to the cylinder walls is decreased, which results in a slight increase in thermal efficiency. The exhaust gas temperature, and thus specific energy at the inlet to the turbine, is also lowered, which leads to a slight reduction in boost pressure. However, the net effect is better air flow through the cycle as a result of the density increase. This increase in air flow allows for increased fuel delivery, and consequently, substantial gains in power output. Fuel consumption is also lowered as a result of the improved efficiency of the cycle (Challen & Baranescu, 1984).

Fuel Injection Technology

Fuel delivery systems have developed considerably since the first diesel engines became popular. Indirect injection (IDI), a method by which diesel is injected into a pre- or swirl chamber to facilitate mixing with the air, has almost completely been phased out in favour of direct injection (DI) engines. Injection pressures have also risen considerably, from 500 bar in early engines to over 2000 bar currently (Challen & Baranescu, 1984).

The distribution pump injection method has been very popular for use in both passenger car and commercial vehicle engines. The method consists of a central

high pressure pump which then supplies fuel pressure to individual pipes leading to injectors. Mechanical distribution pumps are driven and timed through a mechanical connection to the engine crankshaft. The injectors consist of a spring-loaded needle that presses against a seat. When fuel pressure rises it pushes the needle against the force of the spring. As the spring force is overcome, the needle lifts off its seat and fuel is injected into the engine. The spring forces the needle back onto its seat when the fuel pressure drops (Challen & Baranescu, 1984).

Another method, popular in large industrial engines, but also used in some passenger car engines, is the *unit injector*. Unit injectors combine the high pressure pump and injector into one single unit. The high pressure pump is in the form of a plunger, driven either by a modified form of the camshaft for the valves or by an auxiliary camshaft (Heywood, 1988). To have full control over injection quantity, multiple injections and injection timing, modern unit injectors have electronically controlled bleed-off valves. Fuel pressure is bled off through these valves, while the plunger is being actuated until injection is required. The valve is then closed, causing the pressure in the system to rise, the needle to lift and injection to take place. When the valve is again opened, pressure is released and injection terminates. The small volume in the injector means that pressure waves propagate quickly and that injection can be very accurately controlled. This allows for multiple injections per combustion stroke. Small pilot injections can significantly lower the noise of combustion. Furthermore, the fuel in the plunger acts as lubricant to prevent wear (Challen & Baranescu, 1984). Figure 5 shows the unit injectors as well as the camshaft and rockers that drive the plungers.

Currently most modern diesel engines use the *common rail injection system*. This system uses a single pressurised rail which feeds every injector. The rail pressure can be varied to match the requirements of the engine operating condition and provides control over the rate and shape of fuel delivery during injection (Kang et al., 2003). An electronically controlled pressure relief valve manages this rail pressure and a mechanical relief valve acts as failsafe to prevent damage to the system. Injection is controlled through electromagnetic or, more recently, piezoelectric controlled injectors. This system allows for very accurate control over the injection strategy, making multiple pilot injections and even late injections possible. Coupled with variable vane turbochargers, this system can improve combustion, lower noise and lower emissions (Challen & Baranescu, 1984).

Figure 5: Electronically controlled unit injectors of the 1.9 TDI engine.

Exhaust Gas Recirculation

Exhaust gas recirculation (EGR) is a technology mainly used for emission control, more specifically to reduce the formation of NO_x. It entails recirculating some of the exhaust gas back to the intake of the engine through a control valve. The addition of exhaust gas lowers the combustion temperature and, therefore, the formation of NO_x. This will be discussed in more detail in the section on emissions.

In naturally aspirated diesel engines the application of EGR is simple, as the back pressure of the exhaust gas is higher than that of the intake manifold. Flow can thus easily be established from the exhaust side back to the intake manifold through a recirculation passage. In some instances a heat exchanger is used to condition the exhaust gas before entering the intake manifold. This is known as cooled EGR and it is implemented so as not to undo the advantages of intercooling by introducing hot exhaust gas into the charge (Zheng et al., 2004).

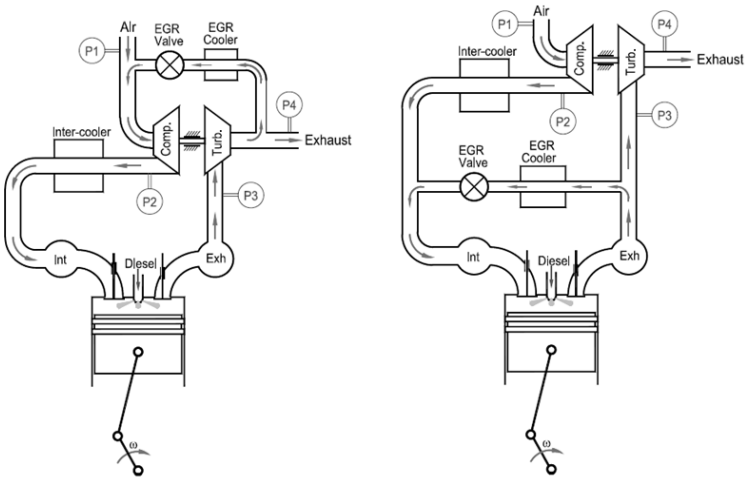

Figure 6: (a) Low pressure and (b) High pressure EGR systems in a turbocharged diesel engine (Zheng et al., 2004).

Turbocharged diesel engines however present more of a challenge. Low pressure, post-turbine exhaust gas can be channelled to the inlet of the compressor as shown in Figure 6(a). Most compressors and intercoolers are, however, not designed to handle the fouling properties and temperature of exhaust gas. Another solution would be to take post turbine exhaust gas and bypass the compressor and intercooler. However, this requires special exhaust gas pumps to overcome the charge pressure. The simplest solution is to channel exhaust gas from the exhaust manifold directly to the intake manifold through an EGR passage and control valve as shown in Figure 6(b). This is known as high pressure EGR and can only be achieved if the exhaust manifold pressure is sufficiently higher than the intake manifold pressure. A strategy to achieve this is by means of a VGT that can vary the exhaust manifold pressure. The control of the EGR valve and VGT must then be closely linked (Zheng et al., 2004).

Piston and Combustion Chamber Shape

Diesel combustion chamber shape is determined by the need to withstand the high combustion pressures and to facilitate fuel-air mixing. In IDI engines the fuel is injected into a pre- or swirl chamber. This chamber is connected to the main combustion chamber through a series of passages. During the compression stroke, air is forced through these passages into the swirl chamber, inducing a high level of turbulence which aids air-fuel mixing and the start of combustion. The combustion then travels through the passages again to the main combustion chamber where further combustion takes place. The piston bowl is usually shallow (Challen & Baranescu, 1984). The advantage of the IDI diesel engine is that ignition delay is low, which reduces combustion noise typically associated with diesel engines.

DI diesel engines are however more fuel efficient and for this reason, now completely dominate the diesel engine design. In DI diesel engines the intake runner and port shape as well as the piston bowl design generate turbulence to aid

fuel-air mixing. There are two main piston bowl designs. The first, *Re-entrant chamber*, has a smaller lip diameter than bowl diameter and is mainly used in light duty engines. The second, *open chamber*, are used predominantly in heavy duty engines. Figure 7 shows the re-entrant chamber on the left and open combustion chamber on the right.

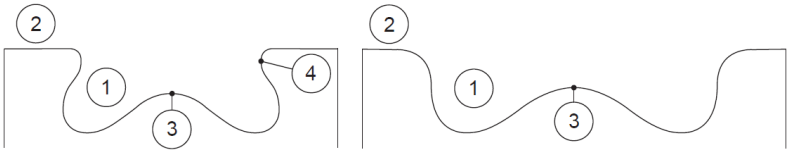

Figure 7: Piston bowl schematics. Re-entrant on the left and open chamber on the right. 1) Bowl; 2) Squish volume; 3) Pip; 4) Lip (Andersson, n.d.).

In these pistons the injector protrudes from the cylinder head wall and injects directly into the piston bowl. The bowl also allows for a flat cylinder head which is a structural advantage. The re-entrant piston bowl was patented by Hippolyt Saurer in 1934, but is still representative of most piston bowl designs (Andersson, n.d.).

2.1.3. Exhaust Gas Emissions

With the drive towards environmentally friendly power units, diesel engines have always been attractive. This is because of their low fuel consumption, when compared to SI engines with the same levels of CO and unburned HC emissions. It is however in NO_x and particulate emissions that CI engines cannot compete with their SI counterparts. Therefore, there has been a large focus on the reduction of these specific emissions. This has largely been accomplished through techniques like oxidation catalysts, advances in fuel formulation technology, injection strategies and exhaust gas recirculation.

The unfortunate problem in diesel engines is that the reduction of one of these usually leads to the increase of the other. This is also referred to as the NO_x-particulate trade-off (Horrocks, 1994).

The following paragraphs give more insight into exhaust gas emissions and the strategies employed in the reduction thereof.

Nitrogen Oxides

The formation of NO, which comprises the largest amount of the NO_x formed during combustion, is highly dependent on temperature and oxygen availability. This is because the oxidation of nitrogen from atmospheric air through thermal processes is a relatively slow and a temperature-dependent process (Andersson, n.d.).

The fundamental design of a diesel engine, with fuel being injected into an excess of air and the resulting lean initial burn phase, results in favourable conditions for the formation of NO_x. During this initial phase, directly after the ignition delay, the burn rate is largely uncontrolled. The rapid pressure rise due to initial combustion and resulting rise in temperature promotes further NO_x formation (Heywood, 1988).

There are, however, newer studies that contradict this. These have found that the premixed phase is too rich for NO formation and that the bulk of NO is formed during the "mixing controlled" phase that follows. During this phase NO is formed on the outskirts of the flame where the fuel concentration is low. Finally, it has been found that NO is also formed during the late stages of combustion as a result of the time the combustion gasses have been subjected to high temperatures (Andersson, n.d.) (Aspiron et al., 2013).

One of the main ways to reduce NO_x formation is through *charge air cooling*. By increasing the engine efficiency and lowering the charge temperature, charge air cooling significantly lowers the NO_x formation for the same power output in turbocharged engines.

An even more important strategy is *exhaust gas recirculation* (EGR). EGR is widely regarded as the most effective way to reduce NO_x emissions. The biggest reason for the reduction is what is known as the *dilution effect*. The recirculated exhaust gas displaces some of the oxygen in the intake manifold of the engine, thus leaving less oxygen to take part in combustion. This lowers the combustion temperature and therefore reduces the NO_x produced. It does however have the adverse effect that the now less complete combustion causes a substantial rise in particulates, CO and unburned HC. It has however been found that if EGR is done supplementary to the inlet charge, thereby increasing the charge mass, favourable NO_x reduction can be achieved without the increase in particulate emissions. This is due to the fact that the increase in mass also increases the total heat absorbing capacity of the inlet charge. The combustion temperature is therefore lowered and so is the NO_x production, without reducing the oxygen required to oxidise the soot particles (Ladommatos et al., 2000) (Zhao et al., 2000).

Carbon Monoxide

The combustion of fuel rich mixtures results in the formation of carbon monoxide. This is due to the lack of oxygen in the mixture and therefore incomplete combustion of the fuel. The nature of diesel combustion, however, requires the air-fuel mixture to be on the lean side of stoichiometric and CO emissions are therefore very low (Heywood, 1988).

Unburned Hydrocarbons

Unburned hydrocarbon emissions, as the name states, are mainly the result of incomplete combustion of the HC molecules of the fuel. Unburned HC emissions are therefore in a large part influenced by the composition of the fuel. Fuels containing olefins and aromatics usually produce relatively high unburned HC emissions. There are however some HC emissions that are synthesized during

the combustion process as is evident from the presence of organic compounds in the emissions that are not found in the fuel.

The unburned HC emissions can be divided into two classes: the non-reactive, methane hydrocarbons and the reactive, non-methane hydrocarbons. Some of these hydrocarbons are known to be carcinogenic.

Diesel fuel composition and the injection spray process results in the composition of the unburned HC emissions in diesel engines being much more complex than that of SI engines and ranges over a far larger density scale. Some of these HC emissions stay in gaseous form whilst others condense and are absorbed in the soot emissions. These condensed hydrocarbons can form up to 45% of the particulate mass and cannot be detected with an analyser, as they get filtered out with the soot.

As already stated, HC emissions are formed as a result of incomplete combustion. In a diesel engine the main ways for this to occur is either when the mixture is too lean to ignite and keep burning or, too rich. During the ignition delay period, the injected fuel disperses in the cylinder and some regions can become too lean for auto-ignition. The fuel then oxidises through thermal-oxidation which is relatively slow and incomplete. This is especially true for part load operation. During the primary stage of combustion, over-injection of fuel could cause over-rich areas which also do not combust completely. Secondary fuel injection also adds to this scenario. When injected fuel is not evaporated completely, it can become impinged on the combustion chamber walls, also resulting in incomplete combustion of this fuel (Heywood, 1988).

Soot and Particulates

Particulate emissions and the understanding of how and when they are formed is probably the most complex part of diesel emissions. The dynamic nature of the combustion as well as the pressures and temperatures present during combustion make modelling and measuring the formation of particulates a very intricate field.

It is widely accepted that soot, which combines with other products of combustion to form particulates, is formed in areas of the cylinder which are overly rich during the combustion process. This has traditionally been considered to be the regions located close to the injection nozzle orifices. Newer studies, as summarized by Anderson (n.d.), have found that even though soot formation starts close to the injection nozzle, the particulates tend to grow as they travels further into the combustion chamber. If these particulates move into the periphery of the flame, they are oxidised as a result of the lean conditions (Andersson, n.d.).

As particulates are produced by an inefficient combustion processes, the main strategies to reduce particulates are through the optimization of these processes. Improved injectors and injector placement have greatly reduced particulate emissions. Injector pressures have also risen considerably to improve spray patterns. The design of the combustion chamber, number and placement of valves and the shape of the piston bowl all contribute to better fuel air mixing. The effect

is thus improved combustion efficiency and less particulate formation. This coupled with after treatment devices like *oxidation catalysts* and *diesel particulate filters* (DPF) have all but eradicated particulate emissions (Hooks, 1994).

2.2. Engine Testing

Engine testing is a field that encompasses a very broad collection of engineering disciplines. It spans all the way from the structural and architectural layout of the facility to the electronic capture and software post-processing of data. It has been noted that it takes carefully managed processes to be able to generate useful and valid test data from a facility. Even then, a test facility would soon become obsolete if the latest technology is not implemented.

2.2.1. Test Facility

"One of the primary purposes, and in most cases the only purpose, of an engine or vehicle test cell is to produce data." (Martyr & Plint, 2007)

With reference to the abovementioned quote, one can however produce gigabytes of data but have it all be void if the test is not well designed and executed. In the engine test facility this design starts from the ground up. An ergonomic layout to the building is essential to engine testing, especially if engines and test bench pallet setups are to be changed regularly. It is important that the intent of the test facility and future scope of work be defined before the layout of the building is done. Changing the layout and purpose of the facility once it has been built is a far more time-consuming and costly exercise than designing the facility from scratch to meet the required specifications.

2.2.2. Performance Testing

The nature of performance testing is inherently governed by what specific component is to be analysed. Manufacturers will also often have their own specified standards for performance and durability tests for instance. These tests will be specifically designed to address known areas of key performance. There are however some standards in use that provide a starting point to most engine performance analysis.

ISO 3046-1:2002 is one such standard. It defines the basic atmospheric conditions under which performance testing should be conducted and also gives directive as to how engine performance should be reported to improve communication (ISO, 2002).

The basic atmospheric conditions specified are:

Atmospheric pressure:	1 bar
Temperature:	25 °C
Relative humidity:	30 %

The standard also addresses how correction factors should be implemented for tests not done at the specified conditions. It is also further specified that an accuracy of ± 3 % for power and ± 3 % for fuel consumption in repeatability is acceptable (Martyr & Plint, 2007).

2.2.3. Emission Testing

With the major focus on environmental impact, the strict legislation governing emissions limitations and the constant drive towards a reduction in fuel consumption, emission testing has become an integral part of engine testing. It is even considered that emission testing might comprise the majority of current development and routine testing (Martyr & Plint, 2007). This becomes even more apparent when the amount of testing done to verify *conformance of production* (COP) is considered. Legislation may require a manufacturer to test new production vehicles throughout the production life span of the vehicle to verify that current production conforms to the limitations set out for that particular vehicle. Typically this would require that a statistical analysis be done to determine how many vehicles of each model must be tested.

The bulk of emission testing is conducted on complete vehicles as legislation is mostly set to govern *vehicle tail pipe emissions*. This entails mounting a complete vehicle to a chassis dynamometer and testing it in accordance with strict guidelines set out by the relevant legislation that is enforced in the specific vehicle market. Comparative tests can however also be done on specially equipped engine test cells as shown in Figure 8. This is aimed at the emissions of stationary engines and those found in industrial equipment, also known as *non-road* engines (Martyr & Plint, 2007). These test cells are also used for fuel development. Although the laboratory might differ greatly, the techniques for analysing the exhaust gas of both vehicle and stationary engines are mostly the same.

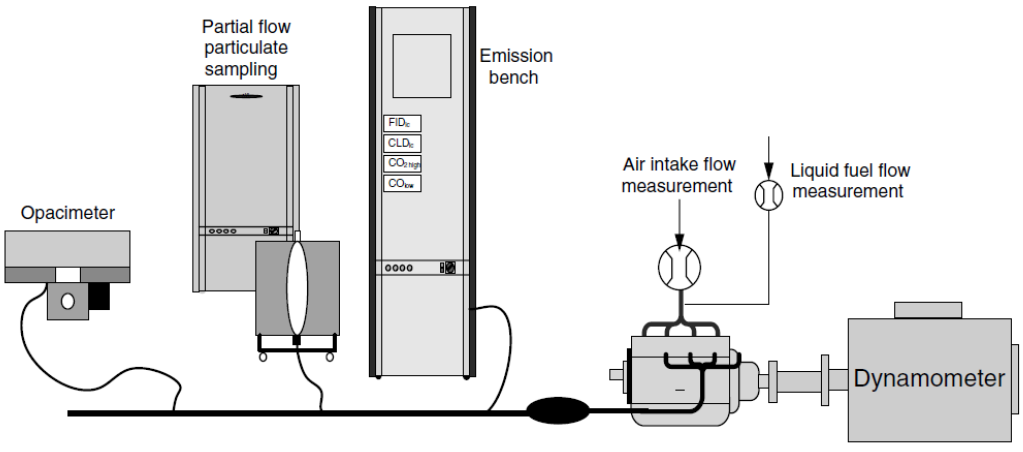

Figure 8: Test setup to test a *non-road* diesel engine (Martyr & Plint, 2007).

The development of instrumentation and techniques to perform emission tests has lagged behind the rapid progress of the emission legislation itself. This is as a result of the sheer cost and complexity of establishing a new test procedure and standard. Test procedures and equipment therefore usually stay constant for some years (Martyr & Plint, 2007).

Table 1 shows the most common techniques for gaseous emissions analysis. The 90 % response times of analysers should be carefully considered when testing is required. Under stable testing conditions enough settling time should be allowed for the analysers at each point. This is however not possible under transient conditions and therefore the response time needs to be considered when data synchronizing is done.

Table 1: Techniques for Emission Analysis (DieselNet, 2007)

Technique	Gas	Typical Range	90% Response Time
Non-dispersive infra-red (NDIR)	CO	0-3000 ppm	2-5 s
	CO_2	0-20%	2-5 s
Chemiluminescence detector (CLD)	NOx	0-10,000 ppm	1.5-2 s
Flame ionization detector (FID)	Total HC	0-10,000 ppm	1-2 s
Fourier transform infra-red (FTIR)	NOx, some HC, etc.	various	5-15 s
Paramagnetic analyzer	O_2	0-25%	1-5 s

Non-dispersive Infra-red (NDIR) and Fourier Transform Infrared (FTIR)

NDIR functions on the principle of passing *polychromatic light* through a gas sample and on to a sensor. In *dispersive* instruments the light is first passed through a filter, reducing the light spectrum to a narrow band, before it is passed through the sample. In *non-dispersive* instruments the filter is only applied after the light has passed through the sensor (Martyr & Plint, 2007). This technique is used to detect the presence of CO_2, CO, HC, N_2O, NO and SO_2 (Horiba, 2014). These molecules have a very unique band of absorbance of infrared light. CO_2 for instance has an absorbance that has a distinctive peak at 4.26 µm wavelength. The analyser for CO_2 therefore has a sensor specifically tuned to detect this wavelength.

FTIR basically works on the same operating principle as NDIR but, by performing a Fourier transform analysis, it can distinguish peaks in multiple waveform lengths. This allows the instrument to measure different components (Martyr & Plint, 2007).

Chemiluminescence Detector (CLD)

CLD's and HCLD's, *Heated Chemiluminescence Detector*, are used to determine concentrations of NO_x. All NO_2 in the sample is converted to NO through a catalytic converter. The converted sample is then reacted with ozone (O_3) which forms NO_2 in an activated state. This discharges light as it returns to

its normal state as shown in Equation [2.1]. The amount of light is indicative of the concentration of NO_X and is measured through a photomultiplier (Stone, 1999).

$$NO + O_3 \rightarrow NO_2^* + O_2 \rightarrow NO_2 + O_2 + photon \qquad [2.1]$$

Flame Ionization Detector (FID)

During hydrocarbon combustion positive ions and free electrons are produced. When this reaction takes place in an electric field, the current flow can be used to approximate the amount of carbon atoms involved in the reaction. In the FID the sampled gas is mixed with oxygen and helium and then burned to induce the reaction and to prevent any further ionisation of N_2. Some FID's are heated (HFID) to prevent the formation of water vapour (Stone, 1999) (Martyr & Plint, 2007).

Paramagnetic Detection (PMD)

Paramagnetic detection analysers are used to measure O_2 concentration. In a PMD cell a magnetic field is generated with varying flux strength. Due to the strong paramagnetic susceptibility of O_2, the molecules collect in the area of highest flux strength. The molecules then displace a balance detector which acts as indicator of O_2 concentration (Martyr & Plint, 2007).

Soot and Particulate Measurement

As with gaseous emissions analysers, particulate measurement instruments have evolved with the tightening of legislation and cleaner burning engines. Some after treatment strategies, like DPF, have even left older technology instruments obsolete.

Diesel particulates can be measured by means of *opacimeters, smoke meters, particulate samplers* and, more recently, *particle counters.* The difference in measurement methods means that results from different methods is difficult to compare (Martyr & Plint, 2007).

In opacimeters meters light is shone through an undiluted sample of exhaust gas. A receptor then determines what percentage of light is blocked by the particulate emissions (Martyr & Plint, 2007).

Smoke meters pass a predetermined amount of sampled exhaust gas through a piece of filter paper. Particulates are caught in this filter and the blackening of the paper is measured by means of a reflectometer. The blackening is compared with clean paper and the difference is an indication of exhaust gas soot content (AVL, 2005).

Particle samplers also use filters to capture the particulates. The filters are made to very exact specification and are weighed before and after testing. The results are compared against a reference filter to determine the mass of particulates that has been caught on the paper (Martyr & Plint, 2007).

Solid particle counters (SPC) are the next generation of particulate analysing equipment. They analyse the non-volatile particle number concentrations. Exhaust gas is first hot diluted at 150°C and then treated in an evaporation chamber to evaporate the remaining volatile components. The particles are then counted by using the *light-scattering* method (AVL, 2014) (Horiba, 2014).

2.3. Combustion Analysis

2.3.1. Pressure Indicating

Pressure indicating is the name given to the process of measuring the combustion chamber pressure of the internal combustion engine. The name stems from a time when steam engines were in general use and when a fully mechanical system was used to indicate the cylinder pressure (Zhao & Ladammatos, 2001).

A typical pressure indicating system uses an in-cylinder piezoelectric pressure transducer to measure cylinder pressures and a shaft encoder to reference the pressure signal to the crankshaft angle. Most current systems intended for heat release analysis, use the signal from the encoder as sample time for pressure measurement. The result is a pressure signal based on discrete crank angle steps and not time. This is needed because the events in the engine are governed by crank angle and not time. For this purpose an incremental type shaft encoder is needed. Figure 9 demonstrates how the encoder signal is used to reference the pressure signal. It is recommended that for diesel engines, the acquisition be done at 0.25°CA or higher to capture the extremely high rate of pressure rise (Zhao & Ladammatos, 2001) (Bueno et al., 2012) (Stone, 1999).

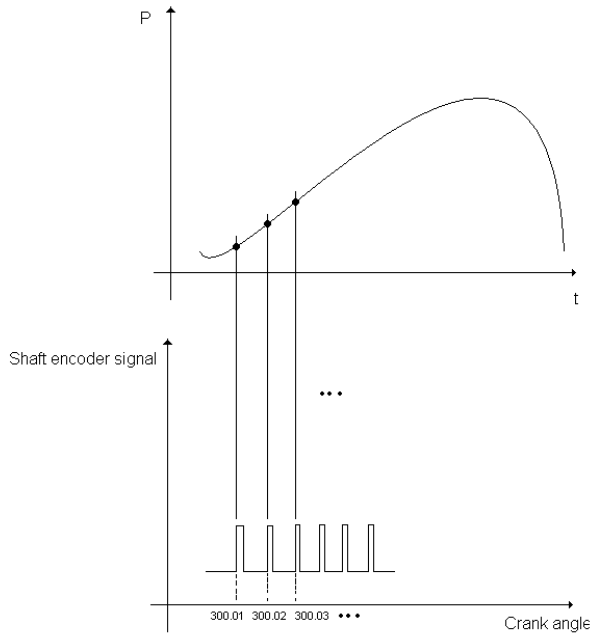

Figure 9: Pressure signal referencing with incremental shaft encoder.

Pressure Transducer Mounting

The mounting position of the transducer has a large influence on the accuracy of the data that can be captured. Positions close to valves or above the squish volume in the cylinder can result in pressure measurement discrepancies as a result of high gas flow rates and pressure oscillations. If however a pressure transducer is placed in or directly above the piston recess, it is subjected to far larger thermal loading as a result of combustion than any other position. Measurements can be negatively affected as a result of *thermoshock* (AVL, n.d.). Figure 10 shows the effect pressure oscillations have on the pressure trace as a result of transducer location.

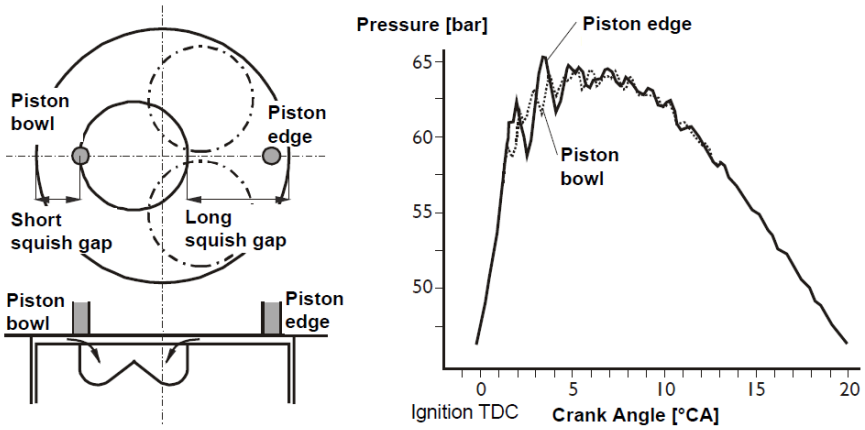

Figure 10: Pressure oscillations as a result of pressure transducer placement (AVL, n.d.).

It is also recommended that pressure transducers be mounted flush with the cylinder head or very slightly recessed. In modified glow plugs or spark plug transducers the pressure transducer is sometimes recessed to minimize the thermal effects. The recess forms an *indicating channel*. This channel can act as an acoustic resonator causing pipe oscillations. The frequency of the oscillation is determined by the pipe length, as shown in Figure 11, and also gas composition. The difference between chamber pressure oscillations and pipe oscillations are not easily distinguishable (AVL, n.d.).

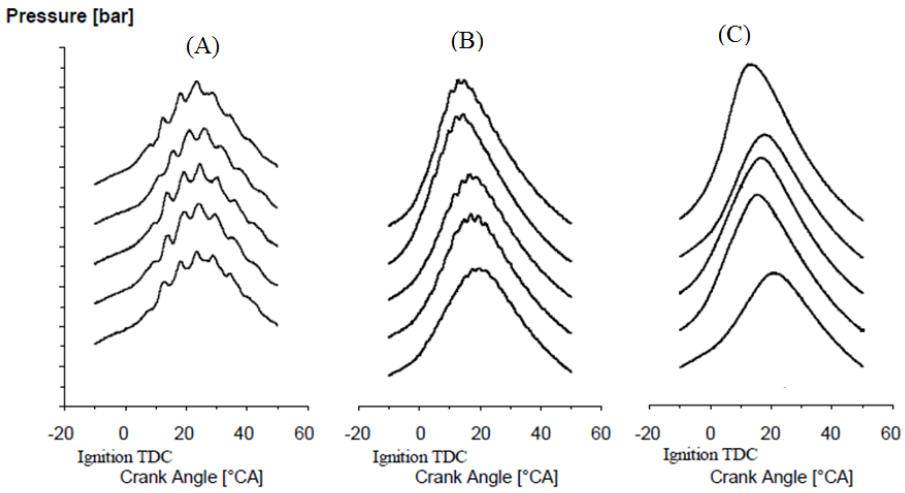

Figure 11: Pipe oscillations as a result of indicating channel length: (A) $L_{channel}$ >37 mm; (B) $L_{channel}$>25 mm; $L_{channel}$>2.7 mm (AVL, n.d.).

The cost of modifying an engine head to accurately position the pressure transducer for best results must be weighed up against the possible inaccurate measurements of using a glow plug or spark plug mounted sensor. The positions of these plugs are usually areas of high thermal loading within the cylinder which

could negatively influence results. There is however development cost involved in establishing a mounting procedure for pressure transducers in a new engine without guarantee of success. The compact layout of modern engines has also made finding a suitable solution a difficult procedure (AVL, n.d.).

Pressure Pegging and Top Dead Centre Determination

Piezoelectric transducers produce a voltage corresponding to a change in pressure through a calibration constant. It also produces a base or bias voltage at atmospheric pressure corresponding to a zero reading. To determine the absolute pressure, the pressure signal must be referenced to a certain pressure. The most used option to accomplish this is to peg the pressure trace to the mean manifold pressure at the inlet bottom dead centre (IBDC). It is assumed that the cylinder pressure at IBDC is equal to the mean inlet manifold pressure as the piston is stopped, the exhaust valve is closed and there is hardly any flow over the partially open intake valve. This is, however, not as accurate if wave effects in the intake manifold runners are present (Lancaster et al., 1975). The equation for cylinder pressure from the electric signal (E) is thus as follow:

$$p = C_E(E - E_{IBDC}) + p_{IBDC} \qquad [2.2]$$

If possible, pegging should be performed on every cycle recorded to counter the drift effect that is found in piezoelectric devices (Zhao & Ladammatos, 2001).

It is recommended that the pressure data from a large number of cycles at an operating point be recorded and averaged to determine the pressure trace for that operating point. This statistically increases the chances of the trace being correct. It is also in line with most other measurements in the engine testing environment that are averaged over time. Averaging will therefore eliminate the cycle-to-cycle variation that is present when an engine runs at a set operating point (Lancaster et al., 1975).

The validity of pressure measurement data should be checked by analysing the data from a motored pressure trace. An estimate of the peak pressure can be made by using the polytropic principle for compression. That is:

$$pV^n = constant \qquad [2.3]$$

The polytropic constant, n, can be assumed to be between 1.25 and 1.35. The peak pressure can then be estimated through the following equation (Zhao & Ladammatos, 2001):

$$p_{max} = p_{IBDC}{r_v}^n \qquad [2.4]$$

With r_v being the compression ratio of the engine.

Peak cylinder pressure should precede TDC in a motored pressure trace. This is as a result of the heat loss and leakage in the cylinder (Yost et al., 1981). This is also the reason why it is important that a motored curve be performed on an engine at operating temperature. The heat loss and leakage would then be in line with what is expected under operating conditions. The angle at which peak pressure precedes

TDC will also reduce with an increase in engine speed (Zhao & Ladammatos, 2001). This is because less time is available for the heat loss and leakage to transpire. If peak pressure precedes TDC by more than 2 degrees crank angle, the pressure data is most likely advanced (Lancaster et al., 1975). *Thermal loss angle* is the angle between the calculated TDC from pressure data and the actual TDC (AVL, n.d.).

In an SI engine, the ignition timing is controlled through the spark timing. In a CI engine this function is fulfilled by the injection timing of the fuel. Late injection timing with late combustion (ATDC) results in less negative work needed during the compression stroke, but also less peak pressure and therefore less power output during combustion. On the contrary, if the peak pressure of a fired pressure trace is close to TDC the pressure rise before TDC results in much more negative work. The Minimum ignition advance for Best Torque (MBT) is the timing when these two effects are optimized for a fixed speed and air fuel mixture (Heywood, 1988) (Ferguson & Kirkpatrick, 2000) (Zhao & Ladammatos, 2001).

More information about combustion can be obtained by analysing the pressure data against the corresponding cylinder volume. A CI engine has no throttle and therefore very little pumping losses during the exhaust and intake stroke, when compared to an SI engine. Some work is however still required during this part of the cycle as a result of friction in the intake and exhaust systems. In a p-V diagram as shown in Figure 12, the pumping work (W_p) is represented by the enclosed area between the exhaust and intake stroke. The gross indicated work ($W_{i,g}$) is represented by the enclosed area between the compression and expansion strokes and gives the work done by the force of combustion acting on the piston. The net indicated work per cycle ($W_{i,n}$) is therefore the difference between these two. The indicated power per cylinder can be determined through the following equation:

$$P_i = \frac{W_{i,n} N}{n_r} \qquad [2.5]$$

Here n_r is the number of crank revolutions needed to perform a power stroke. In a four-stroke engine, it would be 2 whilst in a two-stroke engine it would be 1 (Zhao & Ladammatos, 2001).

P_i represents the amount of power available before frictional losses etc. If the brake power is measured by a dynamometer, it is possible to calculate these losses.

$W_{i,n}$ also allows for the calculation of *Indicated Mean Effective Pressure* (IMEP):

$$IMEP = \frac{W_{i,n}}{V_d} \qquad [2.6]$$

MEP is a measure of the work done per unit volume and is a useful measure as it allows for comparison of engines of different configurations (Ferguson & Kirkpatrick, 2000). IMEP is therefore a measure of an engine's design efficiency regardless of the engine size (Zhao et al., 2000).

Brake Mean Effective Pressure (BMEP) represents the work transferred to the output shaft of the engine and can be calculated based on the measured torque:

$$BMEP = \frac{4\pi T}{V_d} \qquad [2.7]$$

With both IMEP and BMEP known, the *Friction Mean Effective Pressure* (FMEP) can also be calculated (in this equation FMEP includes pumping losses).

$$FMEP = IMEP - BMEP \qquad [2.8]$$

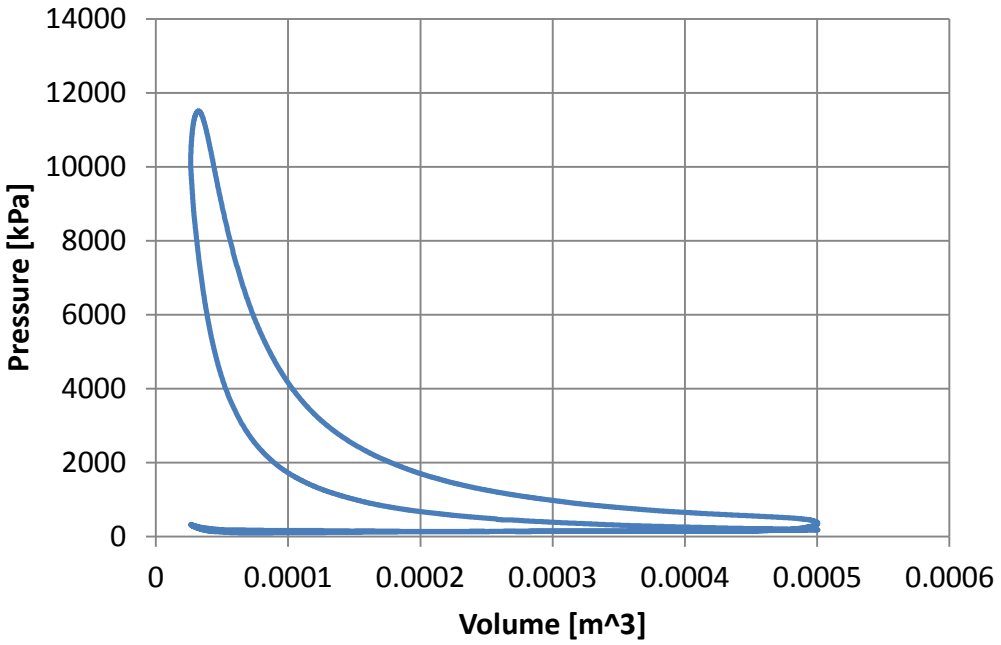

Figure 12: Typical p-V diagram of the 1.9L TDI during a firing cycle. 3000 rpm, 160 Nm, BMEP: 1050 kPa.

As previously stated, the compression curve of an engine can be approximated through the exponential polytropic function shown in Equation [2.3]. This curve will thus represent an almost straight line with slope –n when plotted on a logarithmic scale (Lancaster et al., 1975). The log p-log V diagram is essential to determining and fine tuning the validity of the pressure data.

One of the more important tasks in pressure indicating is to perfectly match the TDC pulse of the shaft encoder with the TDC of the engine. TDC can be measured both directly, through position sensors that monitor the position of the

piston, or indirectly through calculations with the pressure signal. Direct methods are very accurate, but require considerable modification to the engine and difficult mounting procedures. Indirect methods are far easier, but are affected by various factors like engine speed, torque and coolant temperature (Miao et al., 2013).

The task of determining accurate TDC through the indirect method can be simplified by accounting for slight misalignment through an offset angle input during post-processing. Correct phasing can be determined through examining the log p-log V diagram for a hot motoring curve. The pressure trace is correctly phased when there is no crossing or excessive opening of the compression and expansion lines. The two lines should form a sharp spike (Callahan et al., 1985). This method of determining TDC is also known as the *polytropic exponent method*. This is because the angle of the log p-log V line represents the polytropic exponent (Miao et al., 2013).

The diagram can also be used to determine the correct pegging of the reference pressure. An incorrect reference pressure will cause curvature at the bottom end of the straight compression and expansion lines. Similarly, a curvature at the top of these lines indicates that the compression ratio or clearance volume is incorrect and should be adjusted (Lancaster et al., 1975) (Callahan et al., 1985).

2.3.2. Instantaneous Heat Release

Instantaneous heat release is the method of diagnosing the combustion process in an internal combustion engine. By measuring the in-cylinder pressure and crank angle it is possible, through thermodynamics and heat transfer theory, to determine the energy release within the cylinder. This opens a window into exactly how the energy in the fuel is utilized, what theoretical temperatures are present and what type of burn process is active. This also gives an indication as to the origins of certain exhaust gas emissions.

Heat release is an essential tool in evaluating the performance of an internal combustion engine.

The basis for heat release analysis starts with the first law of thermodynamics for a closed system (Ferguson & Kirkpatrick, 2000).

$$\delta Q = dU + \delta W \qquad [2.9]$$

By assuming Ideal Gas Law $pV = mRT$ and with $\delta W = pdV$ and $dU = mc_v dT$ Equation [2.9] becomes:

$$\delta Q = \frac{c_v}{R}(pdV + VdP) + pdV \qquad [2.10]$$

For the purpose of heat release calculations this needs to be re-written in terms of the crank angle:

$$\frac{dQ}{d\theta} = \frac{V\frac{dp}{d\theta} + \gamma p\frac{dV}{d\theta}}{\gamma - 1} \qquad [2.11]$$

To model the heat loss to the cylinder walls, an instantaneous heat transfer term $\frac{\mathrm{d}Q_w}{d\theta}$ is introduced.

$$\frac{\mathrm{dQ}}{d\theta} = \frac{V\frac{dp}{d\theta} + \gamma p\frac{dV}{d\theta}}{\gamma - 1} + \frac{dQ_w}{d\theta} \qquad [2.12]$$

This type of model is known as a single zone, zero-dimensional model for heat release and it assumes the content of the combustion chamber to be homogeneous. More sophisticated quasi-dimensional models have been developed, but these are found to be only slightly more accurate (Stone, 1999) (Goering, 1998) (Lawton, 1987).

2.3.3. Instantaneous Spatially-Averaged Heat Transfer

Heat transfer models can be grouped according to their intended use and the heat flux they predict. Time-averaged heat flux predicts the time and spatially averaged heat flux and is used to predict overall heat release. Instantaneous spatially-averaged heat transfer coefficients are used to predict instantaneous conditions like power output, efficiency and emissions. Local instantaneous heat transfer coefficients are the most complex of the correlations and are used for accurate modelling of the engine (Finol & Robinson, 2006).

It is clear from the above that instantaneous spatially-averaged correlations provide enough information for combustion and emissions analysis without the complexity of a local instantaneous heat flux correlation. To model instantaneous spatially-averaged heat transfer, the in-cylinder heat transfer must be assumed to be quasi-steady. This means that at any instant the rate of heat transfer is directly proportional to the difference between the cylinder wall temperature and the temperature of the gasses in the cylinder. Although this is not theoretically correct and the mechanisms inside the cylinder are in actual fact far more complex, it is argued that more correct correlations become practically unusable in their complexity (Annand, 1963) (Finol & Robinson, 2006). This assumption then allows for a correlation for instantaneous heat transfer coefficient to be developed (Annand, 1963).

Eichelberg developed the basic method for measuring instantaneous heat transfer in the internal combustion engine as far back as 1939.

$$\frac{dQ_w}{dt} = 2.43\mathrm{A}\left(u_p\right)^{1/3}\left(pT_g\right)^{1/2}(T_g - T_w) \qquad [2.13]$$

This correlation is based on one developed by Nusselt for a spherical bomb, but was developed through measurements in a reciprocating engine. The major criticism for the Eichelberg correlation is that it focusses mainly on convective heat transfer and does not explicitly address heat transfer through radiation, although some compensation was made by shaping the exponents. Care should also be exercised when implementing this equation as it is not dimensionally constant. The big advantage of the correlation is that it is simple to use and only

requires pressure and gas temperature data (Stone, 1999) (Finol & Robinson, 2006).

It is worth noting that the Eichelberg and Nusselt correlations are based on the conditions of free convective heat transfer. The heat transfer in the cylinder of the reciprocating engine is, however, a forced convection process. Radiation heat transfer also plays a role in the expansion stroke (Finol & Robinson, 2006). Annand (1963) developed a correlation that takes the above into account and it is still widely used to estimate instantaneous heat transfer.

$$\frac{dQ_w}{dt} = \mathrm{A}[\mathrm{a}\frac{k_g}{B}Re^b\left(T_g - T_w\right) + c\left({T_g}^4 - {T_w}^4\right)] \qquad [2.14]$$

With:

$$Re = \frac{u_p B}{\upsilon} \qquad [2.15]$$

Values for the variables differ with regards to application, but are generally in the region of the following:

a = 0.25 – 0.8

b = 0.7 – 0.8

c = 0 during compression and exhaust strokes

c = 0.57σ

(Annand, 1963) (Stone, 1999) (Finol & Robinson, 2006) (Hountalas & Anestis, 1998) (Zhao & Ladammatos, 2001).

Woschni is another that developed a well-known correlation for heat transfer based on forced convection in turbulent flow. He also approximated the gas velocity in the cylinder by using both the pressure of the motored and combusting cycles at a specific operating point. This vastly increases the complexity of the correlation (Finol & Robinson, 2006). The correlation as represented by Finol and Robinson (2006) and again by Finol Parra (2008):

$$h = 129.9B^{-0.2}p^{0.8}{T_g}^{-0.53}[C_1 u_p + C_2\frac{V_s T_r}{P_r V_r}(p - p_m)]^{0.8} \qquad [2.16]$$

With all pressures measured in bar.

When developing his correlation for heat transfer, Woschni introduced into his equation the difference between the measured pressure data and the motored pressure data for the same point (p_m). This complicates the use of this correlation. It is however suggested that approximating the motored pressure using isentropic compression and a measured index pressure does not introduce any noteworthy error into the calculation (Finol Parra, 2008). Figure 63 in Appendix J shows the small difference that can be associated with this method.

$C_1 = 6.18$; $C_2 = 0$ during gas exchange process

$C_1 = 2.28$; $C_2 = 0$ during compression

$C_1 = 2.28$; $C_2 = 3.24 \times 10^{-3}$ during combustion and expansion

Woschni also at a later stage introduced the rate of swirl into the constants C_1 and C_2 to compensate for its effects on gas velocity:

$C_1 = 6.18 + 0.417C_u/u_p$ during gas exchange process

$C_2 = 2.28 + 0.308C_u/u_p$ for the rest of the cycle

With $C_u = B\omega_p/2$ and ω_p is measured from a paddle wheel used to measure swirl velocity (Heywood, 1988) (Zhao & Ladammatos, 2001) (Finol & Robinson, 2006) (Woschni & Spindler, 1988).

Hohenberg analysed Woschni's correlation and, through correlation with experimental data from different DI diesel engines, simplified the expression:

$$h = C_1 V^{-0.06} p^{0.8} {T_g}^{-0.4} (u_p + C_2)^{0.8} \qquad [2.17]$$

Where

$C_1 = 130$; $C_2 = 1.4$;

(Finol Parra, 2008)

2.4. Fuels, Engine Performance and Emissions

All over the world the diesel engine is the prime mover of choice. The biggest reason for this is its excellent thermal efficiency and fuel economy (Challen & Baranescu, 1984) (Xing-cai et al., 2004). Globally, the transportation sector alone is responsible for 70 % of all carbon monoxide emissions, 40 % of all nitrogen oxide emissions and 19 % of all carbon dioxide emissions (Goldemberg, 2008). As the effects of pollutants become more apparent and global crude oil supplies dwindle, the pressure on engine manufacturers to produce even more efficient engines with far less emissions has increased significantly. Researchers have also focused on advancing fuel technology, especially addressing the reduction of emissions and the use of renewable fuels (Rakopoulos et al., 2007). This is particularly important as most of the world's vehicle fleet consists of older technology engines and one way to improve emissions from these engines is through cleaner burning fuels (Shahir et al., 2014). One of the most important ways to reduce emissions is through the addition of oxygenated components. These include fuels that have potentially renewable sources, like alcohol and biodiesel (Rahimi et al., 2009). It is however key that any petroleum fuel replacement has characteristics that closely resemble those of the original diesel. In South Africa, every batch of biodiesel produced to be commercially sold has to comply with the SANS quality standard for biodiesel (SANS1935) and can only be blended up to an allowable quantity of 5 % by volume. In addition to this, the blended fuel still has to comply with the regular specification for automotive diesel (SANS342) (SAPIA, 2008).

2.4.1. Properties of Diesel

Diesel fuel has certain properties that specifically make it suitable as a liquid fuel for use in compression ignition engines. Some of these are very strictly governed by fuel specifications while others, even though not specifically regulated, still have a large effect on the engine's operation. Deviation from the proper specifications would have a negative effect on engine performance, durability, exhaust gas emissions or a combination of the three. The following sections discuss some of these properties and their importance.

Ignition Quality

Ignition quality determines how well the fuel is suited to combustion in a compression ignition engine (propensity to auto-ignite). *Ignition delay time* is an indication of the ignition quality of a fuel, but is also affected by various other factors. The tests procedure developed to determine ignition quality from ignition delay is therefore carried out under carefully controlled test conditions to ensure that the only variable is the test fuel. To this effect, various tests have been developed.

Cetane Number

The most accepted of these is the *cetane number* (CN) test. The method was developed in the 1930's by the *Cooperative Fuel Research* (CFR) Committee and is standardised as ASTM D613. The test is run on a single cylinder *CFR cetane engine* with continuously variable compression ratio and two reference fuels with which to compare the test fuel.

- *n-hexadecane* (also called cetane) has good ignition qualities and was given a cetane value of 100.
- *1-methylnaphthalene*, has poor ignition qualities and was given a cetane number of 0 (this fuel was later replaced with *2,2,4,4,6,8,8-heptamethylnonane* (isocetane), which, compared to the original fuels, has a cetane number of 15.

The cetane number of a fuel is determined by the volume percent composition of a mixture of the two reference fuels that would give the same ignition delay:

$$cetane\ number = \%cetane + 0.15(\%isocetane) \qquad [2.18]$$

In routine operations the two primary reference fuels will be replaced by two secondary reference fuels that have been calibrated against the primary reference fuels. These are only supplied by one supplier, Chevron Phillips.

The test is very expensive to do as a result of the specialized fuels, equipment, and skills required.

Cetane Index

The correlation for *cetane index* (CCI) was developed to predict the ignition quality of a fuel without having to do the expensive cetane number test.

Cetane index is based purely on the physical properties of the test fuel. Two standards, namely, D976 and D4737, are commonly used. The equations are included in Appendix I.

Derived Cetane Number

The derived cetane number (DCN) test presents an alternative to the expensive CN test. The test is performed using a *Constant Volume Combustion Apparatus* (CVCA) and in accordance with either ASTM D6890 or IP489. During the test, ignition delay is measured from the start of injection into the combustion chamber, causing the pressure to drop slightly, until the combustion chamber recovers the pressure and starts to combust.

$$DCN = 4.46 + 186.6/IND \qquad [2.19]$$

IND = Ignition delay.

This section was adapted from Jääskeläinen (2007).

Energy Content

The energy content (calorific value, heating value) is a very important fuel property. It does not usually form part of any fuel regulations but, it is indirectly controlled through the other defining fuel properties.

Heating value is determined with a bomb calorimeter according to the procedure laid out in ASTM D 240. Some standard procedures for estimating heating value from other key properties like density, aromatics content, mid-boiling point etc. also exist.

Higher heating value (HHV) or gross heating value is the total energy released during the combustion of a fuel. This includes the latent heat released when the water vapour, formed during combustion, is condensed. Lower heating value (LHV) or net heating value is the energy released without this latent heat. In an IC engine the water vapour escapes with the exhaust. The LHV is therefore of more importance (Owen & Coley, 1990).

Diesel fuel's LHV along with its density play a major role in the CI engine's favourable fuel economy over SI engines.

2.4.2. Biodiesel

Biodiesel is synthesized from vegetable oil through transesterification. This is a chemical process that substitutes the glycerol of the glycerides and forms methyl esters. The glycerol is replaced with three molecules of mono alcohols (Agarwal & Das, 2001). This process takes place in the presence of an alkali based-catalyst, although acid and enzyme based catalysts can also be used (Von Gerpen, 2005). Non-catalytic transesterification can also happen under high temperatures and with a large excess of methanol (Dasari et al., 2003). Figure 13 and Figure 14 show the process flow and chemical reaction for biodiesel

production. R represents long hydrocarbon chains. The in-fuel oxygen in the ester group is what gives biodiesel its oxygenation characteristics.

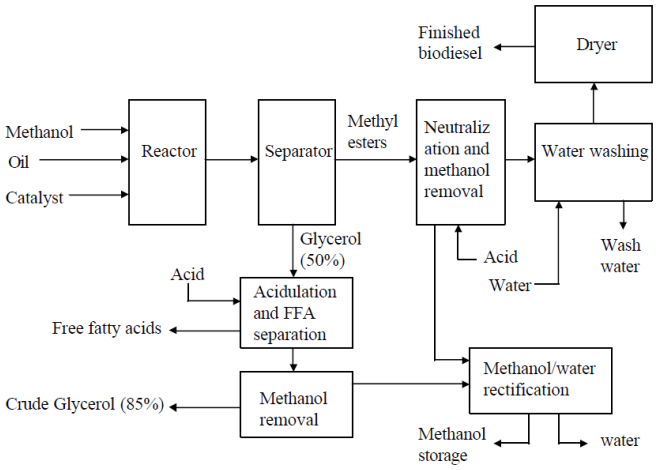

Figure 13: The process of transesterification of vegetable oils (Von Gerpen, 2005).

Vegetable oils mainly contain only five types of methyl ester chains. The combination and quantities of these determine the properties like cetane number, cold flow and oxidation stability of the fuel (Von Gerpen, 2005).

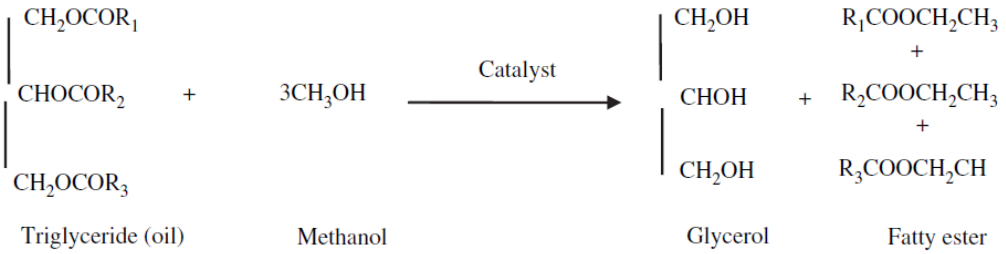

Figure 14: Transesterification reaction (Rahimi et al., 2009).

Biodiesel can be used in diesel engines as 100% biofuel or as a mixture with mineral diesel. Mixtures are designated according to the biodiesel content. As an example, a 20% biodiesel blend is designated as B20, 50% as B50 and pure biodiesel as B100. Blends are almost always in volume percentage.

In South Africa legislation dictates that biodiesel up to blends of 5% by volume (B5) can be commercially sold as long as the blend still conforms to the national automotive diesel specification, SANS 342. In addition, the B100 blend stock should conform to its own standard, SANS 1935. Every batch of biodiesel should

conform to these standards, both at the manufacturing plant and at the point of blending. This means that every batch should be analysed, which is a very expensive exercise and not economically feasible for smaller producers. Careful consideration should also be given to the logistics and storage of biodiesel when distributed, due to its limited shelf life (SAPIA, 2008).

The following is a summary of the most important properties of biodiesel:

Cetane Number and Combustion Quality

The cetane number of vegetable oil derived biodiesel is typically higher than that of mineral diesel. This makes the fuel attractive as a cetane enhancer in blends with other fuels. The high cetane number is as a result of the long-chain structure of alkyl esters. Long-chain, saturated methyl esters have the highest cetane number. The cetane number decreases when the amount of unsaturated bonds in the molecular structure of the fuel increases, as can be seen in Figure 15. The first number denotes the length of the chain and the second the amount of unsaturated bonds (Jääskeläinen, 2009).

The cetane number of biodiesel has been known to increase with prolonged storage. This is as a result of the tendency of biodiesel to oxidise over time. During the early stages of oxidation the peroxide concentration in the fuel will increase. Peroxides possess qualities that increase the cetane number and are often used as cetane enhancers (Knothe et al., 2005).

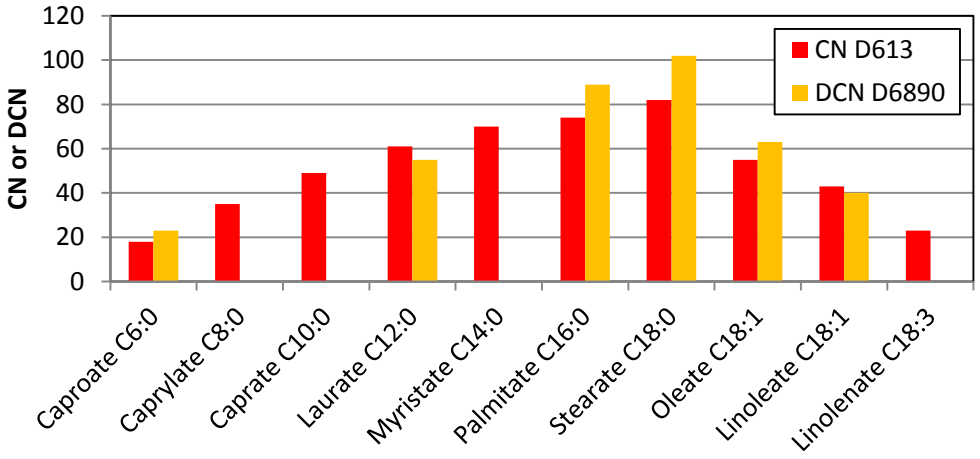

Figure 15: Cetane (CN) and derived cetane number (DCN) of some methyl esters (Jääskeläinen, 2009).

Biodiesel generally has lower calorific values than that of pump diesel. This reduction in energy content is frequently sighted as the reason for reduction in power output and fuel economy when compared to pump diesel (Utlu & Koçak, 2008) (Agarwal & Agarwal, 2007). The SFC for biodiesel blends increases with an increase in biodiesel concentration. In a study done on a turbocharged, DI,

common-rail diesel engine fuelled with biodiesel derived from coconut oil, the SFC was consistently higher than the mineral diesel, regardless of engine load. Figure 16 shows the increase in SFC. This is due to the lower calorific value of biodiesel when compared to the pump diesel (How et al., 2014).

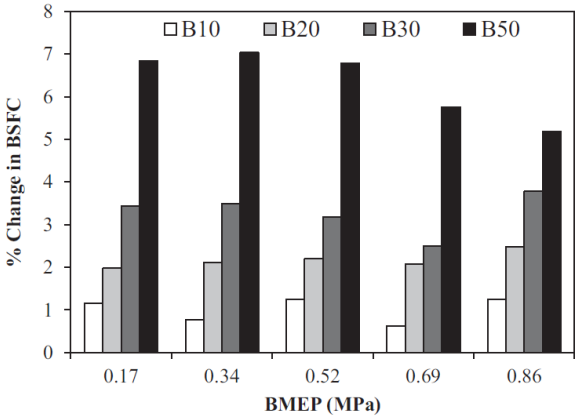

Figure 16: Change in SFC for increase in biodiesel content (How et al., 2014).

Viscosity and Lubricity

The viscosity of diesel fuel is important, as it affects the performance of both the fuel pump and injection system of the engine (SAPIA, 2008).

The kinematic viscosity of biodiesel is slightly higher than that of mineral diesel as a result of the high molecular mass of the fuel. It is, however, very close to and completely miscible in diesel. When blended with mineral diesel, very little difference in viscosity can be discerned (Agarwal & Das, 2001). It is found that the viscosity of the biodiesel increases with the increase in carbon chain length and the degree of saturation (Knothe et al., 2005). The higher kinematic viscosity of biodiesel allows for better spray penetration during injection. This improves air-fuel mixing and aids combustion (Lin et al., 2009).

Viscosity and lubricity of fuels were considered to be linked, as fuels with higher viscosity would also have better lubricity (SAPIA, 2008). More recent studies have however found that it is different chemical constituents, like oxygen and nitrogen content, that contribute largely to the lubricity of a fuel (Knothe et al., 2005).

The lubricity of the fuel used in a diesel engine is of utmost importance as it is the only source of lubrication for many of the fuel delivery components. A single tank of low lubricity diesel fuel could cause catastrophic failure of the diesel pump. The drive towards lower emissions has resulted in the specification for very clean, ultra-low sulphur diesel (ULSD) fuels. It has however been found that these fuels do not meet the lubricity specification and require a lubricity additive to be added before they can be used in a modern diesel engine. It was first thought that it was

specifically the reduction in sulphur that caused the reduction in lubricity. However, more recent studies have shown that it is the desulphurization process that reduces the oxygen and nitrogen content, which reduces the lubricity of the fuel (Knothe et al., 2005).

Biodiesel is known for its high lubricating qualities and could therefore be used as a possible lubricity additive in ULSD. A study was done to determine the compound of biodiesel that most contributes to its lubricating qualities. It was found that although methyl esters do possess some lubricity advancing qualities, it is in fact the common biodiesel contaminants, like monoglycerin and free fatty acids, that contribute most to this quality (Jääskeläinen, 2009).

Cold Flow Properties

As already stated, saturated long chain fatty acids form a significant part of biodiesel. These fatty acids, however, resemble a long chain paraffin molecule which has undesirable cold flow properties and these long chain fatty acids tend to solidify and form waxes in the fuel when subjected to cold temperatures. The formed wax can plug filters causing reduced fuel supply and stalled engines. Similarly, saturated monoglycerides, sterol glucosides and soaps, the contaminants regularly found in biodiesel, can precipitate at low temperatures. This can add to the filter-plugging effect. Biodiesel also has an affinity for water. At temperatures below zero, the water in contaminated biodiesel can freeze, causing ice particles (Jääskeläinen, 2009).

2.4.3. Ethanol-Diesel Fuel Blends

Ethanol is a renewable fuel that can be produced from basically any carbon containing fermentable feedstock. The production of this fuel or alcohol is a very well-known and mature technology.

Ethanol as a SI fuel has been widely used in South American countries like Brazil, where it is used as a fuel enhancer to boost octane levels or as a neat fuel. More recently the addition of ethanol to diesel as a renewable component has been researched (Xing-cai et al., 2004). The use of ethanol in diesel as supplementary fuel or range extender is however not a new concept. Trials on agricultural equipment were, in fact, already performed in South Africa in the 1980's. It was however always considered too expensive to produce ethanol. The dwindling of the world's crude oil supply, and the ever increasing demand for it, has meant that the price of crude based fuel has increased significantly. This has sparked renewed interest in the use of ethanol in diesel (Hansen et al., 2005). Recent advancements in the production of second generation bio-ethanol, that is ethanol produced from surplus biomass and non-food crops, has also attributed to this (Corro & Ayala, 2008). The reason for this is that the production of crops for fuel instead of food has always posed a moral dilemma.

Ethanol is also referred to as an oxygenated fuel. This is as a result of almost 35 % of its mass being oxygen (Rakopoulos et al., 2007).

The mixture of ethanol in diesel does however present some challenges. These include solubility; cetane number and the effect on combustion; viscosity and lubricating properties; and safety. Table 2 shows typical values for these physical properties. The following sections discuss these challenges and some other physical properties of ethanol-diesel blends.

Table 2: Typical physical properties of diesel fuel and ethanol (Rakopoulos et al., 2007).

Fuel properties	Diesel fuel	Ethanol
Density at 20 °C, kg/m^3	837	788
Cetane number	50	5–8
Kinematic viscocity at 40 °C, mm^2/s	2.6	1.2
Surface tension at 20 °C, N/m	0.023	0.015
Lower calorific value, MJ/kg	43	26.8
Specific heat capacity, J/kg °C	1850	2100
Boiling point	180–360	78
Oxygen, % weight	0	34.8
Latent heat of evaporation, kJ/kg	250	840
Bulk modulus of elasticity, bar	16 000	13 200
Stoichiometric air–fuel ratio	15.0	9.0
Molecular weight	170	46

Solubility and Miscibility

The solubility of ethanol in diesel is a major challenge and is mainly affected by two factors, temperature and water content of the mixture. A study by Gerdes and Suppes found that anhydrous ethanol, that is ethanol with a water content of less than 0.5 %, can be blended into diesel up to a concentration of 5 % whilst still keeping the cloud point temperature of the original diesel. The blend is however very sensitive to water contamination. In this case where no additives are used, the aromatic content of the diesel acts as a co-solvent to keep the mixture from separating. It was found that diesel with less or no aromatic content, like Fischer-Tropsch diesel, has far less tolerance to ethanol. (Gerdes & Suppes, 2001). Lapuerta et al. found that ethanol-diesel blends of up to 10 % ethanol by volume can be used in diesel engines in countries where winter temperatures rarely fall to -5 °C (Lapuerta et al., 2007).

It is therefore often required that additives be added to the blend to ensure blend stability. Two types of additives commonly used are surfactants and co-solvents. Both these additives allow for the splash blending of ethanol and diesel. Surfactants are molecules that contain a polar end, attracted to the ethanol molecules, and a non-polar end, attracted to the hydrocarbon molecules in the diesel. Surfactants thus cause micro-emulsions in the blend. These micro-emulsions are smaller than a quarter of a wavelength of visible light and therefore the blend appears clear to the eye. Biodiesel has also been found to act as an

emulsifier for ethanol in diesel. This serves as a very attractive prospect, as it increases the percentage renewable feedstock in the fuel. Co-solvents, on the other hand, have an intermediate polarity between that of ethanol and diesel. This causes the co-solvent to act as a bridging agent, thus creating a homogeneous blend (Jääskeläinen, 2006) (Hansen et al., 2005).

Cetane Number and Combustion Quality

Another challenge is that ethanol has a very low cetane number. It is considered to be in the region of 5 – 15. Blending ethanol with diesel thus also negatively affects the cetane number of the blended fuel. This causes the fuel to resist auto- ignition. It is found that there is a marked increase in ignition delay when ethanol is added to diesel (Jääskeläinen, 2006). The difference also seems to be amplified at lower loads. It has been suggested that the high latent heat of vaporisation of ethanol plays a large role here. At lower loads the evaporated ethanol has a larger effect on the temperature inside the cylinder. This drop in temperature further delays the auto-ignition process (Xing-cai et al., 2004). Figure 17 clearly shows how the rate of heat release and combustion pressure rise is delayed for the E15 mixture when compared to the original neat diesel. It also shows how adding a cetane improving additive can reduce the combustion delay.

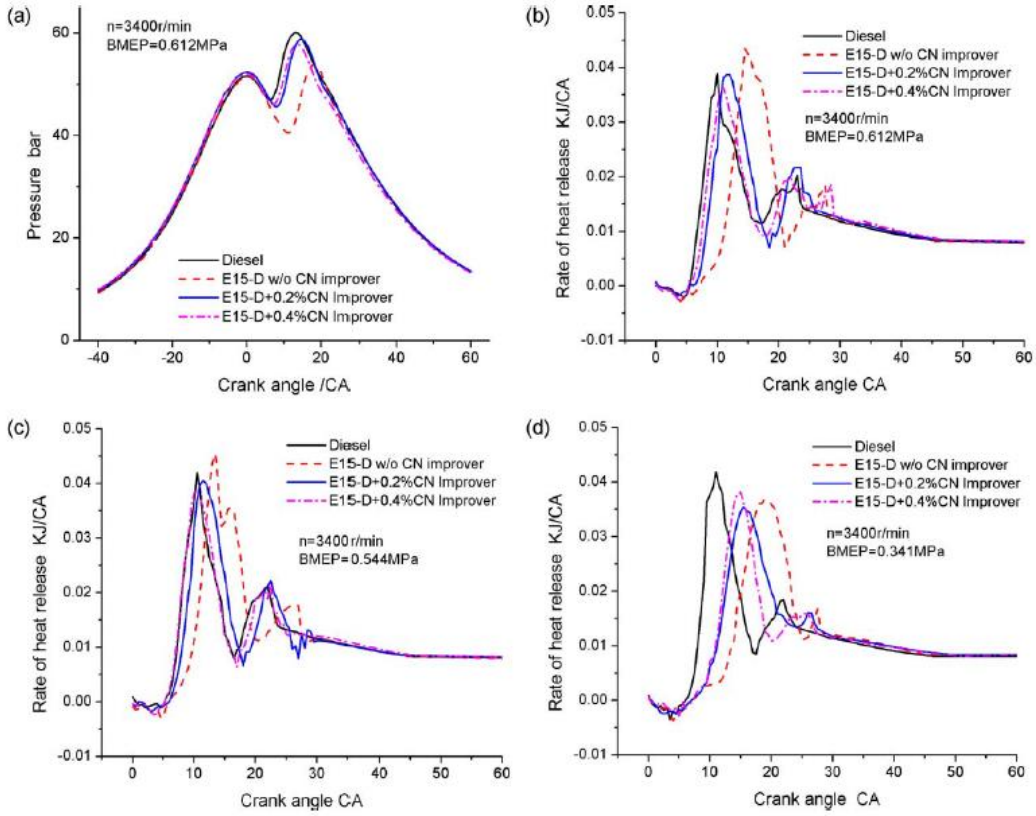

Figure 17: In-cylinder pressure and rate of heat release for ethanol-diesel blends at set speeds and BMEP (Xing-cai et al., 2004).

Similar results were found in other studies when they compared the in-cylinder pressures of neat diesel to that of E10 and E15 at different BMEP. They also echoed the finding of Xing-cai et al. that the relative ignition delay of the ethanol-diesel with respect to neat diesel decreased with an increase in BMEP (Rakopoulos et al., 2007), (Lapuerta et al., 2008).

Ethanol has a lower *gross heating value* than that of diesel and therefore a blend also has a *lower heating value*. Ethanol typically contains about 2/3 the energy of diesel for the same weight, as can be seen in Table 2. This is partly due to the density of ethanol being lower, but also the molecular composition. There is therefore less energy contained in each gram of fuel (Li et al., 2005). Consistent with this lower heating value, it is found that brake specific fuel consumption (BSFC) of the diesel engine increases when run on ethanol-diesel blended fuel. It is however found that this increase in fuel consumption decreases with increase in load and that there is therefore an increase in brake thermal efficiency. Figure 18 depicts this effect (Lapuerta et al., 2008).

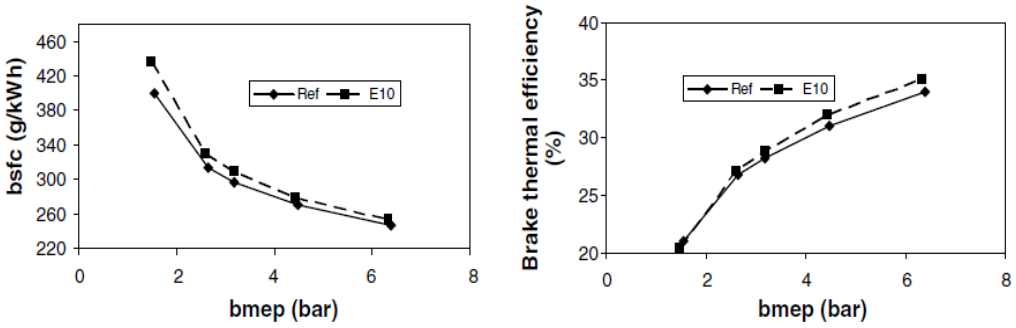

Figure 18: BSFC and BTE of ethanol-diesel compared to neat diesel at different BMEP (Lapuerta et al., 2008).

Viscosity and Lubricity

The lubrication qualities and viscosity of diesel fuel is of utmost importance to the fuel injection system. This is because some of the injection components, for example the high pressure injection pump, rely solely on the fuel to act as lubricant during operation. In unit injector systems the fuel acts as lubricant between the barrel and plunger and it is also important in lubricating the needle guide-nozzle body interface in the injector (Hansen et al., 2005). Lubricity and wear are concerns when blending ethanol with diesel. This is as a result of the much lower dynamic viscosity of ethanol compared to that of diesel (Xing-cai et al., 2004). Additives are therefore necessary to ensure that the mixture still has the correct lubrication qualities. It has been found that the surfactants used as additive to ensure blend stability can also improve the lubricity of the mixture (Jääskeläinen, 2006).

The lowered viscosity of the mixture can also result in greater leakage at the pump and injectors. This reduces the maximum rate of fuel delivery and would therefore reduce power output (Hansen et al., 2005).

The spray characteristics and atomization of the fuel during injection are also affected by the viscosity of the fuel. Smaller *Sauter mean droplet diameters*, a system developed to compare the surface area versus volume ratio of particles, are usually observed for fuels with lower viscosities. This means there is a greater droplet surface area per unit volume, which influences evaporation characteristics (Hansen et al., 2005), (Heywood, 1988).

Cold Flow Properties

Blending ethanol with diesel has been found to lower the pour point of the mixture significantly compared to that of normal diesel. It has, however, also been found that the cloud point can actually increase. This has been attributed to the fact that the micelles in the micro-emulsion of the ethanol-diesel increase in size when the ethanol-diesel cools down, becoming visible to the eye. These micelles are in fact liquid and will pass through a fuel filter, unlike the visible cloud point of normal diesel, which indicates the formation of wax crystals.

It is, in fact, this improved cold flow property which suggests that the blending of ethanol with biodiesel before blending with conventional diesel will have positive effects on the cold flow property of biodiesel/diesel blends. It has been found that if 20 % of a 50:50 mixture of biodiesel and ethanol is blended with 80 % pump diesel, it has cold flow properties comparable to that of the original diesel (Jääskeläinen, 2006).

Safety

In South Africa the minimum flash point specification for diesel is set to 55 °C, which is also the EN590:2004 (Euro 4) specification. However, some countries as well as certain parts of the US do allow a flashpoint lower than this. India, for instance, allow a flashpoint as low as 38 °C. The flash point of diesel does not have a direct influence on the performance of an engine, but it has major implications with regard to fuel handling. All blends of ethanol in diesel reduce the flashpoint from 55 - 60 °C to about 12 °C (SEKAB BioFuels & Chemical AB, 2007). The shipping and storing of the fuel should therefore be adapted to accommodate this.

An ethanol flame burns clear. This has particular implications to the fire-fighting procedure for an ethanol fire. Fire extinguishers for ethanol flames also use a different type of foam compound and different application method than conventional fuel fires (SAPIA, 2008).

2.4.4. Diesel-biodiesel-ethanol Blends

As stated in the section on ethanol-diesel, biodiesel is found to act as an emulsifier when mixed with diesel-ethanol blends. This makes it an attractive fuel, as both have an oxygenation characteristic and both can be produced from

renewable sources. The fuel therefore has potential from both an exhaust emissions and total carbon emissions standpoint. The properties of biodiesel and ethanol are also in some cases of opposing nature. When blended these properties balance each other, which causes blend fuels to mimic the characteristics of petroleum diesel more closely. Some important properties of the blended fuel are further discussed in the following sections.

Blend Stability

The phase diagrams in Figure 19 show the blend stability of both 95 % and 99.5 % pure ethanol mixed with diesel and biodiesel. From the diagrams it is clear that 95 % ethanol does not mix with diesel. Phase separation even takes place in mixtures with 80 % biodiesel, 10 % ethanol and 10 % diesel. The high polarity of the water in the ethanol increases the polar part of the ethanol molecule. This inhibits the ethanol from binding with the non-polar molecules of the diesel. However, the opposite is true for the 99.5 % anhydrous ethanol. This grade of ethanol forms homogeneous mixtures with diesel in all blend ratios (Kwanchareon et al., 2007).

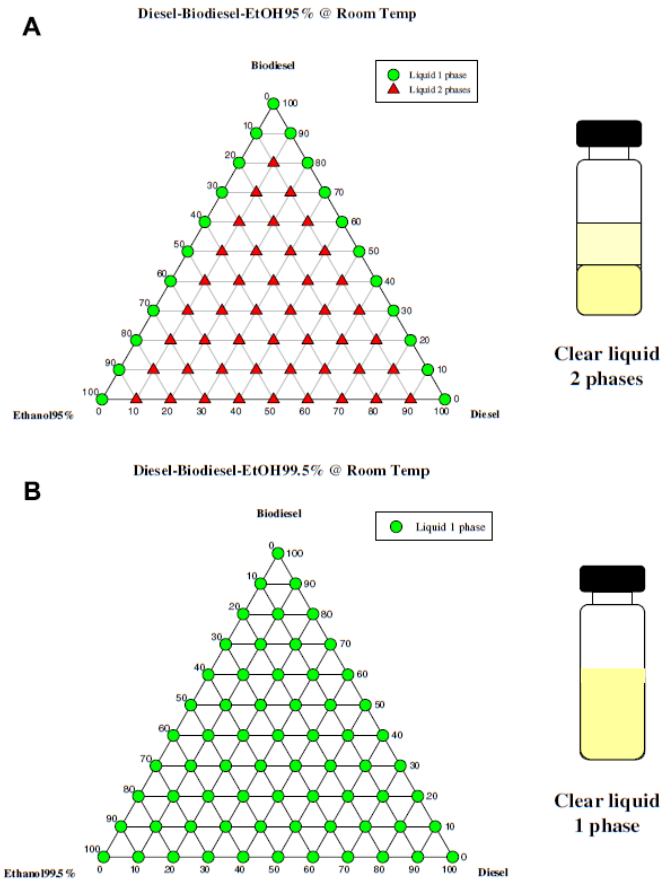

Figure 19: Blend stability of diesel-ethanol-biodiesel blends (Kwanchareon et al., 2007).

Cetane Number and Combustion Quality

As discussed in the previous sections, the cetane number of Ethanol is very low whilst biodiesel, on the other hand, can be used as a cetane improver in mineral diesel. Hulwan and Joshi tested a blend fuel containing 70 % neat diesel, 20 % ethanol and 10 % biodiesel. In their evaluations it was found that the addition of biodiesel raised the cetane number to 50. The neat diesel in the evaluation had a cetane number of 54 (Hulwan & Joshi, 2011). The diesel-ethanol-biodiesel blend therefore has the potential to have a comparative cetane number to that of neat diesel, provided the blend quantities are well chosen.

2.4.5. Exhaust Emission Characteristics of Biodiesel and Ethanol-diesel Blends

The exhaust gas emissions of an engine are as dependent on the physical and chemical properties of the fuel used as it is on the design of the engine. The following sections discuss the emissions characteristic for NO_x, CO, Unburned HC and PM for both mixtures of diesel with ethanol and biodiesel.

Nitrogen Oxides

Ethanol-diesel Blends:

As previously stated, the formation of NO_x is largely dependent on temperature and availability of oxygen during combustion.

In studies done on a 4 cylinder, DI, naturally aspirated diesel engine, it was found that there was a slight decrease in NO_x emissions with the use of ethanol-diesel blends, when compared to neat diesel fuel. This study found that higher the percentage of ethanol, the greater the reduction in NO_x emissions, as can be seen in Figure 20.

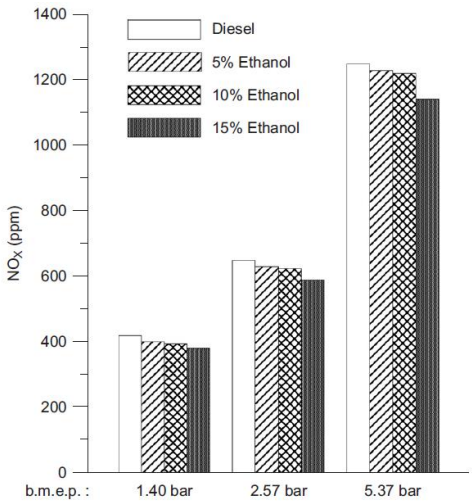

Figure 20: NOx emissions of ethanol-diesel blends compared to neat diesel at different BMEP (Rakopoulos et al., 2007).

This reduction is attributed to the temperature lowering in the cylinder through the latent heat of vaporisation of ethanol (He et al., 2003). Furthermore, the longer ignition delay caused by the low CN shortens combustion and causes less NO_x formation (Jeong et al., 2011). It was however noted that this is a very sensitive balance and that it is largely affected by the type of engine used (Rakopoulos et al., 2007).

The above-mentioned sensitivity was observed in tests using a VW 1.9 L, TDI, intercooled engine for various oxygenated fuels. It is found that oxygen enrichment actually slightly increases NO_x emissions. This follows the usual PM to NO_x trade-off, as explained in Section 2.1.2.1. It is found that the addition of oxygenates increases the heat release during the mixing controlled burn phase, the phase responsible for the most NO_x formation. It is suggested that the higher oxygen concentration causes an increased flame temperature in this usually locally rich phase, which increases NO_x formation (Song et al., 2004).

In another study done on a VW 1.9 L TDI it was found that the effect of ethanol addition was very much dependant on the speed and load of the operating point. Decreases as much as 60 % and increases of up to 25 % were measured with an addition of 15 % ethanol (Cole et al., 2000).

Biodiesel:

Reports on NO_x emissions for biodiesel fuelled compression ignition engines vary from slight improvements (-12 %) to slight increase (12 %) of NO_x emissions for different studies done with different engines, different blend ratios and different feedstock (Xue et al., 2011).

In the case of engines fitted with unit injectors, it has been shown that a slight increase in NO_x can be expected with an increase in biodiesel blend percentage. The reason for this is that the biodiesel blends have higher bulk modulus of compressibility. Pressure waves therefore propagate faster through the fuel and needle lift is attained faster than with normal diesel fuel. This induced advanced timing causes an earlier start of combustion (McCormick & Alleman, 2005). This means that the temperatures that are conducive to the formation of NO_x are attained earlier and are present for longer before cooling due to expansion begins (Szybist et al., 2007).

Carbon Monoxide

Ethanol-diesel Blends:

Studies on ethanol-diesel blends have found that CO emissions are reduced with an increase in ethanol volume percentage. Blends of 5 %, 10 % and 15 % ethanol-diesel all show a reduction in CO emissions. This reduction can clearly be attributed to the increased oxygen availability during combustion as a result of the fuel-bound oxygen in ethanol (Rakopoulos et al., 2007). It is also believed that the increased temperature during the mixing controlled phase further assists the oxidation of CO (Song et al., 2004).

More recent work has stated that CO is in fact reduced at higher loads, and increased at lower loads. The increase at lower loads was attributed to incomplete combustion of the ethanol blends as a result of low combustion temperatures, which contradicts previous work (Jeong et al., 2011).

Biodiesel:

CO emissions for blends of biodiesel decrease with an increase in the percentage of biodiesel added. This is found at both high and low load points. The reason for the reduction, as with ethanol-diesel, is the fuel-bound oxygen that can be found in biodiesel. The added oxygen assists combustion in the locally rich zones of combustion during the mixing controlled phase (Rakopoulos et al., 2006). The improvement is however limited when the CO emissions of the engine are already very low, as is the case with newer technology, high injection pressure, turbocharged engines (Wang et al., 2011).

Unburned Hydrocarbons

Ethanol-diesel Blends:

The unburned HC emissions of an engine running on ethanol-diesel are found to be higher than the corresponding neat diesel. It is believed that the high latent heat of vaporization of the ethanol causes slower fuel-air mixing and thus increased spray penetration. Fuel impingement on the combustion chamber walls and flame quenching at the walls are thus more likely. This results in incomplete combustion of this fuel at the walls and, as a result, HC formation (Rakopoulos et al., 2007). The inhomogeneity of the ethanol-diesel is also suggested as a possible cause of incomplete combustion in lean zones in the combustion chamber (He et al., 2003).

The effect is however also very dependent on operating point. In a report issued by the Argonne National Laboratory increases in HC of 226 % and decreases of up to 42 % were measured, depending on load point and percentage ethanol used (Cole et al., 2000).

Biodiesel:

Literature on the unburned HC emissions of biodiesel blend fuels is mostly inconclusive. Some studies show a substantial decrease in HC emissions whilst others show no effect or even, in some cases, an increase in HC emissions (Lapuerta et al., 2008). In general, the fuel bound oxygen in the biodiesel should improve combustion and therefore lower unburned HC. However, in engines with very low unburned HC emissions, like high injection pressure turbocharged engines, the effects of this fuel-bound oxygen becomes negligible and the effect limited (Wang et al., 2011).

Soot and Particulates

Ethanol-diesel Blends:

Soot reduction is one of the major advantages of blending ethanol with diesel fuel. It is found that soot is significantly reduced through the increase in volume percentage ethanol in ethanol-diesel blends as can be seen in Figure 21.

The cause of this, as with CO, is attributed to the overall leaner combustion as a result of the fuel-bound oxygen in ethanol. As the oxygen is fuel-bound, even the locally rich zones in the combustion chamber experience an increase in oxygen and thus leaner combustion (Rakopoulos et al., 2007).

In a study done on a very similar engine to the one used in this project, it was found that whether oxygenation takes place in the intake manifold (oxygenated fuel added in gas form) or in the fuel, the PM is still reduced (Song et al., 2004).

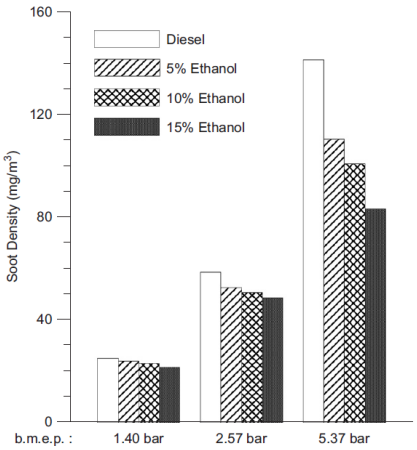

Figure 21: Soot density of ethanol-diesel blends compared to neat diesel at different BMEP (Rakopoulos et al., 2007)

It is also found that, although soot emission is higher at higher loads, the reduction in soot as a result of the addition of ethanol is also more. This can be seen in Figure 22 (He et al., 2003).

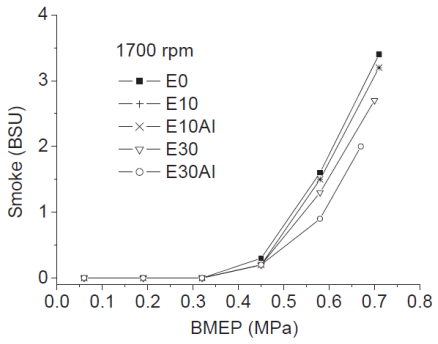

Figure 22: Bosch smoke units of different blends of ethanol-diesel at various BMEP (He et al., 2003).

The exact amount of reduction in soot is very dependent on specific engine and load points. In a summary on ethanol blended with diesel, emission reduction in particulate matter of up to 75 % was found (Hansen et al., 2005).

Biodiesel:

As is the case with CO emissions, soot formation and particulate matter reduce with an increase in percentage biodiesel added in biodiesel blended fuels (Canakci, 2007). Most studies find a reduction of around 50 – 70 % for 100 % biodiesel (Xue et al., 2011). The mechanism for the formation is much the same as with CO and it is therefore again the fuel-bound oxygen in the biodiesel that assists in oxidising the soot more completely (Rakopoulos et al., 2006).

Emissions Summary

To summarize, there are a lot of different findings on the exact influence of ethanol and biodiesel addition to diesel fuel with regard to emissions.

1. There is general consensus among all sources that the addition of ethanol to diesel fuel reduces the exhaust and particulate emissions and it is seen as one of the most important advantages of the use of ethanol-diesel. This is also the case with biodiesel.
2. There are fairly contradicting views on the effect of ethanol-diesel on the emission of NO_x. The main reason for this would be that the physical design of the engine used seems to have a greater effect on NO_x formation than the addition of small percentages of ethanol to diesel. In the case of biodiesel, a slight increase can be expected, but this is heavily reliant on the type of engine and load points tested.
3. The contradicting views are also found when CO emission is analysed. Again the design and calibration of the ECU controlled engines seems to have a greater effect. Biodiesel does seem to have a positive effect on CO emissions, but this effect becomes limited when the engine has very low CO emissions.
4. All sources have found that the use of ethanol-diesel produces more unburned HC than when compared to petroleum diesel. Yet, a slight improvement in unburned HC emissions can be expected with biodiesel addition to petroleum diesel.

3. TEST FACILITY DEVELOPMENT

The Biofuels Testing Facility is the culmination of work done by both Palmer (2008) and Kotzé (2010) as part of the fulfilment of their masters' theses. Palmer built up the test bed and control room and fitted a Toyota turbo-diesel engine to test biodiesel blends (Palmer, 2008). Kotzé built on this by exchanging the older technology engine for a modern VW 1.9 L TDI and integrating the newer technology into the test cell. Kotzé also set out to develop and instrument the engine with a cost effective indicating system (Kotzé, 2010).

Part of the objectives of this project is to build on the work done by both Palmer and Kotzé to enhance the fuel-to-fuel test capability of the test facility.

3.1 Test Bench

In an effort to further increase the capability of the test cell hardware, some improvements were introduced. These include upgrading the functionality and, in some cases, improve the operational safety of the various systems on the test bench.

3.1.1. Driveshaft

The initial driveshaft used by Kotzé consisted of a solid shaft with a CV-joint on either side. The use of CV-joints ensured that the engine's rotational velocity was transmitted directly to the dynamometer and speed pick up, whilst misalignment between engine and dynamometer could still be handled. This is shown in Figure 52(a). Further improvements to the driveshaft later incorporated a rubber damper between the dynamometer side CV-joint and the dynamometer. This type of rubber damper is used to counteract torsional vibrations between the engine and the dynamometer (Kotzé, 2010).

The addition of the rubber damper can however make the driveshaft unstable. This is because the rubber damper adds an extra pivot point along the shaft's axis as shown in Figure 52(c). This, combined with the two CV-joints, will then allow part of the shaft to be offset to the rotation axis under torque and high speed load. This eccentricity could cause vibration and result in shaft failure.

The solution was to re-develop a driveshaft that would only consist of two pivot points, the CV-joint at the engine side and a flexible rubber coupling at the dynamometers side, as shown in Figure 52(b). The two pivot points would still be able to handle some misalignment and the flexible coupling would dampen torsional vibrations.

The type of flexible coupling that was chosen for this application is often used to dampen shock loading between the gearbox, driveshaft and differential of vehicles. It can therefore withstand far greater loading than could be expected between the engine and the dynamometer. To this effect, it was decided that fitting two dampers in series would increase both the flexibility and damping ability of the coupling. It is also very important that this type of coupling be

centred at a central pivot point, preventing the coupling from distorting under load and to run with ecentricity. To achieve this, a shaft spigot was designed to fit through both dampers and locate inside a spherical bearing on the dynamometer connector flange. The spherical bearing keeps the shaft centred, but is unable to transmit torque. Further information on the design of the driveshaft can be found in Appendix A.

A final modification to the driveshaft was to introduce a central flange in the shaft guard. This flange encapsulates the shaft and would act as a constraint to restrict the radial movement of the shaft. Figure 23 shows the final driveshaft assembly.

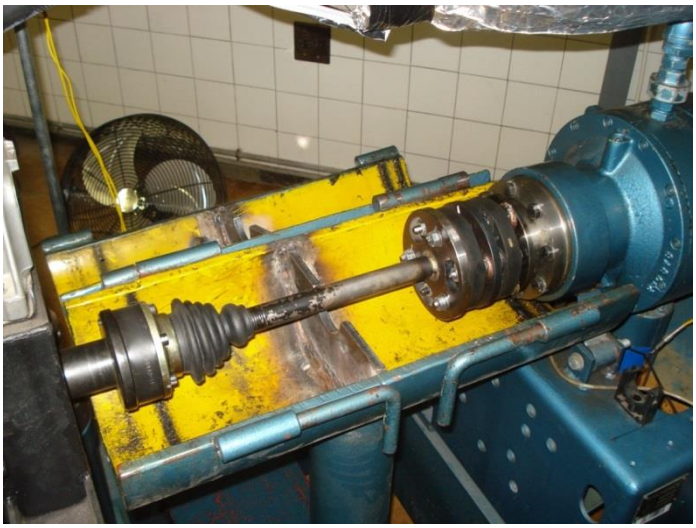

Figure 23: Final dynamometer driveshaft assembly

3.1.2. Engine Cooling Setup

The engine cooling setup had to be improved to provide stable operating temperatures. This section provides some background to engine cooling in a test cell and the design, installation and commissioning of the improved system.

Automotive engine cooling systems are designed to utilize the movement of the vehicle to facilitate heat transfer. Most modern passenger vehicle engines are liquid cooled and use air flow through a liquid-to-air radiator to disperse the heat generated by the engine. These cooling systems are not designed for stationary applications and therefore must be modified when the engine is fitted to a test bench. Engine testing also has additional stability requirements which necessitate improved control.

The most widely accepted test cell engine cooling setup is to exchange the radiator for a liquid-to-liquid heat exchanger. Engine coolant is circulated in what is known as a closed loop system between the engine and the heat exchanger. The cooling is controlled by managing the amount of engine coolant that is circulated through the heat exchanger or bypassed directly back into the engine.

Previous Setup

The diesel test cell was equipped with a closed loop liquid-to-liquid cooling system, by means of a tube-in-shell heat exchanger, to cool the engine. To manage the amount of coolant that is circulated through the tube-in-shell heat exchanger, an electronically actuated 3-way mixing valve was used. The actuation of this valve was then determined by a subroutine written into the PLC program. The operator could specify the required inlet temperature and the subroutine would automatically control the actuation of the valve by comparing the required temperature to the measured value (Palmer, 2008).

With the upgrade of the diesel test cell to the modern 1.9TDI engine it was found that efforts to try and control the coolant through both the subroutine written by Palmer (2008) and by implementing the Honeywell temperature controller, were unsuccessful. Automatic control was therefore substituted for manual control by means of toggle switches (Kotzé, 2010).

Automatic Control

For this project the automatic and accurate control of the coolant temperature was earmarked as one of the crucial upgrades needed for the test cell. Through discussions with Kotzé it was concluded that two aspects of the cooling system needed specific attention. The first was that the capacity of the tube-in-shell heat exchanger used in the test cell at that moment far exceeded the requirements of the test setup. This resulted in overshoot each time coolant was passed through the exchanger. Another possible solution was to replace the valve actuator with a faster acting model. This would reduce the response time of the valve.

A smaller, previously used heat exchanger was obtained to replace the larger version. A calculation of the heat dissipation capability of the new heat exchanger was performed to estimate if this one shell pass, double tube pass type heat exchanger was suitable. The estimation was done according to guidelines given by Çengel (2006). Refer to Appendix B for further calculations. It was estimated that the heat exchanger has a heat dissipation capability of almost 50 % of the engine power output and should therefore be adequate for this application. This would, however, have to be verified with testing. The heat exchanger was refurbished and pressure tested to ensure that there would be no leaking of fluid between the engine coolant and the cooling water sides.

The Honeywell ML6420A3007-3 valve actuator fitted to the system had a rated actuation speed of 20 mm in 1 minute. To increase the actuation speed this was replaced with a Honeywell ML6420A3023 which has a rated speed of 20 mm in 30 seconds. The interface of the two actuators with the mixing valve and the controller unit is completely interchangeable.

The actuator was reconnected with the PID controller unit, as per Honeywell's specifications. A remote setpoint can be supplied to the controller unit via an analogue signal, but due to a lack of open analogue outputs on the PLC, this was not possible. Manual setting of the controller setpoint was thus used.

In a cooling setup like this, the engine can either be operated with normal thermostat functionality or the thermostat could be blocked open. The latter allows the operator more control over the engine temperature, especially if irregularly hot or cold engine temperatures are to be tested. Feedback control of the coolant temperature would then be done on the coolant leaving the engine as this would represent the temperature of the engine. As the purpose of this test facility is to test the performance of the fuel more than that of the engine, it was decided that normal thermostat operation would be adequate and more representative of the engine's normal operating conditions. In this case the engine is allowed to regulate its own temperature through normal thermostat and coolant flow operation. The temperature of the coolant fed to the coolant inlet of the engine is controlled to a temperature above thermostat opening temperature and about 10 °C lower than the operating temperature of the engine. This allows for adequate heat exchange in the engine without thermally stressing the engine.

Figure 54 in Appendix B shows a flow diagram of how the coolant temperature control system is laid out and how the feedback control functions.

The system was checked first during warm-up procedures and then during a full load performance curve. It was found that the system controls temperature very well under all operating conditions. Figure 24 shows how the coolant at the coolant inlet to the engine slowly rises in temperature during warm-up. This is due to the proximity of the sensor to the engine. As soon as the coolant inside the engine reaches a temperature high enough for the thermostat to open, coolant flow causes the inlet temperature to drop again. At the same time, the coolant outlet temperature rises sharply due to the hot coolant leaving the engine. This temperature then stabilizes as the engine starts to regulate its own temperature. The hot coolant flows out of the engine toward the mixing valve and back into the engine. The rise in inlet coolant temperature then occurs. Finally, there is a small overshoot in inlet coolant temperature before it settles to stable control.

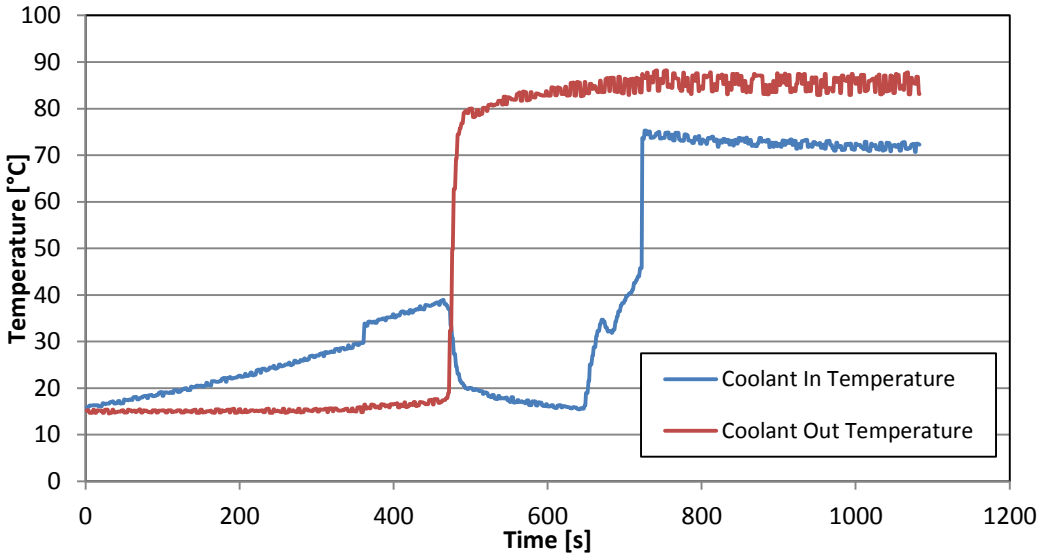

Figure 24: Thermostat operation and temperature control during warm up.

3.1.3. Fuel Mass Flow Measurement

A very important requirement of the test cell is the ability to accurately determine fuel consumption at set operating conditions. The test cell is fitted with an AVL 730 fuel mass flow measurement device. It consists of an AVL 7030 module and an AVL 7130 dynamic fuel balance that measures the fuel mass consumption rate. It operates by filling a central vessel with fuel to supply the engine. The vessel is mounted on a leaf spring capacitive bridge that allows it to continuously monitor the mass flow rate of fuel consumed. When the vessel drains completely, it momentarily stops measuring to refill. During this time a zero measurement is returned. The vessel has both a supply and return line to allow fuel that is not used to return to the vessel. A fuel pump is wired to the refill valve relay to pump fuel from the fuel tank to the measurement vessel when the fuel balance goes into refill mode (Palmer, 2008).

During the upgrade from the Toyota engine to the VW TDI, it was realized that the fuel consumption could not be accurately measured. Kotzé determined that there was no fault with the AVL equipment and that it was the hot fuel returning from the cylinder head of the engine that caused the erratic measurements. In attempts to rectify this, a fuel cooler was installed as it could be observed that the fuel in the system warmed to such an extent that some of its more volatile components started to vaporize. Unfortunately, stable measurements could not be achieved (Kotzé, 2010).

Kotzé's idea that the engine was the cause of the erratic measurement initiated a new concept for the fuel flow layout. The 1.9 L TDI ATD's fuel system layout is designed to use the fuel for both cooling and lubrication of the unit injectors. For

this reason, the fuel supplied to the engine by the diesel lift pump far exceeds the requirement of the engine at that operating condition. The fuel enters the head where it is warmed up considerably. The plunger action of the pump unit injectors also induces pressure waves in the diesel fuel and warm, pulsating fuel is then returned via the return line to the fuel system. The return line could therefore be the cause of the erratic measurement if it is fed directly back into the measurement vessel. It was decided to experiment with feeding the return line back into the supply line to the engine. The bulk of the fuel would therefore circulate around the engine and the measurement vessel would only supply the (relatively small in comparison) amount of fuel used to operate the engine. Preliminary tests showed this concept to produce favourable results.

Further improvements to the setup also included: The addition of one way valves in the fuel lines to prevent pressure pulses from travelling to the AVL vessel; a large diesel filter with water trap to prevent damage to the engine; optimized air flow circulation fan placement to avoid turbulent air flow over the AVL equipment; and finally, the implementation of a fuel conditioning unit to accurately control the fuel temperature supplied to the engine. More on this system will be explained in the following section.

The fuel mass balance was calibrated according to the AVL 730 user manual. An extract of the procedure is included in Appendix K.

Fuel Conditioning Unit

In preliminary tests it was soon established that the recirculated fuel from the engine would quickly rise to temperatures in excess of 60 °C. The need for an accurate fuel conditioning unit was therefore soon realised. As part of his final year project, Uys developed a fuel conditioning unit for use in the test cell environment and specifically for diesel engines. The unit was developed to cool and heat diesel fuel as well as pressurize the feed to the engine (Uys, 2010). These capabilities far exceeded the requirements of the current diesel test setup. The volume of fuel in the system also meant that a large amount of fuel would have to be flushed each time a new fuel was tested. Due to the high temperatures of the returning fuel, it was decided to simplify the setup to incorporate only fuel cooling. The basic design principle of Uys' setup was however kept.

The fuel conditioning unit system diagram is shown in Figure 25. The system uses chilled water to cool the fuel through two plate-type heat exchangers. Fuel returning from the engine passes through the first heat exchanger where most of the heat is dissipated. If any vapour bubbles were formed inside the engine, this exchanger serves to condense it back to liquid. The cooled fuel then feeds back into the fuel supply from the AVL mass balance through a set of configurable valves. The valves are set up to allow the operator to change between feeding the return fuel into the AVL or back into the supply line. Tests showed that feeding the fuel back into the supply line produced the most stable and repeatable measurements. The fuel supply is then passed through a second heat exchanger. The chilled water feed to this heat exchanger is controlled through a three-way mixing valve. The PID controller actuates the mixing valve according to the

feedback loop from a thermocouple in the fuel line. The fuel then passes through both an aftermarket and the OEM specification fuel filter, both equipped with water traps, before being supplied to the engine.

During commissioning tests the main chilled water supply line valve was throttled until approximately 50 % of the mixing valve's stroke equated to the desired fuel temperature. This allows for enough of a buffer on either side of the controller range to prevent it from reaching its minimum or maximum cooling capacity. The controller setpoint was set to 30 °C. During all fuel tests the temperature of the fuel was constantly monitored to ensure deviation never exceeded 1 °C from the setpoint temperature.

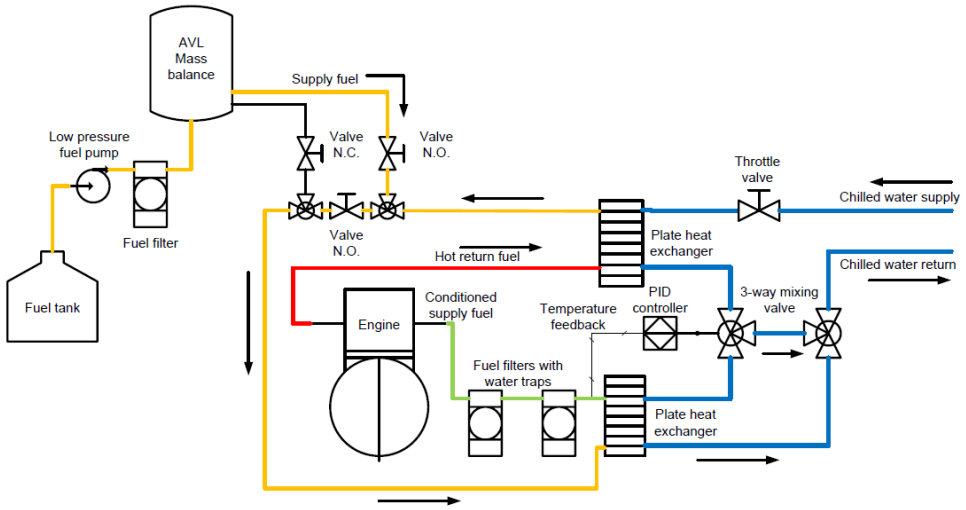

Figure 25: Fuel conditioning unit diagram.

Fuel Mass Flow Validation

To validate the performance of the AVL fuel mass balance it was important to analyse the accuracy and repeatability of the data. Initially, the tests signals were very unstable which resulted in very poor repeatability. Early part load tests showed that the raw measurements of fuel mass flow rate every 0.2 s had a standard deviation of more than 30 % of the measured value. This reduced to 6 % of the measured value after improvements to the fuel system layout and introducing temperature control. Figure 26 shows the improvements to the measurements that were achieved by depicting the maximum, minimum, median and 25^{th} and 75^{th} percentile of the respective test. During fuel testing, the fuel mass flow rates were captured over a period of time and the mean value was used. This also improved the repeatability of the results.

The reliability of the fuel flow measurement can also be determined by checking the repeatability of the SFC values. A repeatability test was conducted with both

the engine and fuel flow measurement equipment switched off between runs. With very stable load control and stable inlet air temperature, engine coolant temperature and fuel temperature, a 1 % deviation in repeatability could be achieved on SFC.

It should be noted that this type of accuracy is only achievable if the test bed as a whole functions correctly and stable. The test therefore also served as good validation for the rest of the test bed.

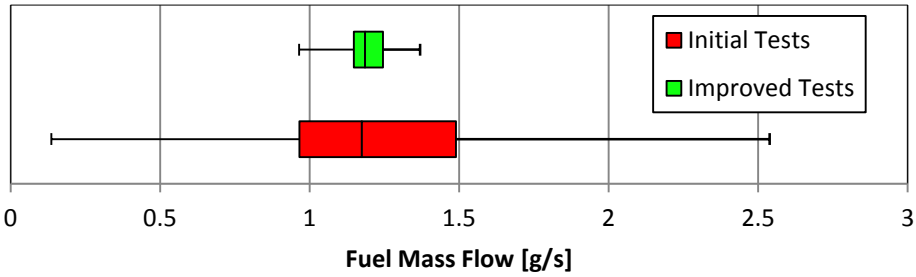

Figure 26: Box and whisker representation of raw fuel flow measurements done both before and after improvements to the measurement system.

As final form of validation for both the fuel mass flow meter and the rest of the test bed, the *Friction Mean Effective Pressure* (FMEP) was calculated using the *Willan's line method*. More on this is discussed in Section 3.3.5. Figure 34 shows that the data points to calculate the FMEP were found to be very linear with R^2 values very close to 1. This is an indication that the fuel consumption data, dynamometer control and calibration and the rest of the test bed as a whole was acceptable.

3.1.4. Inlet Air Temperature Control

For accurate fuel-to-fuel comparative testing it is important that the inlet air temperature be controlled. Although ECE correction factors in the test cell control software does compensate for the drift in ambient conditions when calculating the corrected torque and power, a drift in inlet air temperature would still affect the charge air temperature. A change in charge air temperature would result in unstable exhaust emissions as already discussed in Section 2.

As part of his final year project, Van Zyl built an air conditioning unit for use in the BTF. The conditioning unit is equipped with two automotive type radiators to cool down the incoming air to below the required setpoint by circulating chilled water through them. This also functions to dehumidify the air. The cooled air then passes through a feedback controlled heater bank which heats the air to the required temperature. Air is forced through the system by means of a centrifugal fan (Van Zyl, 2010).

A bypass valve is fitted in parallel to the radiators. By changing the setting on the bypass valve, the amount of cooling over the radiators can be managed. The valve

is set so as to allow adequate cooling of the ambient air, without overstraining the heating elements to get the supply air back to the setpoint temperature.

As part of the validation tests to check the controllability of the heating bank, a step change to the air temperature fed to the heating bank was induced. This was done by allowing the system to settle at a pre-set temperature with a set chilled water bypass setting and then suddenly altering the flow through the bypass valve. Figure 27 shows how the bypass valve was closed at 150 s. The temperature drops initially, but then climbs back to the set temperature within 50 s and then stays within 1 °C of the setpoint.

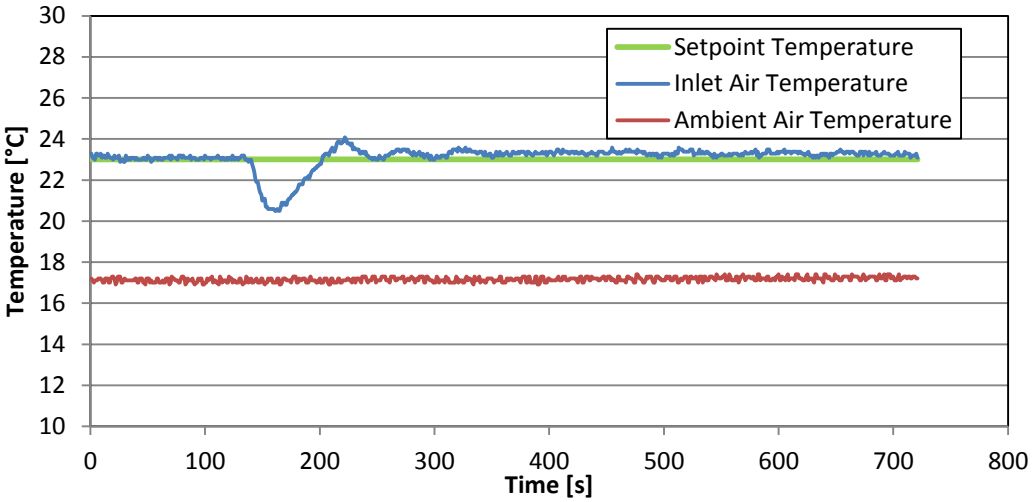

Figure 27: Air conditioning unit heater control.

3.2. Emissions Measurement

Emissions measurement is a key component in analysing the performance of a fuel in an engine. The results of good emission measurements give crucial insight into the combustion of the fuel in the engine and without it, complete understanding of the performance of the fuel is impossible.

3.2.1. Signal Emissions Equipment

Signal analysers were used to measure CO_2 and O_2. Sampling points were installed both before and after the catalytic converter to aid future investigations as seen in Figure 28. For the current project, only emissions before the catalytic converter were analysed.

The analyser system has a heated line that runs from the sampling point, through a pre-filter cabinet, and again via heated line to the analyser cabinet. The heated lines are to prevent any condensate formation and keep the sampled gas at 190 °C (Signal Group Ltd, 2009). To protect the expensive filters in the pre-filter cabinet from congesting too quickly, a ceramic wool filter was installed between the sampling point and the pre-filter.

The analysers were allowed to heat up each morning before zero-span checks were performed before each test in the afternoon. This is to allow the electronics to heat up and attain stable operating conditions.

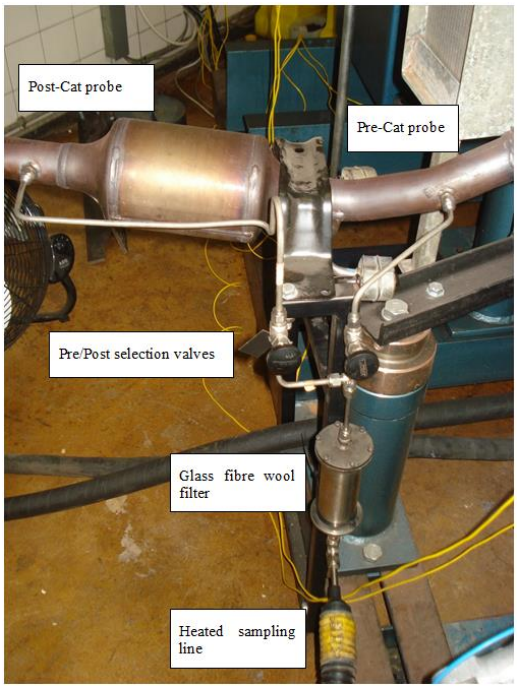

Figure 28: Signal emissions analysers sampling probe layout.

A zero-span check was performed both before and after every fuel test for the CO_2 and O_2 analysers. For the zero checks pure nitrogen gas was used and for the span checks a cocktail gas with known properties of 14.4 % CO_2. Additional information is attache in Appendix D. The gas was supplied by Air Products. Both the CO_2 and O_2 sensors were very stable and repeatable during these checks.

3.2.2. Dräger Emissions Equipment MSI-150 Euro-E

The Dräger MSI-150 Euro E equipment is a multiple channel instrument designed for emissions measurements on diesel engines. The instrument can provide measurements for CO, NO, NO_2 and a combined measurement for NO_x (Dräger, n.d.).

A probe for the instrument was fitted before the catalytic converter (CAT). To protect the instrument against moisture and particulates, two filters were placed in series in the measurement line. This caught any excessive particulate matter that would quickly contaminate the built-in filter in the Dräger instrument and also allowed the measured sample gas to cool down. This was especially necessary as the instrument is designed to take tailpipe emissions where exhaust gas temperatures would be far less than those measured just before the catalytic converter. The cooling down of the sampled gas causes the vapour to condense in these filters and prevents damage to the instrument function. The condensate

could however have an effect on NO_x measurement. For this reason the filters were placed upside down on clean paper to dry overnight. A third filter was also used to exchange with the finest filter in the line after every test. This further prevented any condensate from forming in the line.

The Dräger MSI 150 Euro E has a built-in zero calibration function. The instrument should be exposed to fresh air while this functionality is being executed. The zero calibration was performed both before and checked after every fuel test.

The equipment has a high accuracy level and was calibrated by Dräger South Africa before the start of the tests. The technical specification of the equipment is included in Appendix D.

3.2.3. AVL 415 Smoke Meter

An AVL 415 smoke meter was used for analysis of the soot content in the exhaust gas of the engine.The AVL 415 smoke meter works on the principle of sucking a quantity of exhaust gas through a filter paper. Blackening of the filter paper, as a result of the soot deposit, is measured through a reflectometer. This formulates an indication of the soot content of the exhaust gas (AVL, 2005).

A probe was designed to fit into the exhaust pipe of the engine after the catalytic converter. It was fitted in a straight section of pipe so as to sample from the stable flow. The probe tip was designed to avoid forcefull soot entry by the flow of the exhaust and to prevent soot buildup between sampling. Every sample would therefore only contain the soot sucked in during that sampling time. To prevent soot buildup in the sampling line, the AVL 415 purges the line both pre- and post-sampling.

Tests done at stable operating conditions showed the smoke meter to be very repeatable. The probe design is attached in Appendix D.

3.3. Pressure Indicating

During his work on the diesel engine test cell, Kotzé developed a cost-effective in-cylinder pressure indicating system for the 1.9 L TDI ATD engine. He was successful in capturing pressure traces and to formulate heat release from these traces. However, he suggested that the system be modified to further improve its accuracy and reduce noise in the signal (Kotzé, 2010).

3.3.1. Optrand PSIglow-A Pressure Transducer

The pressure transducer used for the pressure indicating system is a glow plug type transducer manufactured by Optrand Incorporated. The glow plug type transducer allows in-cylinder pressures to be measured without the need to modify the cylinder head. It was specified by Kotzé as a cost-effective solution with comparable performance to more expensive solutions like Kistler or AVL (Kotzé, 2010).

The Optrand PSIglow-A transducer is a fibre-optic pressure transducer. Light is shone through a glass fibre tube at a diaphragm, reflected and then shined through a second tube to a sensor. When pressure from combustion acts on the diaphragm, it distorts, changing the way the light is reflected back to the sensor. The change in light is correlated to pressure change. As with piezo-electric type transducers, the Optrand can only measure changes in pressure and not absolute pressure. The measured pressure therefore has to be *pegged* to a known pressure.

In a study done by Optrand Incorporated, a fibre-optic Optrand transducer was performance tested against a reference, water-cooled, head mounted, piezoelectric pressure transducer from Kistler (Kistler 6121). A combined error for non-linearity, hysteresis and thermal shock of ± 0.5 % of full scale was attainable if the Optrand transducer was thermally optimised (Wlodarczyk et al., 1998).

The static calibration of the pressure transducer is checked by means of a dead weight tester. Certified weights are used to produce pressures in the dead weight tester. The known pressures are applied to the transducer. The respective voltage from the transducer is used to formulate the voltage-to-pressure correlation. The calibration details are included in Appendix C.

The transducer is fitted inside the glow plug hole of the first cylinder. This is important to keep the error due to torsional deflection between the cylinder measured and the mounting point of the shaft encoder to a minimum.

3.3.2. Shaft Encoder

The shaft encoder was the main improvement that Kotzé cited. He opted for a Kübler 3671 single turn absolute encoder for both its cost and the fact that it produced a 0 – 10 V output, which could be easily captured.

The limitation of this encoder is, however, that both crank angle and in-cylinder pressure are recorded on a time based system. This makes synchronizing the pressure trace to a crank angle based trace complicated. This, in turn, complicates heat release calculations and means that averaging over several cycles is not feasible.

Through literature survey on heat release it was found that an incremental type shaft encoder, producing a set amount of pulses per revolution, would be better suited to this application. It was found that a resolution of at least 1440 pulses or 0.25° per pulse would be preferable although 0.1° per pulse had also been used in some studies (Goering, 1998) (Assanis et al., 2000) (Zhang et al., 2006).

With this in mind a specification for the shaft encoder was drawn up:

- Incremental type;
- Preferably 3 600 pulses per revolution on one channel;
- One trigger pulse per revolution on separate channel;
- Speed rating of up to 5 000 rpm;
- Temperature rating of more than 50° C to withstand test cell conditions;

- IP65 or higher rating;
- Vibration resistant;
- Power supply compatible with that of pressure transducer (9 – 18 V);
- RS422 communication;
- Hollow shaft mounting;
- Local supplier;

The Kübler 5020 optical incremental encoder was found to comply with the set of criteria. The encoder supplies 3 600 pulses per revolution and one trigger pulse per revolution of the crankshaft. All pulses are on one channel, thus allowing the encoder to be used as sample timer. Kübler also supplied a mounting flange for the encoder that suited the application.

A mounting system was developed for the encoder that would allow it to be indexed with regard to crank orientation. The mounting system also helped to isolate the encoder from harsh diesel vibrations. The mounting system can be seen in Figure 29. More information is added in Appendix C.

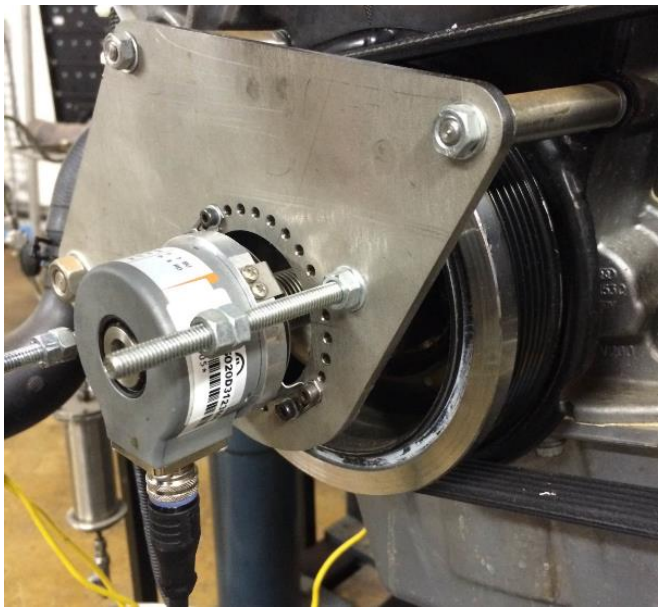

Figure 29: Kübler shaft encoder mounted to crank pulley of the 1.9 L TDI ATD engine.

Shielded cable was used to wire the encoder to the data acquisition system to prevent any interference by other electrical components in the test cell.

The pulse rate of the encoder was validated by using a digital edge counting function in the data acquisition software to count the number of pulses per revolution. By implementing a trigger function, the single turn pulse and the wiring thereof to the data acquisition hardware was also validated.

3.3.3. Data Acquisition Hardware

Finding the correct data acquisitions system (DAQ) was fundamental to the success of the indicating setup.

The first, and possibly biggest challenge, was the rate at which data needed to be captured. Due to the fact that the preferred encoder pulse rate was 3 600 pulses per revolution (0.1° crank angle increments) and the engine could operate to a speed in excess of 4 000 revolutions per minute, the acquisition system needed to be able to handle data at a rate of more than 240 kHz. It would also be preferable if the same indicating setup could be used on other engines with speed ratings closer to 6 000 rpm. This would mean an acquisition rate of 360 kHz. To prevent aliasing, it was decided that a safe buffer rate of acquisition would be at least three times faster than this, thus more than 1 MHz.

Another key feature was the capability to use an external trigger as the sample rate for acquisition. This was necessary to allow the pressure trace to be captured on crank angle base. The system thus also needed to have the capability to process both digital and analogue inputs.

A loose standing unit would also have preference over the PCI slot card type. This was to allow the system to be moved between test cells as needed. The communication system between the DAQ and the PC would however have to be fast enough to process the rate of data capture. Finally the system also had to conform to the budget constraints of the project.

The DAQ system used was the X-series USB-6351 from National Instruments. The unit is capable of sampling at a rate of 1.25MHz which conforms to the speed requirements. It has both analogue and digital inputs and the digital inputs can act as frequency counters or sample time inputs. The sample timing and data capture buffer are done on-board the 6351 chassis, thus reducing the data transfer speed needed via the USB connection.

Another advantage of the National Instruments system is that data acquisition programming is done with the NI LabVIEW graphical user interface (GUI) based software. This vastly optimised the programming time needed to develop a functional data capture routine.

3.3.4. Data Acquisition Software

As stated above, the data capture was controlled through a routine developed in the NI LabVIEW software. This software allows the user to develop a front panel used during the testing procedure. The front panel is linked to a block diagram which contains the programming. Together, this forms what National Instruments call a “virtual instrument” or “VI” as it emulates an actual instrument.

The aim of the VI is to capture the analogue signal from the pressure transducer with sample timing supplied by the digital pulses from the shaft encoder. When

the VI is started, the first trigger pulse received will prompt the start of pressure data monitoring. The pressure trace of combustion is displayed in real time on the front panel display as can be seen in Figure 30. The user can also see the engine speed in real time.

During engine testing the user can prompt the start of data capture. The VI will then record the amount of cycles specified by the user. Once the recording is complete the VI will write the captured data to an Excel spreadsheet. The captured data is only written to Excel after the log has completed, as this process would make the VI slow if done during data capture.

There are two revolutions and thus two trigger pulses during one cycle of the engine. It could therefore happen that two different measurements could be offset by 360°. To aid the user in the phasing of the captured data, a reset trigger resets the data monitor. The user can thus reset the VI until the correct trigger pulse puts the data in phase. It was found that in pressure indicating and heat release it is preferable that the trigger pulse be given just before the start of the compression stroke. This is to prevent capturing thousands of data points before the start of injection and the combustion process.

The LabVIEW software also allows the developer of the VI to build an executable program (.exe) from the VI. The executable can then be run without allowing the end user to alter the block diagram.

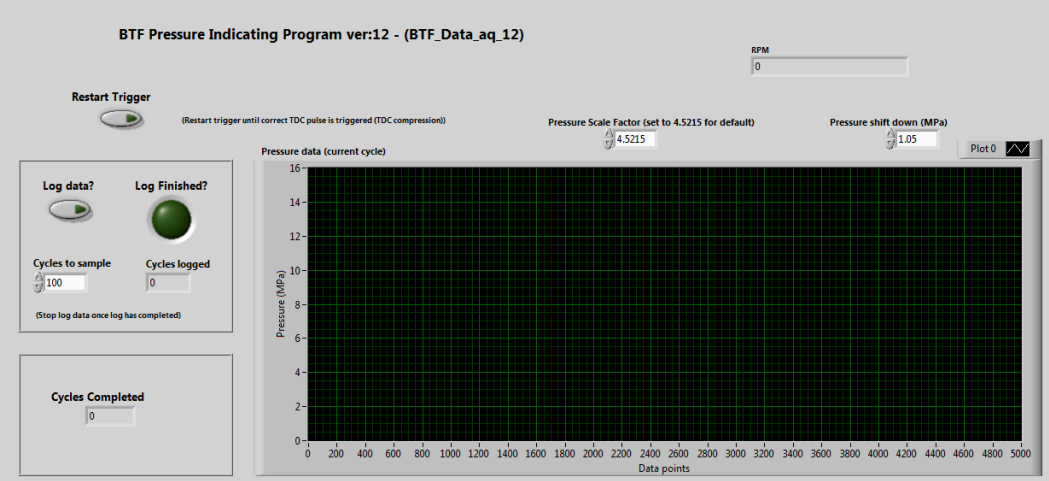

Figure 30: Pressure indicating program front panel.

More on the development of the VI and a detail description of the block diagram can be found in Appendix E.

3.3.5. Validation of Pressure Indicating Setup

Analysis of the pressure data shows the setup to perform very well. Data is easily captured, even with high engine speeds. The use of shielded cables reduces

noise in the pressure signal considerably. This, coupled with the fact that a hundred cycles can be logged and then averaged, produces a very clean pressure trace.

Oscillations were captured in the pressure trace as can be seen in Figure 31. These resemble the oscillations previously discussed and could be a combination of both pressure oscillation (due to transducer placement) and pipe oscillations (due to the indicating channel in the glow plug transducer). These oscillations are constant throughout the 100 cycles that were logged to form the averaged pressure trace. It is also clearly visible in Figure 31 that the oscillation is induced by combustion, with no oscillation visible before the start of fuel injection.

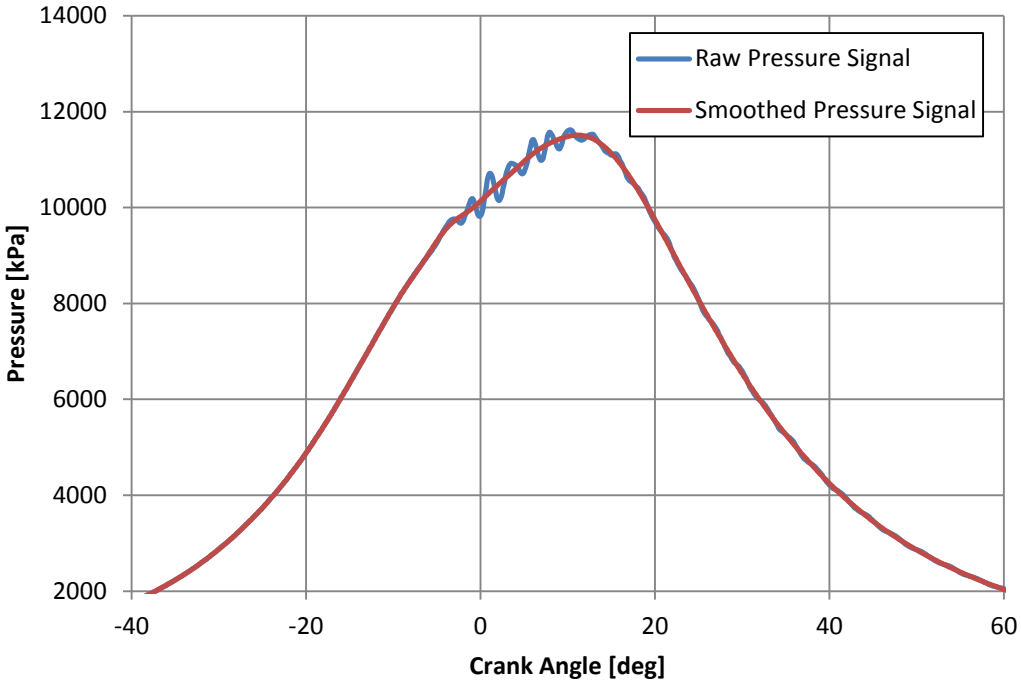

Figure 31: Pressure trace with pipe oscillations and smoothed trace of 1.9L TDI at 3000 rpm and 160 Nm torque.

To minimize the effect of the location of the pressure transducer it should be mounted flush with the roof of the combustion chamber and away from the initial combustion process. This is however not possible as the location and angle of the pressure transducer in this application is pre-determined by the orientation of the glow plug and length of the glow plug transducer. The elimination of the oscillations will require the sourcing of a new pressure transducer and design of an indicated cylinder head.

The solution is to apply filter smoothing to the data during post-processing. A moving average filter proved to be ineffective when a small sample of points are used and also shifts the pressure curve too much when a large number of points are used. Goering's smoothing technique is also ineffective in smoothing out the

oscillations (Goering, 1998). A low pass Butterworth filter proved effective in smoothing the oscillations, without losing the characteristics of the ignition process. The MATLAB® function "filtfilt" is used to implement this filter. The function processes the data in both forward and reverse directions, thus producing a result with zero phase shift. This is especially advantageous when taking into account the importance of phasing in pressure trace analysis. The filtered result can be seen in Figure 31.

Hot motored curves are captured by running the engine at test speeds and then cutting the ignition or by running the hot engine with the injector on cylinder one isolated. The traces are phased by analysing the log p-log V diagram drawn from the motored data as seen in Figure 32. A completely sharp spike is attained between the compression and expansion lines through using the *polytropic exponent method*. The phase angle is adjusted until the gradient of the polytropic exponent changes at TDC. The overturn in polytropic exponent represents the correct TDC (Miao et al., 2013). The phasing for motored curves taken at both 1800 rpm and 3000 rpm were 0.32 crank angle degrees from each other. This deviation is less than the deviation in thermal loss angle found with varying engine speed, load and temperature (Miao et al., 2013). It could therefore be considered to be sufficiently accurate.

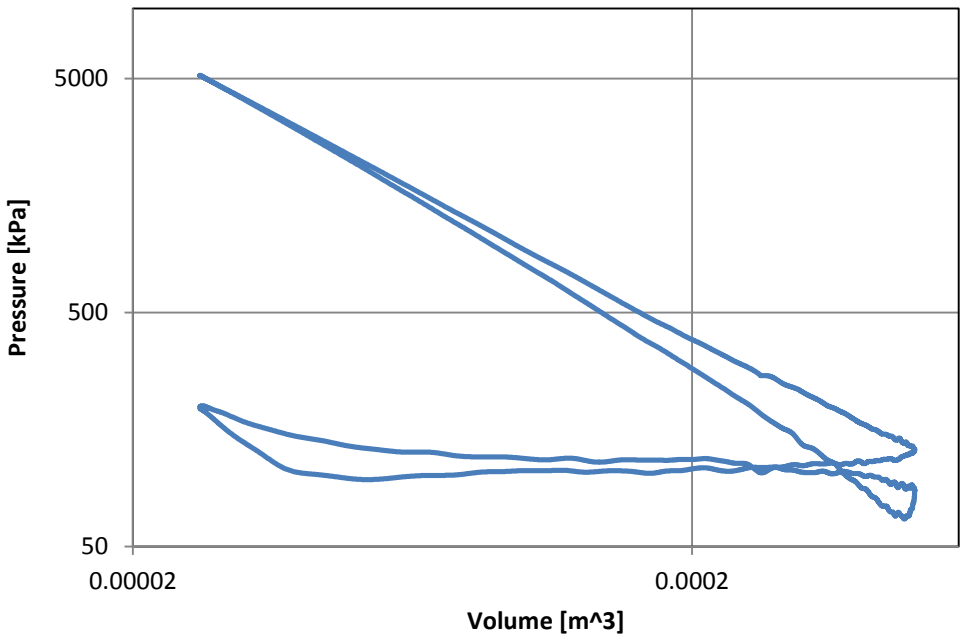

Figure 32: Log p-Log V diagram for motored curve in 1.9 L TDI ATD.

Pressure traces are pegged or referenced using the boost pressure readout from the engine's control unit. The calibration of this readout was checked by means of a calibrated pressure gauge. The readout was found to be linear with minimal

correction required. The calibration is included in Appendix G. The average polytropic exponent during compression for the motored curves at 1 800 rpm and 3 000 rpm where found to be approximately 1.25 and 1.27 respectively. This agrees with values discussed in the literature review. Figure 64 in Appendix J shows the compression and expansion lines associated with a logarithmic plot of a pressure-volume plot during a firing cycle.

In Figure 32 the gas exchange cycle pressure lines cross at the beginning of exhaust and end of intake strokes. This is known as the *bow tie effect* and is due to thermal loading on the transducer, also known as *thermal shock* (Lancaster et al., 1975). This is seen as one of the factors that has the biggest influence on the accuracy of an in-cylinder pressure transducer. Thermal shock changes the response of the pressure transducer through the physical deformation of the transducer and by affecting the sensitivity. Heat propagation into the transducer from the combustion process deforms the metal housing of the transducer to the point where it affects the measurement (Rosseel et al., 1999).

A fibre-optic transducer is especially susceptible to thermal shock as any type of deformation to the transducer body could affect the shape of the pressure diaphragm and therefore the pressure measurement.

Thermal shock can also have an effect on the cycle-to-cycle pressure data. This is known as *Short Term Thermal Drift* (STTD). The susceptibility of a transducer to STTD can be evaluated through Equation [3.1]:

$$|\Delta p_i| = |p(\alpha)_i - p(\alpha)_{i-1}| \qquad [3.1]$$

Where i denotes the number of the cycle and α is a reference crank angle. The reference crank angle can be evaluated at any angle, but the combustion stroke should preferably be avoided as combustion factors like oscillations can have a bigger effect than thermal drift (Rosseel et al., 1999).

The mean values for STTD ($|\Delta p_i|$) of the Optrand transducer are evaluated with both unfiltered and filtered cycle data and can be seen in Table 3. From the table it is possible to see that the STTD value is much higher during combustion. The effectiveness of the filter is also visible. The values for the filtered data are comparable to that found in literature for the same type of sensor but also to water cooled sensors (Rosseel et al., 1999).

Table 3: Mean STTD values ($|\Delta p_i|$) for Optrand PSIglowA pressure transducer in bar.

	Compression	Combustion	Exhaust	Intake
Unfiltered	0.1180	0.1549	0.1133	0.1269
Filtered	0.0438	0.1060	0.0317	0.0310

Figure 33 shows the distribution of STTD values for filtered data compared to the mean value and standard deviation. This shows that although the influence of

thermal shock is clearly visible in the bow tie effect during the gas exchange process, the effect is constant from cycle to cycle when a proper filter is applied.

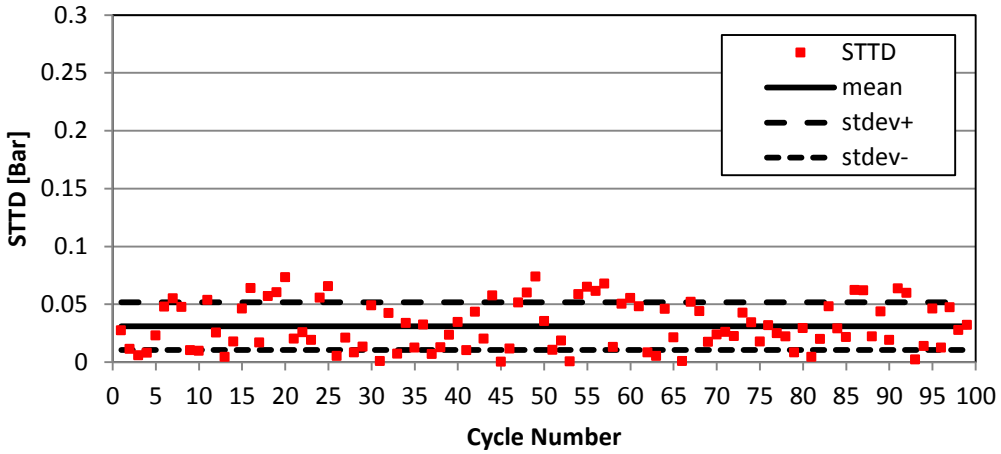

Figure 33: STTD values for filtered Optrand transducer data during intake stroke.

The final method of validating the pressure trace is by comparing the *Mean Effective Pressures* (MEP) obtained from both the indicating and torque measurement instruments. Equations [2.5] to [2.8] in Section 2.3.1 are used to evaluate both IMEP and BMEP.

There are multiple methods to calculate the FMEP but, for this study the *Willan's line method* is found to be the most practical. Fuel consumption versus BMEP or power output is plotted for the engine running at a constant speed and different load points as shown in Figure 34. A linear fit line is then extended to the point where it intersects the horizontal axis. This point represents the theoretical BMEP or power when no fuel is used (Heywood, 1988) (Kumar et al., 2013). It differs with engine speed as a result of differing friction dynamics. A good linear fit can be obtained for low load test conditions.

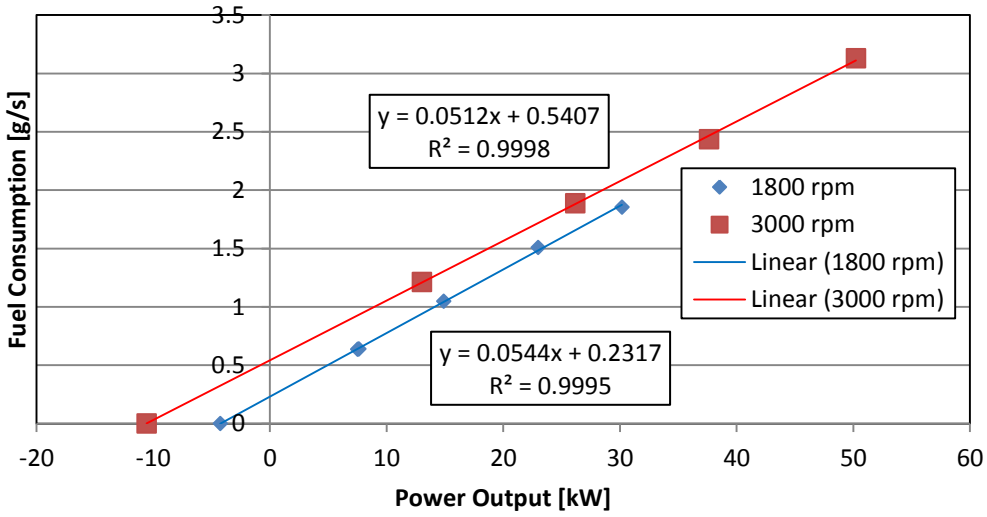

Figure 34: Willan's lines for the 1.9 L TDI ATD.

Table 4: IMEP comparison for 2 indicated points at approximately 160 Nm torque.

Calculation:		$IMEP = BMEP + FMEP$		$IMEP = \frac{W_{i,n}}{V_d}$	
Measuring equipment:		• Dynamometer • AVL 730		• Optrand PSIglow-A • Kübler shaft encoder	
N	**BMEP**	**Willan's FMEP**	**IMEP**	**IMEP**	**%Deviation**
1800 rpm	1061 kPa	150 kPa	1211 kPa	1176 kPa	2.9 %
3000 rpm	1060 kPa	223 kPa	1283 kPa	1231 kPa	4.0 %

Table 4 shows that there is an acceptable correlation between the two methods for the two test speeds. To obtain more accurate IMEP measurements, a water cooled pressure transducer should be used. A study by Wlodarczyk, the founder of Optrand Inc. showed the transducers to have a 1.5 % variance when compared to water cooled piezoelectric sensors (Wlodarczyk, 2012).

3.4. Instantaneous Heat Release Program

The heat release program for this study is developed in Excel. It is based on the program by C. Goering (1998). The program is therefore completely post processed. An example on the use of the program is included in Appendix H.

Pressure pegging and phasing is also done in the heat release program. The pressure at IBDC is pegged to the average manifold pressure. The instantaneous piston displacement, cylinder wall area and cylinder volume is calculated from the incremental crank angle and the engine's physical dimensions.

Fuel flow data from the AVL 730 mass balance is entered into the program and converted to kilogram per stroke. Mass air flow, EGR percentage and intake manifold pressure is collected from the ECU variables. The corrections for mass air flow and intake manifold pressure is also done in the program. The mass air flow sensor was correlated against a calibrated Meriam air flow sensor and the values adjusted accordingly. The correlation is included in Appendix G. The mass of cylinder charge is then calculated using these parameters. The air mass is adjusted for % EGR flow.

Various heat transfer correlations were examined. The correlation developed by Hohenberg was finally selected as it was specifically developed for DI diesel engins. Cylinder wall temperature is taken as the average coolant temperature (Callahan et al., 1985).

Analysis of motored curves serves as a test to confirm that the heat release program is functioning correctly. The motored curve shows no heat release during both compression and expansion cycles. The noise usually associated with heat release calculations can be seen at the beginning of the compression stroke and end of expansion stroke in Figure 35.

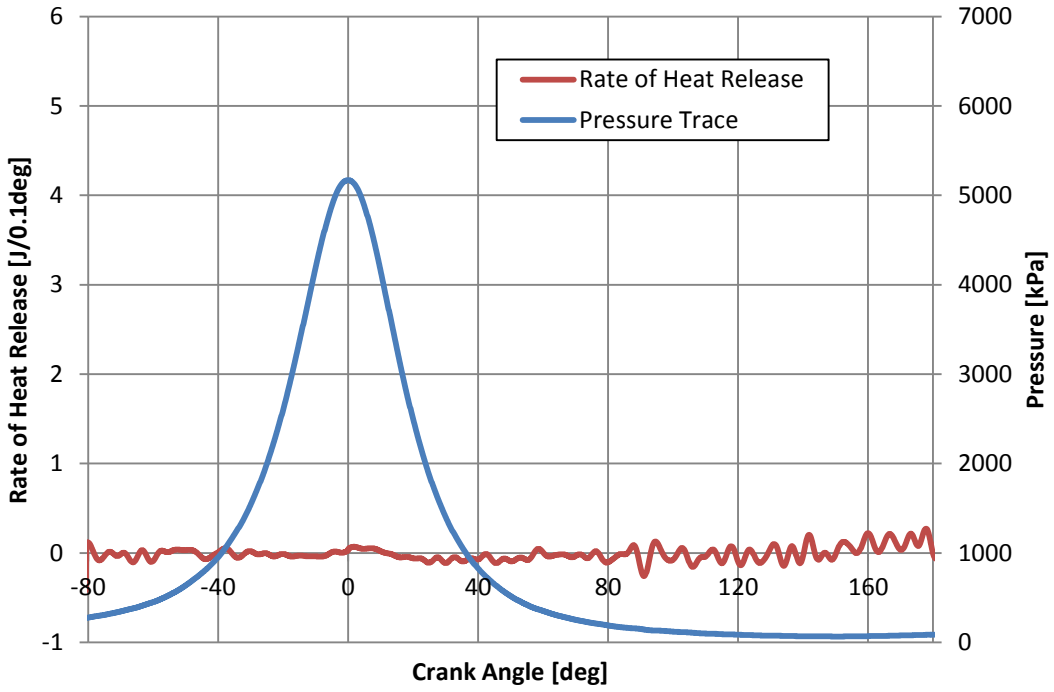

Figure 35: Heat release and pressure data of motored curve.

3.5. Test Engine

The engine used in this test setup is a 1.9 L TDI ATD, 4 cylinder, direct injection diesel powered unit manufactured by Volkswagen Group AG. This is a passenger vehicle engine used in various platforms, but most noticeably in South Africa in the Volkswagen Polo.

Table 5: Test engine specifications (Volkswagen, 1998).

1.9L TDI ATD Engine	
Physical parameters	
Cylinders	4 in line
Valves	2 per cylinder
Swept volume	1896 cc
Bore	79.5 mm
Stroke	95.5 mm
Compression ratio	19/1 ± 0.2 %
Performance	
Rated power	74 kW
Rated torque	240 Nm
Technologies	
Direct injection	Bosch unit injector
Turbo charged	Garret GT1749V variable vane
Exhaust gas emissions reduction	EGR and oxidation catalyst
ECU	Bosch EDC 15

The ATD PD engine was developed by taking a 1.9 L TDI engine with distribution pump fuel injection and changing the cylinder head to accommodate pump unit injection. Figure 36 shows a schematic of the unit injector used. Additional cam lobes where added to the single overhead camshaft to drive the pistons of the unit injectors. Two fuel galleries run through the head to supply fuel to the unit injectors and return the excess fuel back to the fuel tank. An excess amount of fuel is supplied to the unit injectors for cooling purposes.

Pressure in the unit injector is established through a piston driven by a roller-type rocker arm of the cam lobe. The pressure is managed through a solenoid activated bleed-off valve that returns fuel back into the supply/return fuel system. When injection is required the solenoid closes this valve, causing pressure to build up inside the injector. At 180 bar the pressure force of the fuel overcomes the injector spring and forces the needle to lift. Pre-injection then commences. The amount of fuel injected during this cycle is controlled by a fuel filled hydraulic damper. The injection is stopped when the pressure in the fuel causes the retracting piston to lift off its seat. The volume in the high pressure chamber is increased, causing pressure to drop and the injection needle to close.

The movement of the retracting piston has now pre-loaded the injector spring. The pressure needed to lift the needle is therefore increased. Pressure in the high pressure chamber will continue to rise as the piston travels downward. At approximately 300 bar the needle is again forced from its seat and the main injection commences. During the injection the pressure will continue to rise as the amount of fuel that is able to pass the needle is less than the decrease in volume of the high pressure chamber. The pressure peaks at 2 050 bar. The main injection concludes when the ECU stops activating the solenoid valve. Pressure can then escape into the fuel supply/return lines and the injector needle and retracting piston will return to their seats. Only after this action does the pump piston stop compressing fuel and retract.

The ability to attain high injection pressures has a favourable effect on combustion as fuel is better atomized during injection. The accurate control of injection timing and pre-injection also allows for reduction of combustion noise (Volkswagen, 1998).

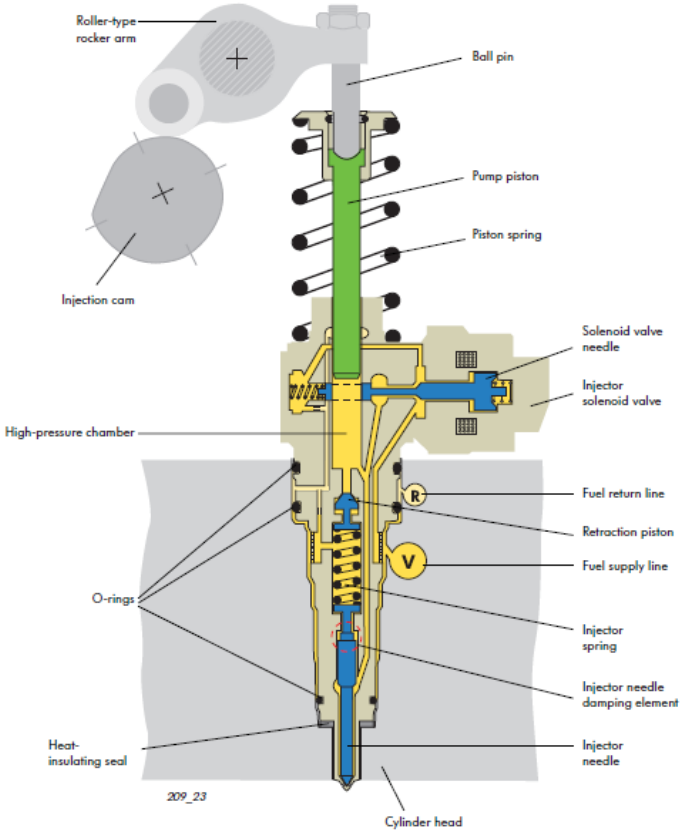

Figure 36: Schematic of pump unit injector fitted to 1.9L TDI ATD PD engine (Volkswagen, 1998).

4. FUELS PERFORMANCE TESTING

4.1. Test Fuels

In South Africa older engine and fuel technology still form the bulk of the country's vehicle fleet. Diesel with a sulphur content of 500 ppm is still readily available across the country and, with its favourable cost compared to 50ppm level, is still the most widely used.

It was therefore decided to test blends of 500 ppm pump diesel with varying percentages of ethanol content, starting at 5 % and leading up to 15 %. Tests were also done on 50 ppm pump diesel from the same manufacturer to gauge the performance of the 500 ppm diesel to what could be considered a more modern fuel.

All fuel blending was done manually and all percentages represent volume percentage and not weight percentage.

Anhydrous ethanol was used and no mixing additives were added to the mixture to prevent phase separation. Blend percentages of up to 15 % ethanol were expected to be soluble as discussed in Section 2.3. Three blends, 5 %, 10 % and 15 % ethanol were tested. These were designated as:

- D(500)E5 - 500 ppm diesel with 5 volume % ethanol
- D(500)E10 - 500 ppm diesel with 10 volume % ethanol
- D(500)E15 - 500 ppm diesel with 15 volume % ethanol

Two blend fuels that used biodiesel as emulsifier were also tested. Initially a blend of 500 ppm sulphur content pump diesel, 20 % biodiesel and 15 % ethanol was tested. During flushing procedures it was noticed that under the heat and pressure of the injection system, the blended fuels reacted and formed a black residue. This could have been from impurities in the biodiesel or detergency of the blend and has to be investigated further. Blends of decreased percentage biodiesel showed this effect to a lesser extent. It was therefore decided to investigate the effect of adding 10 % biodiesel to a D(500)E15 mixture. This mixture was designated E15(500)B10.

In addition to the ethanol blends, B20 (20 % biodiesel by volume) blends were also tested to determine the effect of biodiesel alone. B20 was chosen as it is currently a popular blend ratio tested and used internationally. The biodiesel feedstock was used sunflower oil.

4.2. Test Procedure

The fuel comparison tests were initiated and finished with full load performance curves using the same fuel to bracket the engine performance over the test period. The decision was taken not to perform full load performance curves on each test fuel, as full load conditions are less frequently achieved and therefore less representative of normal driving conditions.

An eight point partial load test was chosen as a better comparison method. These tests consist of four BMEP points at 1 800 rpm and 3 000 rpm respectively. The engine speeds were chosen to be representative of the range of usual driving speeds of a vehicle. The 8 points, as shown in Figure 37, cover an area that represents typical load conditions of the engine during urban and extra-urban driving cycles. The maximum torque points were selected at 160 Nm, which is low enough to still be attainable, even if the test fuel reduced the performance of the engine significantly. The rest of the points were equally spaced at 40 Nm intervals.

In addition to the 8 test points, 4 of these test points were also repeated for pressure indicating measurements. Partial load bracket tests were also done using 500 ppm diesel to ensure repeatability of the test setup at partial load. The tests done before and directly after the blended fuel tests showed good repeatability.

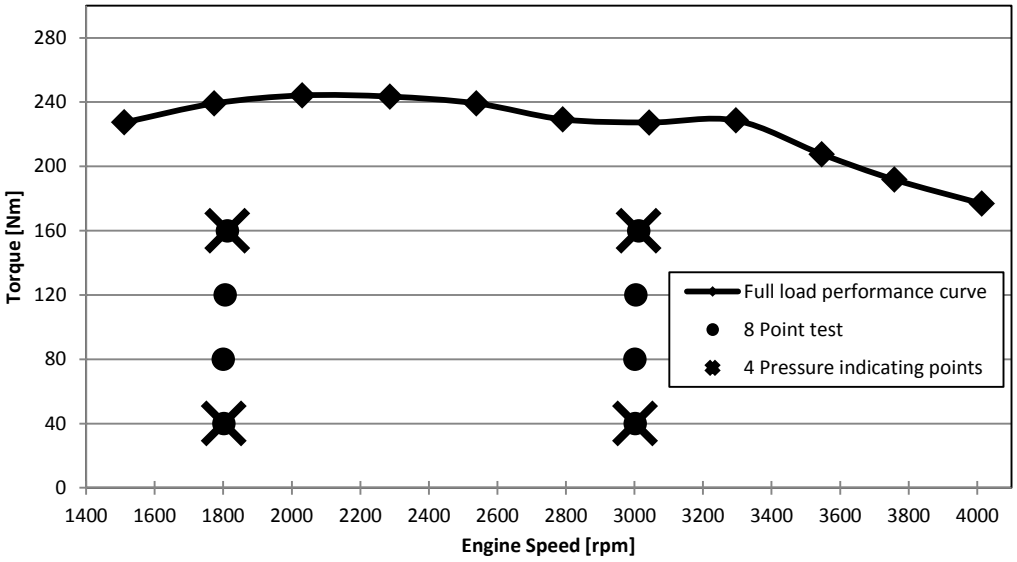

Figure 37: Selected test points for fuel to fuel comparisons.

The functionality of the engine was kept standard as far as possible. Both the EGR and the actuation of the VGT were left to function as normal. The ECU of the engine was a production ECU supplied by the manufacturer. The error codes present on the ECU when operational would suggest that this ECU is running standard production software and not test bench specific software. All combustion controlling functionality should therefore operate normally. During testing this was confirmed by monitoring ECU variables, like EGR percentage. The functionalities and strategies active in the ECU are however still a black box and closely guarded by the manufacturer. Testing is, however, aimed at analysing the performance of a fuel in such an engine with modern control. Leaving all functionality to operate as normal is therefore in line with the aim of the testing.

The dynamometer calibration was done before testing commenced. Additional calibration checks were performed daily. Calibration of the dynamometer was only done once the dynamometer had run and warmed up.

The calibration of the exhaust emissions test equipment was also checked daily. Zero and Span gasses were used for the Signal equipment. The Dräger has a built in calibrating function which was performed as per manufacturer's specifications.

The calibration of thermocouples and channels were checked using boiling and ice water.

The engine tests were conducted by manually controlling the speed and torque setpoints of the engine. Some parameters had to be recorded by hand as automatic electronic capture was not possible. It was therefore more practical to manually set each test point once all data had been captured, other than run an automated test on engine test automation software (ETA). A test sheet was developed to provide space to record certain data and to serve as checklist at each test point. The sheet is attached in Appendix F.

At start-up on test days the engine was warmed up on pump fuel. Batches of test fuel were only mixed immediately before testing. The pump fuel was drained and the fuel system flushed with test fuel. The engine was then run for a minimum of 5 minutes at load on the test fuel to ensure that all remnants of warm up fuel had been removed or consumed.

At the conclusion of each day of testing, all test logs were digitised to ensure that all testing had been done, all data was present and also that all test data had been backed up.

4.3. Test Fuel Performance

4.3.1 External Observation

The test engine started and idled normally on D(500)E5 and D(500)E10. Start performance was however poor on D(500)E15. Audible misfire was also present under idle conditions. Under heat soak conditions starting was very poor.

These performance issues can be attributed to the formation of ethanol vapour in the fuel system under hot conditions. This vapour will negatively affect fuel pressure and delivery. Under loaded conditions the effects are less evident. The large volume of supply fuel coupled with the reduction in supply rail temperatures resists the formation of vapour. The fuel in the supply rail has less residence time in the rail before it gets used and therefore has less time to increase in temperature.

The engine also had no problem running and starting on the B20 blends. No differences could be distinguished, both at idle and load.

The final test fuel, E15(500)B10 developed a slight misfire and the engine had difficulty starting after the engine reached operating temperature. The residue formation in the fuel persisted and it was therefore decided not to include further results from this fuel until the origin could be investigated.

4.3.2. Engine Performance

Specific Fuel Consumption

The 1.9 L TDI ATD engine had interesting responses to the use of test fuels regarding SFC. For pump diesel, SFC was higher for the 500 ppm fuel and this was consistent throughout the repeat tests.

For ethanol-diesel blend fuels the SFC for low load test points decreased with low percentage blends of ethanol when compared to 500 ppm diesel. At high load points very little difference in SFC could be observed, but there is a trend of increased SFC with increase in ethanol percentage. Test results suggest that, even though the energy content of ethanol-diesel blends are lower when compared to diesel, the efficiency with which energy is released is increased resulting in little

to no increases in SFC. This corresponds with findings by Li et al (2004). Hansen (2001) also found that SFC increased, but that specific energy consumption (SEC) in MJ/kWh was the same or slightly better for ethanol-diesel blends.

B20 blends show an increase in SFC at low load test points which is consistent with the lower LHV. At high loads the increase is less than the cycle-to-cycle variation in test shown in Appendix J. This suggests that the addition of biodiesel increases combustion efficiency at these points. This could be as a result of the better air-fuel mixing from improved plume penetration and the higher combustion temperatures improving the vaporisation of the lower volatile biodiesel. The additional oxygen in the fuel would also aid combustion at these loads.

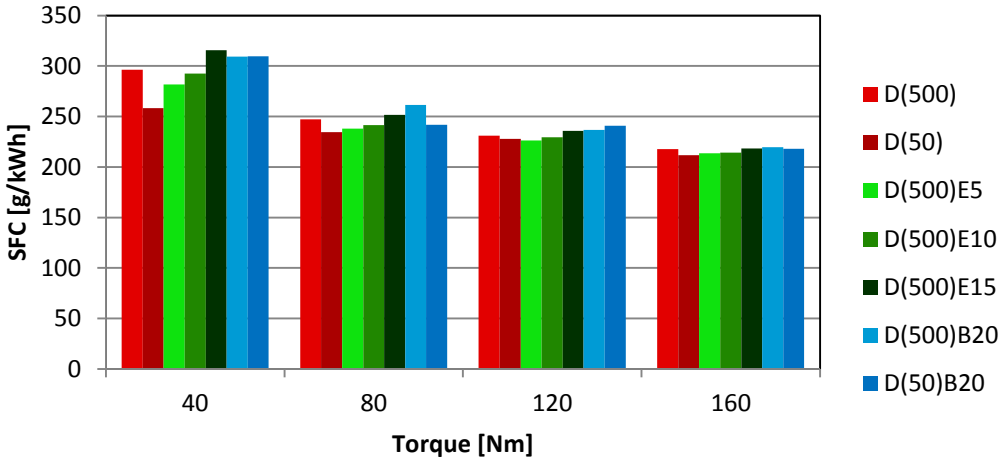

Figure 38: SFC for test fuels at 1 800 rpm.

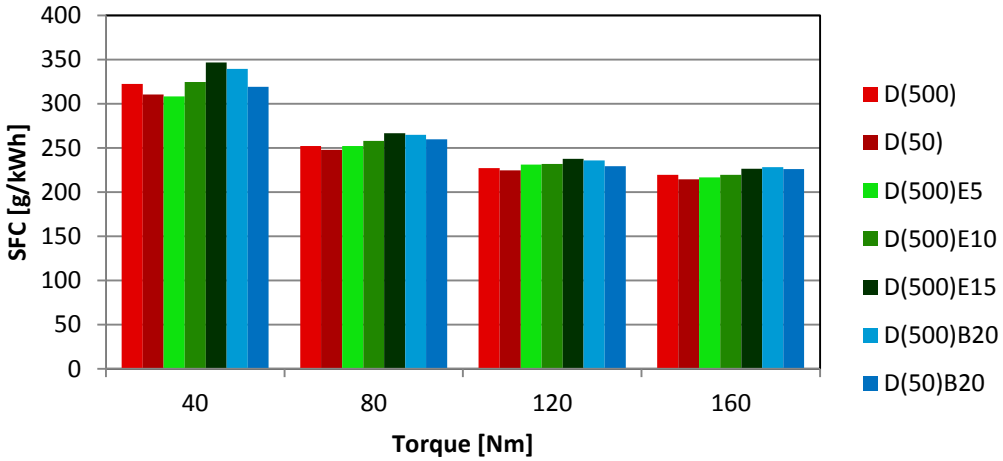

Figure 39: SFC for test fuels at 3 000 rpm.

Exhaust Gas Temperature

On average the exhaust gas temperature decreased with increase in ethanol blend percentage as can be seen in Figure 40 and Figure 41. The effect is also increased at higher load points with a reduction of almost 50 °C at 3 000 rpm and 160 Nm torque. The high volatility of ethanol increases the amount of fuel prepared for combustion during the increased ignition delay period from a lower cetane number. This results in a greater percentage of premixed combustion and therefore an increase in the initial rate of heat release, reducing the combustion duration. This can be seen in Figure 43. The reduction in temperature can also be attributed to the high latent heat of vaporization of ethanol, causing the combustion to be lower in temperature.

B20 blends also show a slight reduction in exhaust gas temperature when compared to pump diesel. A possible explanation for this is the increased oxygen in the biodiesel component which lessens the decrease in oxygen content due to EGR. The improved oxygen concentration increases the rate of heat release, resulting in shorter combustion duration and lower exhaust gas temperatures. The improvement in the combustion rate due to increased oxygen content can be seen in Figure 45 for the load point with lower % EGR. Also, when more fuel is injected in the cylinder, as is the case with B20, more heat is necessary for vaporization, resulting in lower combustion and exhaust gas temperatures.

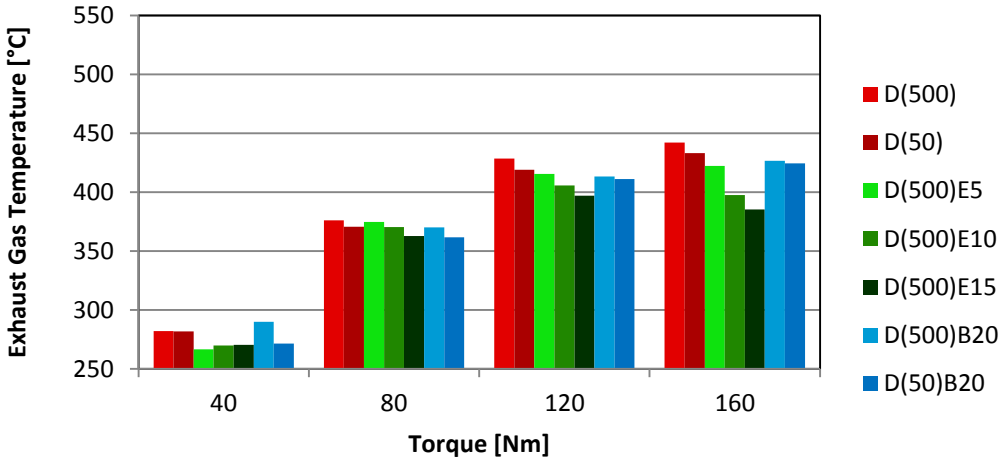

Figure 40: Exhaust gas temperature for 1.9 L TDI ATD at 1 800 rpm.

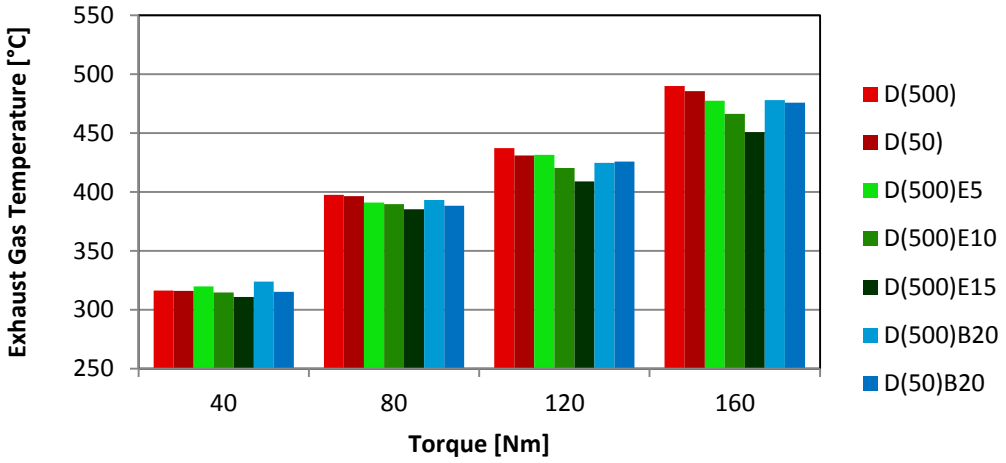

Figure 41: Exhaust gas temperature for 1.9 L TDI ATD at 3 000 rpm.

Peak Pressure and Heat Released

Figure 42 and Figure 43 show low speed, low torque and high speed, high torque graphs of the pressure trace and *rate of heat release* (ROHR) curves for the ethanol-diesel fuel blends.

At lower loads the combustion delay results mainly from the small increase in the ignition delay due to the lower cetane number for ethanol. The small increase in peak rate of heat release in Figure 42 is due to additional fuel prepared during the ignition delay period. At the higher loads the increased temperature and high volatility of ethanol increases the amount of fuel prepared for combustion during the ignition delay period. This results in a greater percentage of premixed combustion and therefore an increase in the initial rate of heat release, reducing the combustion duration. There is also an increase in the peak rate of heat release. This can be seen in Figure 43. The increased oxygen content and improved mixing from smaller droplet size could also result in improved combustion. The peak pressure for E5 is lower than the rest. This was possibly caused by a smaller EGR valve opening than measured. This would cause less mass in the cylinder and therefore lower peak pressure.

The B20 blends, shown in Figure 44 and Figure 45, also exhibit higher rates of heat release. The effect was enhanced at higher engine speed and load as seen in Figure 45. This is a combined result of the improved cetane number and higher viscosity of the biodiesel and agrees with literature. The improved cetane promotes start of combustion while the viscosity enhances fuel penetration for improved air-fuel mixing. This improved air-fuel mixture with increased oxygen content from the biodiesel component also speeds up initial heat release, resulting in higher peak pressures and peak rates of heat release (Nagaraju et al, 2008).

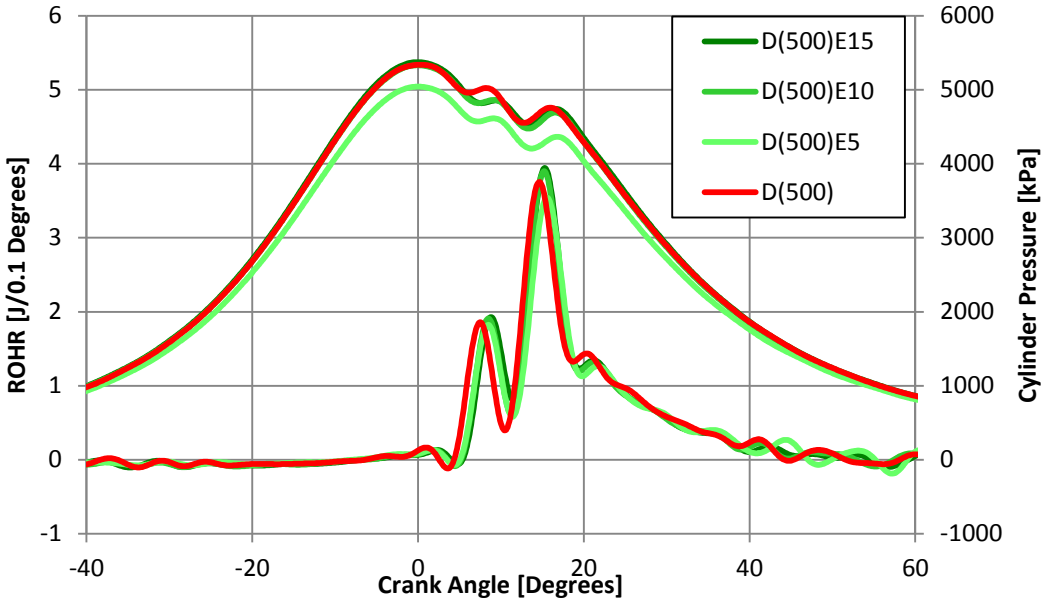

Figure 42: Ethanol-diesel ROHR and pressure trace for 1.9 L TDI ATD engine at 40 Nm torque and 1 800 rpm.

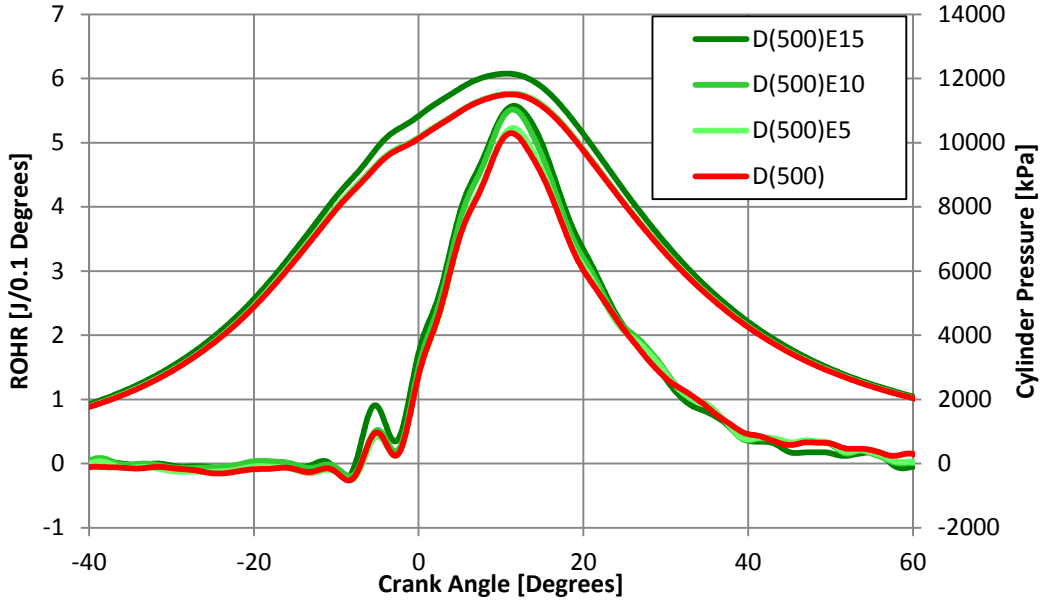

Figure 43: Ethanol-diesel ROHR and pressure trace for 1.9 TDI at 160 Nm and 3 000 rpm.

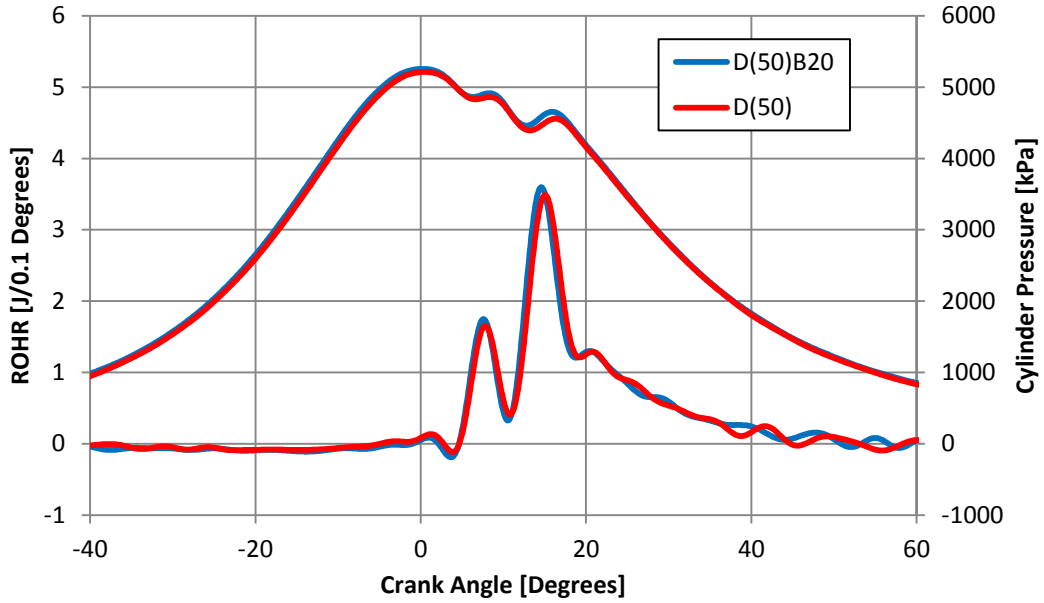

Figure 44: Biodiesel ROHR and pressure trace for 1.9 L TDI ATD engine at 40 Nm torque and 1 800 rpm.

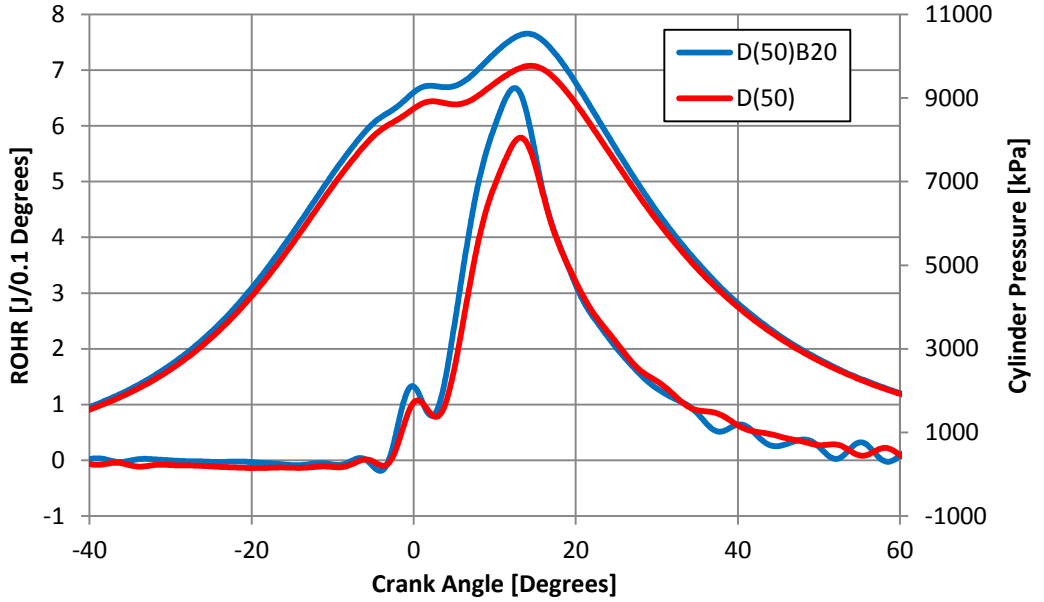

Figure 45: Biodiesel ROHR and pressure trace for 1.9 L TDI ATD engine at 160 Nm torque and 3 000 rpm.

4.3.3 Nitrogen Oxides

Analyses of the NO_x emissions of the ethanol-diesel blends show a minimal difference particularly at low loads. It is clear from both Figure 46 and Figure 47 that the variance in NO_x emissions between ethanol-diesel blends and petroleum diesel at most points is less than the corresponding variance between

50 ppm and 500 ppm petroleum diesel. A slight increase in NO_x can be distinguished at higher loads for both 1 800 rpm and 3 000 rpm. This small difference corresponds with the literature on NO_x emissions for ethanol-diesel blends (Xue et al., 2011).

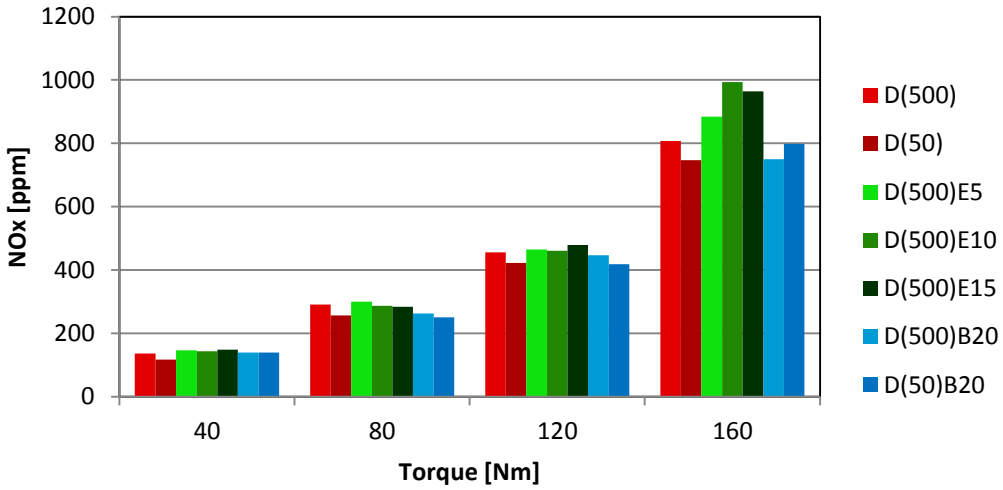

Figure 46: NO_x emissions of test fuels at 1800 rpm.

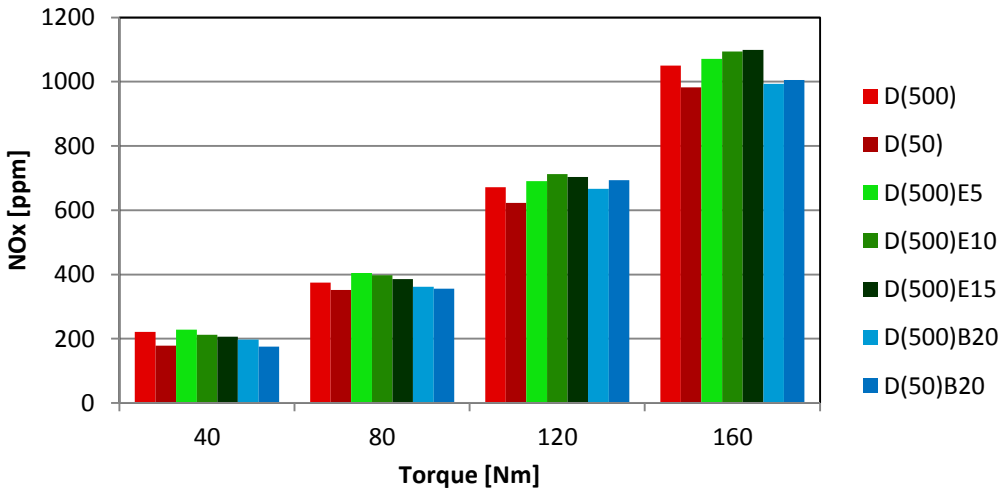

Figure 47: NO_x emissions of test fuels at 3 000 rpm.

The reason for the increase in NO_x emissions at both speeds for the 160 Nm load point becomes apparent when the percentage specified EGR from the ECU for these tests is analysed. It can be seen in both Figure 61 and Figure 62 that the EGR function was switched off by the ECU for the specific fuels that showed a slight increase in NO_x emissions (4.8 % is the default ECU value when no EGR is present). The increase in throttle position to compensate for the slight increase in SFC at this point, coupled with boost pressure, could have caused the ECU to run

in a different map setting. The fact that there is only a slight increase in NO_x with a big difference in EGR could point to the fact that the lowered combustion temperatures, as stated earlier, have a positive effect in limiting NO_x emissions.

The NO_x emissions for B20 blends are similar to those for pump diesel. These small changes agree with the results found in the literature for low blend ratios (Miana, 2014).

4.3.4 Carbon Monoxide

CO emissions, as shown in Figure 48 and Figure 49, were found to have a clear increase with increase in ethanol percentage at the lowest load point tested. This correlates with the work done by Jeong et al. (2009) in that ethanol addition lowers combustion temperature and therefore inhibits complete combustion. A slight reduction is also visible at 160 Nm which would further correlate with literature, but this is too little to accurately determine, given the accuracy of the equipment.

The 1.9 L TDI ATD engine's response to biodiesel blends with regard to CO emissions was again neutral with only very slight improvements visible at the higher load test points and an increase noted at low load high speed point. It should be noted that the CO exhaust emissions for this particular engine is already low. The neutral response therefore correlates with literature on CO emissions (Wang et al., 2011).

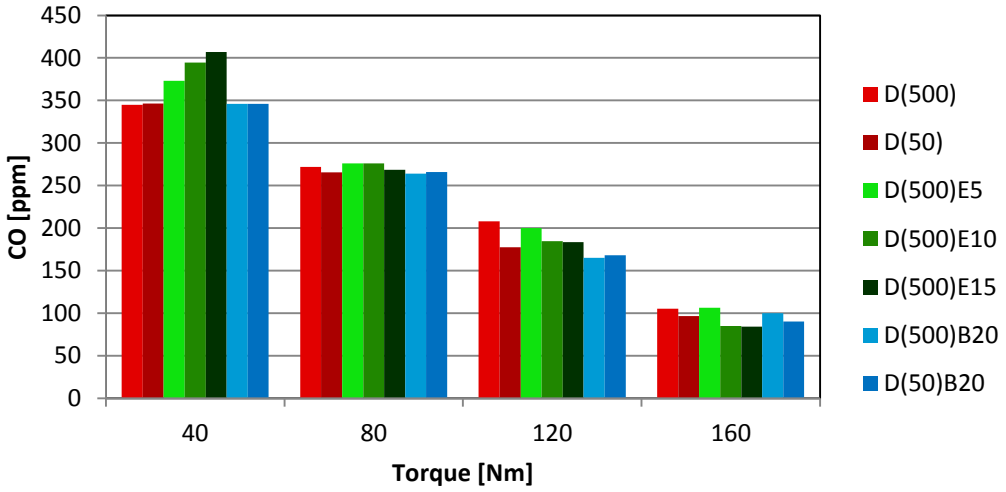

Figure 48: CO emissions of test fuels at 1 800 rpm.

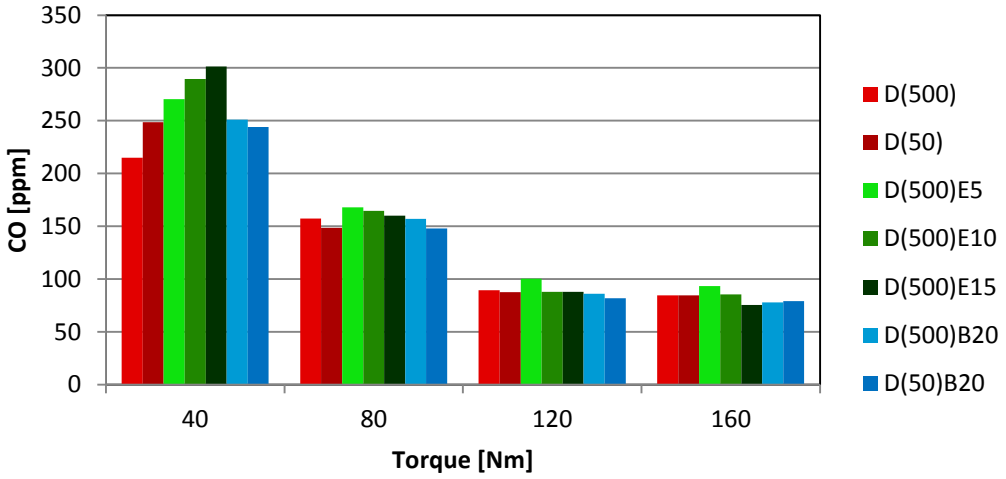

Figure 49: CO emissions of test fuels at 3 000 rpm.

4.3.5 Soot and Particulate Emissions

Ethanol addition to diesel has a favourable effect on soot emission. In Figure 50 and Figure 51 it can clearly be seen that there is a decrease in filter smoke number (FSN) at every load and speed point with the increase in percentage ethanol. This corresponds to the literature on soot emission of ethanol-diesel fuel blends (Song et al., 2004).

The reduction in soot is also visible for the B20 blends with soot reduction mostly correlating with E5 and E10 fuels. The reduction in soot corresponds with literature and confirms that the oxygenated nature of the test fuels is the main contributor to the reduction in soot (Rakopoulos et al., 2006).

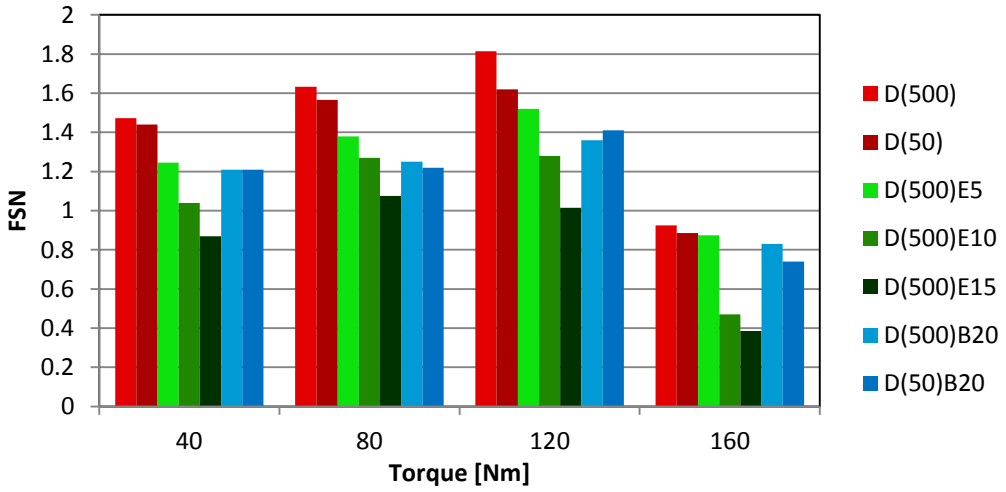

Figure 50: FSN of test fuels at 1 800 rpm.

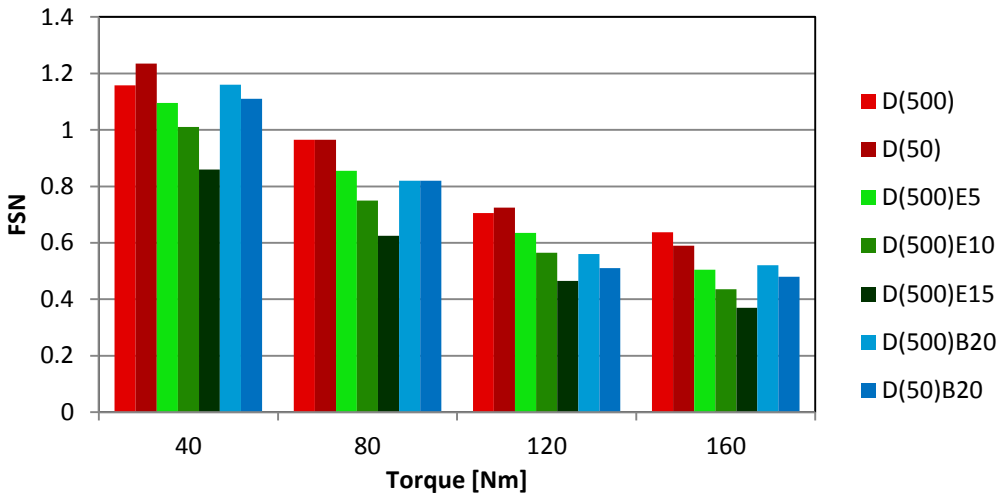

Figure 51: FSN of test fuels at 3 000 rpm.

5. CONCLUSION

The 1.9 L TDI ATD diesel engine test cell was upgraded for improved capability with regard to fuel-to-fuel comparative testing. Air temperature control and fuel temperature control was installed and commissioned to aid repeatability. Coolant temperature control was upgraded, automated and commissioned. Fault finding was done on the AVL fuel mass balance and, with the addition of the fuel conditioning unit, fuel mass flow measurement was improved to good repeatability and accuracy. The driveshaft was upgraded to incorporate a flexible coupling between engine and dynamometer. The exhaust system of the engine was instrumented with probes to allow for emission testing. Finally, a pressure indicating system was developed based on a previously used Optrand PSI-glowA glow plug transducer, a Kübler high resolution shaft encoder and data acquisition software and hardware from National Instruments. Software was developed in-house and the system could successfully capture 100 consecutive engine cycles of 3600 pulses per revolution at 4 000 rpm. Pressure traces were analysed with a spreadsheet based heat release program.

Tests were performed on blends of ethanol and biodiesel with pump diesel. exhaust gas emissions (Soot, CO and NO_x) and engine performance (SFC, exhaust gas temperature and in-cylinder pressure data) were evaluated at 8 part-load set points. Apart from controlled temperatures and instrumentation, the engine setup was kept as close possible to the in-vehicle configuration.

Ethanol-diesel blends showed consistent reduction in soot emission across all the test points. This was accomplished without any significant increase in NO_x emissions. At high load points an increase in NO_x was visible. This was mostly due to EGR deactivation at these set points, but also to the advance in ignition timing at high loads. EGR deactivation occurred as a higher throttle setting was needed to achieve the required set point. This is as a result of the slight decrease

in LHV for ethanol-diesel blends. It is expected that NO_x emission should increase as a result of the additional oxygen availability. This effect seems to be counteracted by a decrease in the mean combustion temperature, visible in exhaust gas temperature, and a varying effect on ignition timing. CO emission is neutral, except at very light loads where the drop in combustion temperature could have a negative effect on complete combustion.

The addition of biodiesel to pump diesel revealed a reduction in soot at every test point. The oxygenated nature of the fuel coupled with better air-fuel mixing seems to aid more complete oxidation of soot. This is again without any significant effect on NO_x. This type of gain in soot emission without the NO_x trade-off is very difficult to attain through other means. CO emission is neutral as is expected with a low CO emission diesel engine. The improvement in CO emissions that could be attained through additional oxygen is also to some extent counteracted by the reduction in combustion temperature, visible in the reduced exhaust temperature. The reduction in combustion temperature could be as a result of increased fuel delivery as seen through the increased SFC. The addition of biodiesel decreases the ignition delay period, as was expected with an improved cetane number. The effect is however far more visible at higher loads and engine speeds.

6. RECOMMENDATIONS

A project is not complete without proper reflection on the final result and the process followed to achieve it. Learning points and especially room for improvement should be noted so as to assist future work on similar projects.

6.1. Test Facility Recommendations and Improvements

Although the facility was able to attain good repeatability, there are some improvements that would improve and also simplify testing:

1. ECU data captured through the VAG-Com software is very handy, but too slow to use as accurate data for heat release purposes. It also does not allow for synchronization with other data. Intake manifold pressure, temperature and MAF should be captured with high speed accurate sensors and synchronized with the in-cylinder pressure data. The multiple open channels and acquisition capability of the current DAQ would allow for this.
2. A fuel pressure sensor in the unit injector would allow for accurate determination of injection timing. Optrand Incorporated manufacture unit injectors with both fuel pressure and in-cylinder pressure transducers (Wlodarczyk et al., 1998). This could also be captured in the current DAQ.
3. The LabView software is very powerful and this project has not even skimmed the surface of what is possible. Using the current VI as basis for further development and incorporating the above instrumentation, the VI could be upgraded to provide realtime pegging of cylinder pressure data, calculation of polytropic exponent, peak pressure and heat release.

4. The current dynamometer configuration does not allow for torque mode control. This would be very advantageous when testing part load points. An investigation into the capability of the current dynamometer controller with regard to pedal control could provide information as to if a new controller is needed or if the current controller has the capability. The current method of actuating the accelerator pedal functions well, but could be improved by building a circuit to mimic pedal feedback. A sacrificial accelerator pedal could provide the info needed to build such a device. By electronically mimicking the pedal, torque mode control could be improved.
5. The current PLC does not have the capability to be expanded. An upgraded version would allow for coolant temperature control, fuel temperature control and monitoring and emissions data to be synchronized into the ETA test environment.
6. Charge air cooling is still dependent on ambient conditions in the test cell. Developing a controlled charge air cooler, capable of maintaining a set charge air temperature will improve repeatability from an engine performance and exhaust emissions point of view.

6.2. Test Procedure Improvement

By improving the test procedure, human error can be eliminated. This would ensure better accuracy of data captured.

1. By implementing the above facility improvements, the test procedure could be automated to run without human intervention. Automated tests would lessen the load on the operator and therefore the chances of errors. Standardized tests could be developed which would allow for the building of a database with which to compare future results.
2. The possibility of testing fuels in the engine with EGR deactivated should be investigated. EGR introduces an unknown in the form of air mass flowing into the cylinder that cannot be accurately measured. It also has more of an effect on some emission results than the fuel would have on its own.
3. Cross-departmental collaboration, especially drawing on the expertise of Process Engineering, could improve areas like test fuel mixing and analysis.

7. REFERENCES

Agarwal, A. K., 2007. Biofuels (alcohols and biodiesel) applications as fuels for internal combustion engines. *Progress in Energy and Combustion Science,* Volume 33, pp. 233-271.

Agarwal, A. K. & Das, L. M., 2001. Biodiesel Development and Characterization for Use as a Fuel in Compression Ignition Engines. *Transactions of the ASME: Journal of Engineering for Gas Turbines and Power,* Volume 123, pp. 440-447.

Agarwal, D. & Agarwal, A. K., 2007. Performance and emissions characteristics of Jatropha oil (preheated and blends) in a direct injection compression ignition engine. *Applied Thermal Engineering,* Volume 27, pp. 2314-2323.

Andersson, Ö., n.d. Diesel Combustion. In: *Handbook of Combustion.* s.l.:s.n.

Annand, W., 1963. Heat transfer in the cylinders of reciprocating internal combustion engines. *Procedings of the Institute of Mechanical Engineers,* 177(36), pp. 973-990.

Ashok, M. P. & Saravanan, C. G., 2007. The performance and emission characteristics of emulsified fuel in a direct injection diesel engine. *Proceedings of the Institution of Mechanical Engineers, Part D: Journal of Automobile Engineering,* Volume 221, pp. 893-900.

Aspiron, J., Chinellato, O. & Guzzello, L., 2013. A fast and accurate physics-based model for the NOx emissions of Diesel engines. *Applied Energy 103,* pp. 221-233.

Assanis, D. N., Filipi, Z. S., Fiveland, S. B. & Syrimis, M., 2000. A Methodology for Cycle-By-Cycle Transient Heat Release Analysis in a Turbocharged Direct Injection Diesel Engine. *SAE 2000-0101185.*

AVL List GmbH, 1987. *Operating Instruction - AVL 730 Dynamic fuel consumption measuring equipment.*. Graz: AVL.

AVL, 2005. *Smoke value measurement with the filter-paper-method.* 2nd ed. Graz: AVL list GmbH.

AVL, 2014. *AVL Particle Counter.* [Online]
Available at: https://www.avl.com/particle-counter
[Accessed August 2014].

AVL, n.d. *Engine Indicating - User Handbook.* s.l.:s.n.

Bueno, A. V., Velásquez, J. A. & Milanez, L. F., 2012. Internal Combustion Engine Indicating Measurements. In: Z. Haq, ed. *Applied Measurement Systems.* s.l.:InTech, pp. 23-44.

Callahan, T. J., Yost, D. M. & Ryan III, T. W., 1985. Acquisition and Interpretation of Diesel Engine Heat Release Data. *SAE, 852068.*

Canakci, M., 2007. Combustion characteristics of a turbocharged DI compression ignition engine fueled with petroleum diesel fuels and biodiesel.. *Bioresource Technology,* Volume 98, pp. 1167-1175.

Çengel, Y. A., 2006. *Heat and Mass Transfer - A Practical Approach.* 3rd ed. New York: McGraw-Hill.

Challen, B. & Baranescu, R., 1984. *Diesel Engine Reference Book.* Second ed. Oxford: Butterworth-Heinemann.

Cole, R. L. et al., 2000. *Effect of Ethanol Fuel Additive on Diesel Emissions,* Illinois: Argonne National Laboratory.

Corro, G. & Ayala, E., 2008. Bioethanol and diesel/bioethanol blends emmissions abatement. *Fuel,* pp. 3537-3542.

Dasari, M. A., Goff, M. J. & Suppes, G. J., 2003. Noncatalytic Alcoholysis Kinetics of Soybean Oil. *Journal of the American Oil Chemists' Society,* 80(2), pp. 189-192.

DieselNet, 2007. *DieselNet Technology Guide - Gas Phase Measurement.* [Online]
Available at: http://www.dieselnet.com/tech/measure_gas.html
[Accessed 30 July 2014].

DieselNet, 2010. *Fuel Regulations - European Union - Automotive Diesel Fuel.* [Online]
Available at:
http://www.dieselnet.com.ez.sun.ac.za/standards/eu/fuel_automotive.php
[Accessed 23 10 2014].

DieselNet, 2012. *Emission Standards - European Union - Heavy-duty Truck and Bus Engines.* [Online]
Available at: http://www.dieselnet.com.ez.sun.ac.za/standards/eu/hd.php
[Accessed 23 10 2014].

DieselNet, 2013. *Emission Standards - European Union - Cars and Light Trucks.* [Online]
Available at: http://www.dieselnet.com/standards/eu/ld.php
[Accessed 23 October 2014].

Dräger, n.d. *Dräger MSI 150 EURO-E Diesel exhaust tester.* [Online].

Ferguson, C. R. & Kirkpatrick, A. T., 2000. *Internal Combustion Engines - Applied Thermoscience.* 2nd ed. New York: John Wiley & Sons Inc..

Finol Parra, C. A., 2008. *Heat Transfer Investigations in a Modern Diesel Engine,* Bath: University of Bath.

Finol, C. A. & Robinson, K., 2006. Thermal modelling of modern engines: a review of empirical correlations to estimate the in-cylinder heat transfer coefficient. *Proceedings of the Institution of Mechanical Engineers, Part D: Journal of Automobile Engineering,* Volume 220, pp. 1765-1781.

Gerdes, K. R. & Suppes, G. J., 2001. Misciblity of Ethanol in Diesel Fuels. *Ind. Eng. Chem. Res.*, pp. 949-956.

Goering, C. E., 1998. Engine Heat Release via Spread Sheet. *Transactions of the ASAE volume 41(5)*, pp. 1249-1253.

Goldemberg, J., 2008. *Environmental and ecological dimensions of biofuels.* Washington, s.n.

Hansen, A. C., Lyne, P. W. L. & Zhang, Q., 2001. Ethanol-diesel blends: A step towards a bio-based fuel for diesel engines. *ASAE: 01-6048*, Volume UILU 2001-7011.

Hansen, A. C., Zhang, Q. & Lyne, P. W., 2005. Ethanol–diesel fuel blends—a review. *Biosource Technology*, Volume 96, pp. 277-285.

Hawley, J. G., Wallace, F. J., Horrocks, R. W. & Bird, G. L., 1999. Variable geometry turbocharging for lower emissions and improved torque characteristics. *Proceedings of the Institution of Mechanical Engineers, Part D: Journal of Automobile Engineering*, Volume 213, pp. 145-159.

He, B.-Q., Shuai, S.-J., Wang, J.-X. & He, H., 2003. The effect of ethanol blended diesel fuels on emissions from a diesel engine. *Atmospheric Environment*, Volume 37, pp. 4965-4971.

Heywood, J. B., 1988. *Internal combustion engine fundamentals.* s.l.:McGraw-Hill Inc..

Hooks, R., 1994. Light-Duty Diesels - an Update on the Emissions Challenge. *Proceedings of the Institution of Mechanical Engineers, Part D: Journal of Automobile Engineering 208*, pp. 289-298.

Horiba , 2014. *Automotive test systems - Mexa 7000.* [Online]
Available at: http://www.horiba.com/automotive-test-systems/products/emission-measurement-systems/analytical-systems/standard-emissions/details/mexa-7000-version-3-930/
[Accessed August 2014].

Horiba, 2014. *Automotive Test Systems - Mexa 1000 SPCS.* [Online]
Available at: http://www.horiba.com/automotive-test-systems/products/emission-measurement-systems/analytical-systems/particulates/details/mexa-1000-spcs-52/
[Accessed August 2014].

Horrocks, R. W., 1994. Light-duty diesels - an update on the emissions challenge. *Proceedings of the Institution of Mechanical Engineers, Part D: Journal of Automobile Engineering 1994 208*, pp. 289-298.

Hountalas, D. T. & Anestis, A., 1998. Effect of Pressure Transducer Position on Measured Cylinder Pressure Diagram of High Speed Diesel Engines. *Energy Conversion and Management*, 39(7), pp. 589-607.

How, H. G., Masjuki, H. H., Kalam, M. A. & Teoh, Y. H., 2014. An investigation of the engine performance, emissions and combustion characteristics of coconut

biodiesel in a high-pressure common-rail diesel engine. *Energy*, Volume 69, pp. 749-759.

Hulwan, D. B. & Joshi, S. V., 2011. Performance, emission and combustion characteristic of a multicylinder DI diesel engine running on diesel–ethanol–biodiesel blends of high ethanol content. *Applied Energy*, Volume 88, p. 5042–5055.

ISO, 2002. *ISO 3046-1:2002.* [Online]
Available at: http://www.iso.org/iso/catalogue_detail.htm?csnumber=28330
[Accessed August 2014].

Jääskeläinen, H., 2006. *Dieselnet Technology Guide - Ethanol-Diesel Blends.* [Online]
Available at: http://www.dieselnet.com/tech/fuel_ediesel.html
[Accessed 26 7 2011].

Jääskeläinen, H., 2007. *DieselNet Technology Guide - What is Diesel Fuel - Fuel Property Testing: Ignition Quality.* [Online]
Available at:
http://www.dieselnet.com.ez.sun.ac.za/tech/fuel_diesel_ignition.php#hf
[Accessed 15 November 2014].

Jääskeläinen, H., 2009. *DieselNet Technology Guide - Biodiesel Standards and Properties.* [Online]
Available at: www.dieselnet.com.ez.sun.ac.za/tech/fuel_biodiesel_std
[Accessed 11 2013].

Jääskeläinen, H., 2009. *DieselNet Technology Guide - Low Temperature Operability of Biodiesel.* [Online]
Available at: http://www.dieselnet.com/tech/fuel_biodiesel_lowtemp.html
[Accessed 11 2013].

Jeong, K., Park, S. H. & Lee, C. S., 2011. *Injection spray and emisssions characteristics in a diesel engine using diesel-bioethanol blended fuels.* Estoril, Portugal, ILASS.

Kang, J., Bae, C. & Lee, K. O., 2003. Initial development of non-evaporating diesel sprays in common-rail injection systems.. *International Journal of Engine Research,* 4(4), pp. 283-298.

Khair, M. K. & Jääskeläinen, H., 2011. *DieselNet Technology Guide - Diesel Engine Fundamentals.* [Online]
Available at: www.dieselnet.com.ez.sun.ac.za/tech/diesel_fund.php
[Accessed 11 2013].

Knothe, G., Van Gerpen, J. & Krahl, J., 2005. *The Biodiesel Handbook.* Champaign, Illinois: AOCS Press.

Kotzé, J., 2010. *MscEng Thesis: A Comparitive Study on the Performance of Biodiesel in a Mordern 1.9 Litre Turbo Diesel Engine,* Stellenbosch: s.n.

Kumar, M., Singh, B. & Jain, V., 2013. Friction Analysis and Reduction in a Single Cylinder Four Stroke Diesel Engine. *International Journal of Emerging Research in Management &Technology ISSN: 2278-9359,* 2(10).

Kwanchareon, P., Luengnaruemitchai, A. & Jai-In, S., 2007. Solubility of a diesel–biodiesel–ethanol blend, its fuel properties, and its emission characteristics from diesel engine. *Fuel,* Volume 86, pp. 1053-1061.

Ladommatos, N., Abdelhalim, S. & Zhao, H., 2000. The effects of exhaust gas recirculation on diesel combustion and emissions.. *International Journal of Engine Research Vol. 1 no. 1,* pp. 107-126.

Lancaster, D. R., Krieger, R. B. & Lienesch, J. H., 1975. Measurement and Analysis of Engine Pressure Data. *SAE Technical Paper 750026.*

Lapuerta, M., Armas, O. & Garcia-Contreras, R., 2007. Stability of diesel-bioethanol blend for use in diesel engines. *Fuel,* Volume 86, pp. 1351-1357.

Lapuerta, M., Armas, O. & Herreros, J. M., 2008. Emissions from a diesel-bioethanol blend in an automotive diesel engine. *Fuel,* pp. 25-31.

Lapuerta, M., Armas, O. & Rodríguez-Fernández, J., 2008. Effect of biodiesel fuels on diesel engine emissions. *Progress in Energy and Combustion Science,* Volume 34, p. 198–223.

Lawton, B., 1987. Effect of Compression and Expansion on Instantaneous Heat Transfer in Reciprocating Internal Combustion Engines. *Proceedings of the Institution of Mechanical Engineers,* 201(A3), pp. 175-186.

Li, D.-g.et al., 2005. Physico-chemical properties of ethanol-diesel blend fuel and its effect on performance and emissions of diesel engines. *Renewable Energy,* Volume 30, pp. 967-976.

Lin, B.-F., Huang, J.-H. & Huang, D.-Y., 2009. Experimental study of the effects of vegetable oil methyl ester on DI diesel engine performance characteristics and pollutant emissions. *Fuel,* Volume 88, pp. 1779-1785.

Martins, D. B., 2013. *Sapia Annual Report - Forword by the Minister of Energy,* s.l.: Sapia.

Martyr, A. J. & Plint, M. A., 2007. *Engine Testing Theory and Practice.* 3rd ed. Oxford: Butterworth-Heinemann.

McCormick, R. L. & Alleman, T. L., 2005. Effect of Biodiesel Fuel on Pollutant Emissions from. In: G. Knothe, J. Van Gerpen & J. Krahl, eds. *The Biodiesel Handbook.* Champaign, Illinois: AOCS Press.

McCormick, R. L. & Parish, R., 2001. *Advanced Petroleum Based Fuels Program and Renewable Diesel Program - Milestone Report: Technical Barriers to the Use of Ethanol in Diesel Fuel,* Golden: National Renewable Energy Laboratory.

Miana, P., 2014. Investigation of fuel properties and engine analysis of Jatropha biodiesel of Kenyan origin. *Journal of Energy in Southern Africa,* 25(2), pp. 107-116.

Miao, R., Li, J., Shi, L. & Deng, K., 2013. Study of Top Dead Center Measurement and Correction Method in a Diesel Engine. *Research Journal of Applied Sciences, Engineering and Technology,* 6(6), pp. 1101-1105.

Nagaraju, V., Henein, N., Quader, A. & Wu, M., 2008. Effect of Biodiesel (B-20) on Performance and Emissions in a Single Cylinder HSDI Diesel Engine. *SAE Technical Paper 2008-01-1401.*

Owen, K. & Coley, T., 1990. *Automotive Fuels Reference Book.* 2nd ed. Warrendale: SAE.

Palmer, D., 2008. *MscEng Thesis: The Development of a Biofuelsl Engine Testing Facility.* Stellenbosch: s.n.

Rahimi, H. et al., 2009. Diesterol: An environment-friendly IC engine fuel. *Renewable Energy,* Volume 34, pp. 335-342.

Rakopoulos, C., Antotnopoulos, K. & Rakopoulos, D., 2007. Experimental heat release analysis and emissions of a HSDI diesel engine fueled with ethanol-diesel fuel blends. *Energy,* pp. 1791-1808.

Rakopoulos, C. D. et al., 2006. Comparitive performance and emissions study of a direct injection Diesel engine using blends of Diesel fuel with vegetable oils or bio-diesel of various origins.. *Energy Conversion and Management,* Volume 47, pp. 3272-3287.

Rosseel, E., Sierens, R. & Baert, R. S. G., 1999. Evaluating Piezo-electric Transducer Response to Thermal Shock from In-cylinder Pressure Data. *SAE Technical Paper 1999-01-0935,* pp. 1431-1446.

Sahin, Z., Durgun, O. & Kurt, M., 2015. Experimental investigation of improving diesel combustion and engine performance by ethanol fumigation-heat release and flammability analysis. *Energy Conversion and Management,* Volume 89, pp. 175-187.

SAPIA, 2008. *Petrol and Diesel in South Africa and the Impact on Air Quality,* s.l.: South African Petroleum Industry Association.

SEKAB BioFuels & Chemical AB, 2007. *Short report from the Swedish experience of using low blend of ethanol derivative in diesel, ED-diesel,* Stockholm: City of Stockholm, Environment and Health Administration.

Shahir, S. A. et al., 2014. Feasibility of diesel-biodiesel-ethanol/bioethanol blends as existing CI engine fuel: An assessment of properties, material compatibility, safety and combustion. *Renewable and Sustainable Energy Reviews,* Volume 32, pp. 379-395.

Signal Group Ltd, 2009. *Model 351/352 pump, filter & distribution oven operating manual.* Camberley: Signal Group Ltd.

Song, J., Zello, V. & Boehman, A. L., 2004. Comparison of the Impact of Intake Oxygen Enrichment and Fuel Oxygenation on Diesel Combustion and Emissions. *Energy & Fuels,* 18(5), pp. 1282-1290.

Stone, R., 1999. *Introduction to Internal Combustion Engines.* 3rd ed. London: Macmillan Press Ltd.

Subbaiah, G. V. et al., 2010. Rice Bran Oil as an Additive in Diesel-Ethanol Blends for Diesel Engines. *IJRRAS,* 3(3), pp. 334-342.

Szybist, J. P., Song, J., Alam, M. & Boeman, A. L., 2007. Biodiesel combustion, emissions and emission control. *Fuel Processing Technology,* Volume 88, pp. 679-691.

Utlu, Z. & Koçak, M. S., 2008. The effect of biodiesel fuel obtained from waste frying oil on direct injection diesel engine performance and exhaust emissions. *Renewable Energy,* Volume 33, pp. 1936-1941.

Uys, D., 2010. *Final year project: The development of a fuel conditioning unit.,* Stellenbosch: s.n.

Van Zyl, A., 2010. *Final year project: Air temperature control unit for engine testing,* Stellenbosch: s.n.

Volkswagen, 1998. *Self-Study Program 209 1.9-ltr. TDI Engine with Pump Injection System Design and Function.* Wolfsburg: Volkswagen AG.

Von Gerpen, J., 2005. *Biodiesel Production and Fuel Quality,* Moscow: Department of Biological and Agricultural Engineering, Univesity of Idaho.

Wang, X. G. et al., 2011. Performance and emissions of a turbocharged, high-pressure common rail diesel engine operating on biodiesel/diesel blends. *Proceedings of the Institution of Mechanical Engineers Part D: Journal of Automobile Engineering,* Volume 225, pp. 127-139.

Wlodarczyk, M. T., 2012. Fiber optic-based in-cylinder pressure sensor for advanced engine control and monitoring.. *Combustion Engines,* Volume 4.

Wlodarczyk, M. T. et al., 1998. In-Cylinder Fiber-Optic Pressure Sensors for Monitoring and Control of Diesel Engines. No. 981913. *SAE Technical Paper.*

Woschni, G. & Spindler, W., 1988. Heat Transfer with Insulated Combustion Chamber Walls and its Influence on the Performance of Diesel Engines. *Transactions of the ASME: Journal of Engineering for Gas Turbines and Power,* Volume 110, pp. 482-502.

Xing-cai, L., Jian-guang, Y., Wu-gao, Z. & Zhen, H., 2004. Effect of cetane number improver on heat release rate and emissions of high speed diesel engine fueled with ethanol-diesel blend fuel. *Fuel,* Volume 83, pp. 2013-2020.

Xue, J., Grift, T. E. & Hansen, A. C., 2011. Effect of biodiesel on engine performance and emissions. *Renewable and Sustainable Energy Reviews,* Volume 15, pp. 1098-1116.

Yost, D. M., Ryan III, T. W. & Owens, E. C., 1981. *Installation of a Diesel Engine Combustion/Ignition Evaluation Facility,* San Antonio: U.S. Army Fuels and Lubricants Research Laboratory, Southwest Research Institure, U.S. Army Mobility Equipment Research and Development Command, Energy and Water Resources Laboratory.

Zhang, J. et al., 2006. Performance and Emissions of Direct Injection Diesel Engine Fueled with Diesel Fuel Containing Dissolved Methane. *Energy and Fuels Vol.20 no.2,* pp. 504-511.

Zhao, H., Hu, J. & Ladommatos, N., 2000. In-cylinder Studies of the Effect of CO2 in Exhaust Gas Recirculation on Diesel Combustion and Emissions. *Procedings of the Institute of Mechanical Engineers, Part D: Journal of Automobile Engineering 2000 214,* pp. 405-419.

Zhao, H. & Ladammatos, N., 2001. *Engine Combustion Instrumentation and Diagnostics.* Warrendale, Pa.: SAE inc..

Zheng, M., Reader, G. T. & Hawley, J. G., 2004. Diesel engine exhaust gas recirculation – a review. *Energy Conversion and Management,* Volume 45, pp. 883-900.

APPENDIX A – DYNAMOMETER DRIVESHAFT DESIGN

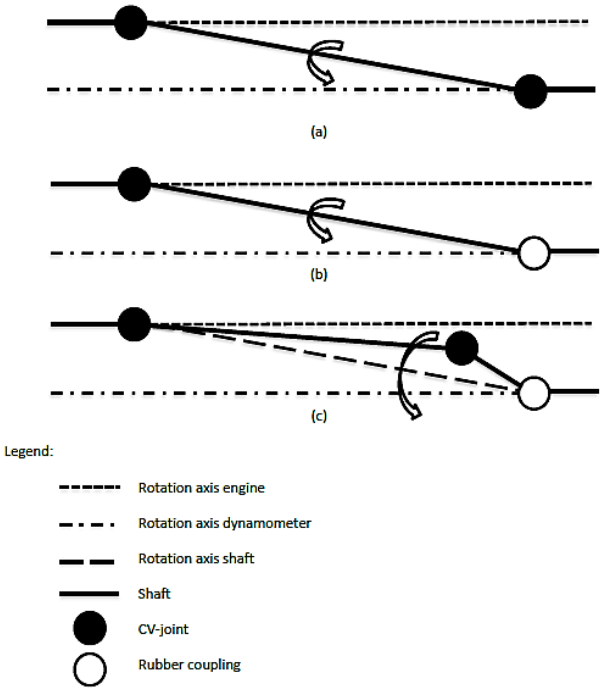

Figure 52: Dynamometer driveshaft diagram

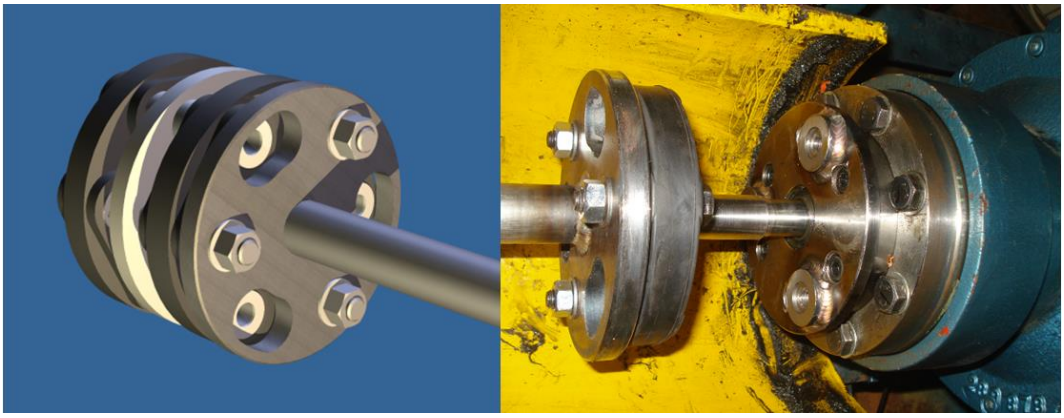

Figure 53: Vibration damper 3D model and during assembly showing central spherical bearing and locating spigot.

Table 6: Drive shaft maintenance components.

Part	Part number	Description	Quantity
CV-joint	Löbro type 104 or similar	Side shaft from VW micro bus (Palmer, 2008)	1
Flexible coupling	N/A	Mercedes Benz 190 flexible drive shaft coupling. 6 x M10 bolts, PCD 90mm	2
Centre bearing	GE20C	Radial spherical plain bearing. OD: 35mm ID: 20mm W: 12mm	1

APPENDIX B – COOLANT TEMPERATURE CONTROL SYSTEM

B.1. Heat Exchanger Calculations

Heat Exchanger Design

Specs			Temperatures			
#tubes	72		Cold inlet	15	°C	
OD	6.5	mm	Warm inlet	95	°C	
ID	4	mm	Cp cold	4.185	kJ/kg.°C	Cp of water @ 15°C
length	600	mm	Cp hot	2.27	kJ/kg.°C	Cp of water @ 95°C
U	850	W/m^2.°C	from Table 11-1 (Çengel,2006)			

Thin walled ε-NTU method ex.11-9 (Çengel, 2006)			
A	0.542867	m^2	
Ch	2.27	kW/°C	
Cc	3.348	kW/°C	
Cmin	2.27	kW/°C	
c	0.678017		
Q'max	181.6	kW	
NTU	0.203276		
ε	0.172917	Fig 11-26 Çengel	
Q'	31.40171	kW	

Mass flow		
Cold	1	kg/s
Hot	0.8	kg/s

B.2. Coolant Temperature Control Flow Diagram

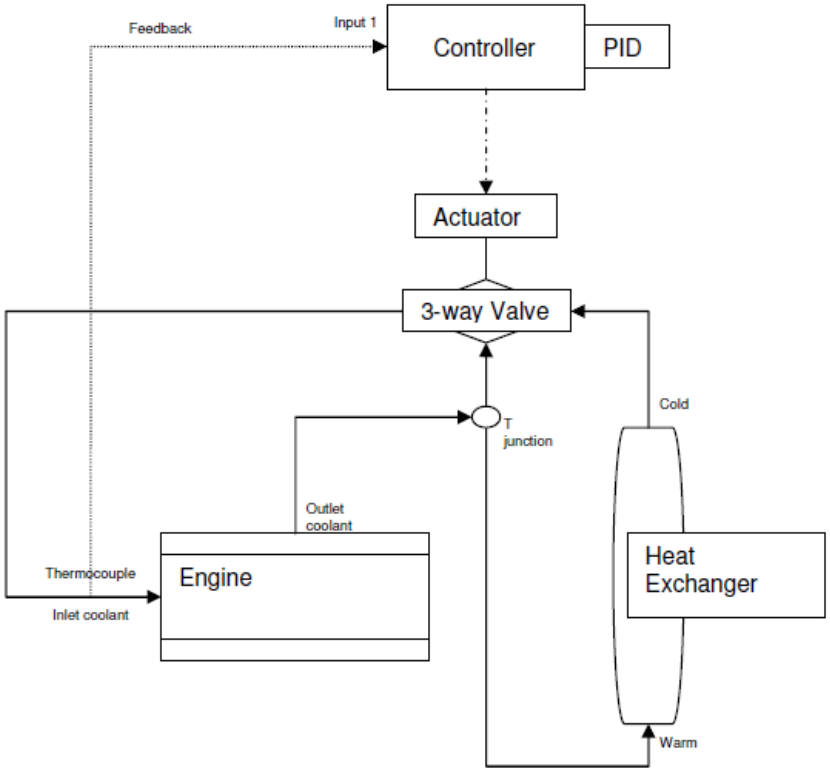

Figure 54: Flow diagram of coolant temperature control system

APPENDIX C – ADDITIONAL INFORMATION ON PRESSURE INDICATING SET UP.

C.1. Pressure Transducer Calibration.

The static calibration of the Optrand PSIglow-A pressure transducer was done using a dead weight tester. Certified weights to generate the pressure needed to calibrate the entire range of the transducer were unavailable. A Wika master gauge was used to check the pressure generated by weights for the 0 – 3 000 kPa range of the gauge. The transducer was found to be linear over this range. The calibration deviated from the default calibration stated on the transducer. Figure 55 shows the difference in calibration.

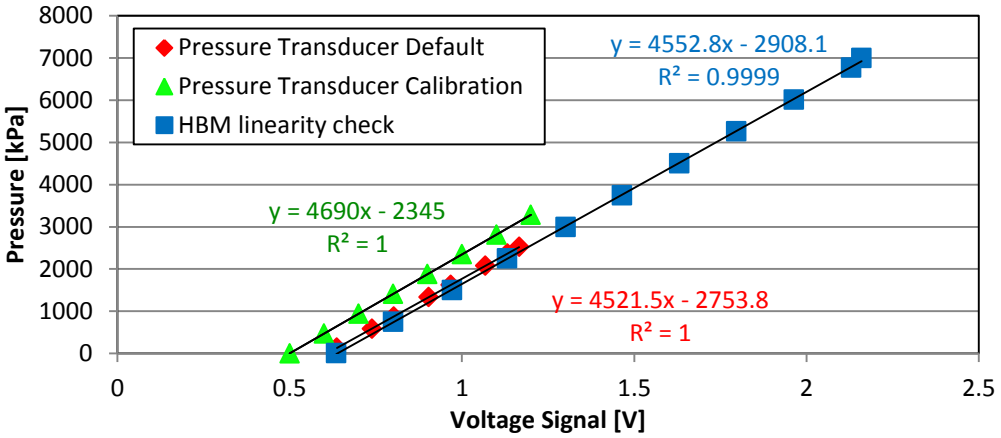

Figure 55: Pressure transducer actual calibration curve compared to indicated default calibration on transducer.

To check the calibration of the Optrand pressure transducer over a broader range, a HBM pressure transducer was used. The linearity of the HBM transducer was checked over the range of 0 – 7 000 kPa which was the maximum pressure rating for the dead weight tester. The linearity of the Optrand pressure transducer was then checked over the same range and was found to be acceptable.

Table 7: Calibrated gauge information on date of use.

Wika Master Gauge	
Asset Number:	MEG NO-01 302637
Range:	0 – 3000 kPa
Calibration Certificate Number:	1101170
Last Calibration:	2011/06/06

C.2. Shaft Encoder Mounting

A mounting system for the encoder was developed which made use of standard front cover bolt holes on the engine. It had to allow the encoder to be indexed for the trigger pulse location. It also had to incorporate an adaptor spigot to mount to the crankshaft. This spigot used the standard crank pulley mounting bolts. The mounting system allowed for slight run-out on the shaft by means of a flexible coupling. To keep vibration to a minimum, the shaft was centred using a clock gauge. The mounting system also incorporated high density, vibration damping foam to protect the encoder from the harsh diesel combustion vibrations.

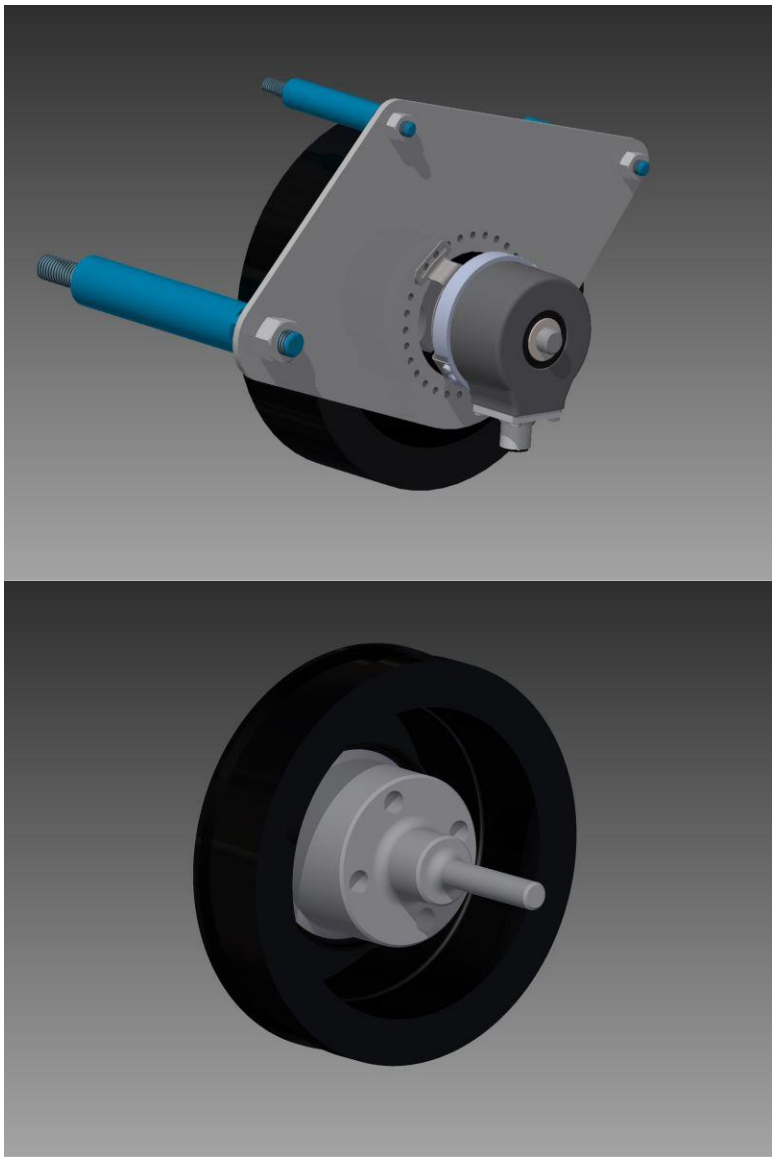

Figure 56: Shaft encoder mounting plate and crank pulley spigot.

Vibration analysis

A vibration analysis was done on the shaft encoder to ensure it could withstand the harsh vibration produced by diesel engine combustion. Initial test showed that the vibrations on the engine far exceeded the shaft encoder vibration rating of 100 m/s^2 (10 g).

It was decided to remove any rigid mountings between the encoder and the engine. A flexible shaft was installed and the encoder was encapsulated in high density foam. It can be seen in Figure 57 that the vibration damping technique had a considerable effect at 1 000 rpm. Vibration measurements of the rigid mounting plate were not taken above this speed for fear of damaging the accelerometer. A measurement of the damped system at 4 000 rpm however still shows the vibrations to be within specification.

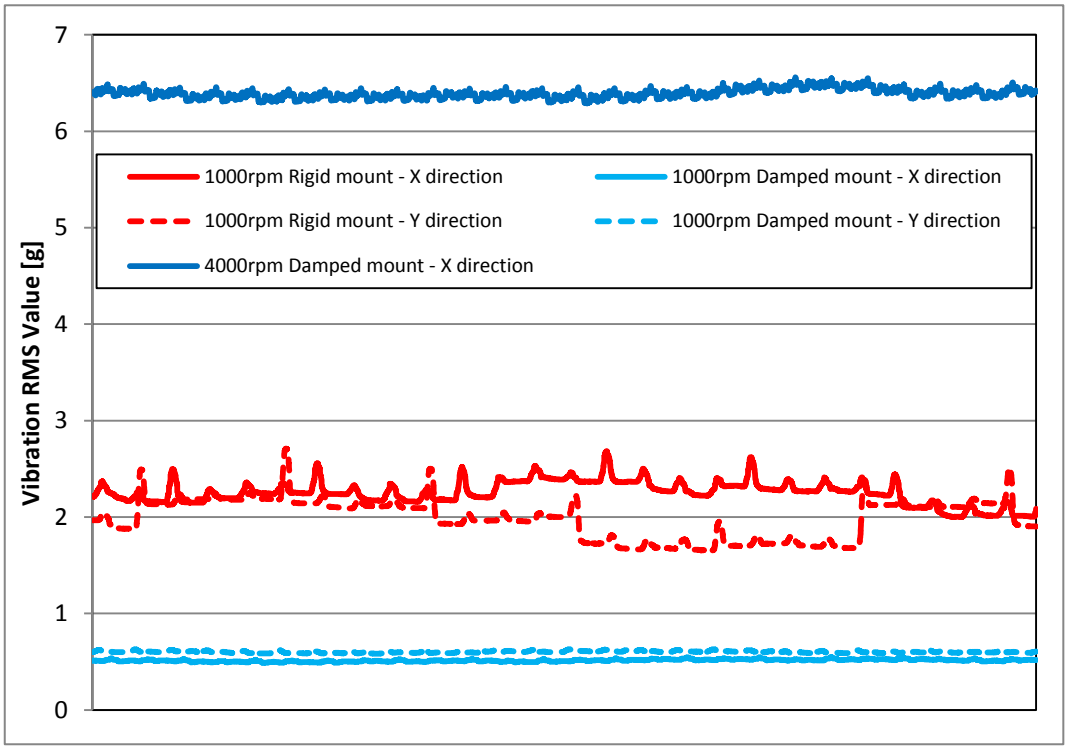

Figure 57: Vibration RMS value for the damped shaft encoder and rigid mounting plate.

APPENDIX D – ADDITIONAL EXHAUST GAS EMISSIONS INFO

D.1. Signal Emissions Equipment

Table 8: Calibration gas information.

Gas:	Cocktail Gas (span gas)	
Supplier:	Air Products	
Cylinder number:	31AL359	
Date:	2011/11/11	
Components:		**Concentration**
	Nitrogen Oxide:	2044 ppm
	Carbon Monoxide:	5084 ppm
	Carbon Dioxide:	14.4 %
	Nitrogen:	Balance
Final Pressure:	140 bar at 21 °C	
Expiry Date:	November 2013	
Analysed By:	M.J.L	

D.2. Dräger Emissions Equipment MSI-150 Euro-E

Table 9: Technical specifications for Dräger MSI-150 (Dräger, n.d.)

Display	Measurement Principle	Range	Display Resolution	Accuracy
T-low	PTC Thermistor	-20 to 100 °C	0.1 °C	≤ 1 °C
T-high	Thermocouple	0 to 1000 °C	1 °C	0 to 250 °C: ≤ 2 °C 250 to 1000 °C: ≤ 4°C
CO	Electrochemical Sensor H_2 compensated	0 to 4000 ppm	1 ppm	0 to 2000 ppm: ≤ ± 20 ppm Or < 5 % of MV
NO	Electrochemical Sensor	0 to 2000 ppm	1 ppm	± 10 ppm or < 5 % of MV
NO_2	Electrochemical Sensor	0 to 200 ppm	1 ppm	± 5 ppm or < 5 % of MV
Air Pressure	Semiconductor	800 to 1700 hPa	1 hPa	

MV = Measured value

D.3. AVL 415 Smoke Meter Probe

The smoke probe is designed to prevent forceful entry of smoke particles. The sampling pipe terminates halfway into the smoke probe head. The probe faces into the exhaust gas stream, but the sampling holes face the opposite direction. AVL suggests that the probes be fitted in a straight piece of exhaust pipe (AVL, 2005). Figure 58 show the probe to be installed in the most suitable position, facing into a straight length of pipe.

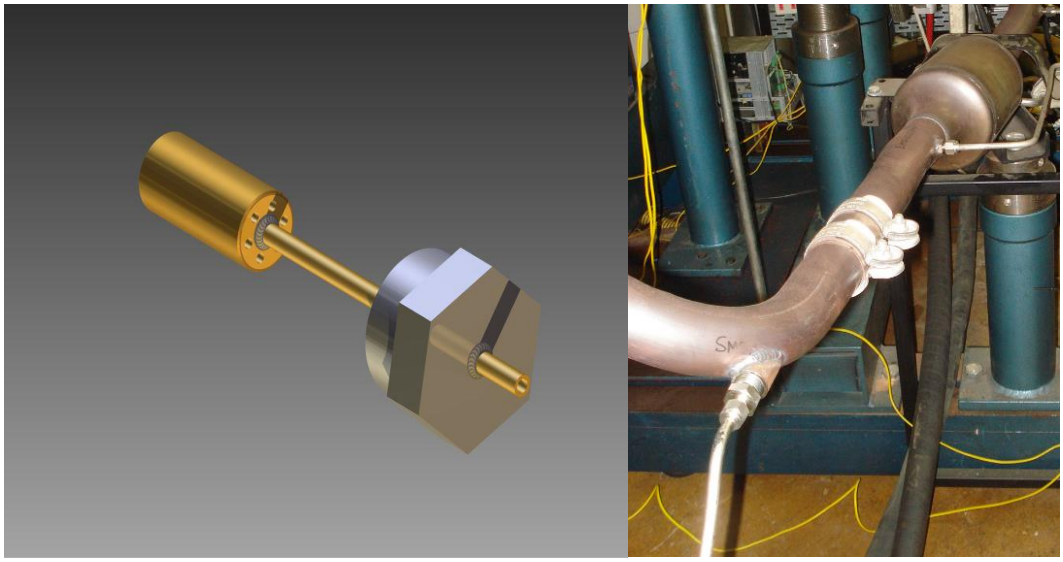

Figure 58: Smoke probe and exhaust pipe location.

APPENDIX E – VIRTUAL INSTRUMENTATION DEVELOPMENT

The following section contains the block diagram of the LabView Virtual Instrument developed to capture and correctly index the pressure with the signal from the shaft encoder. The program is also capable of doing scaling calculations and storing the desired amount of data in Excel format for post processing.

The LabView VI programming works with block diagrams. Blocks perform programming tasks while the lines transfer information or data between blocks. The fenced areas are loops in the programming. Information can be transferred by means of shift registers from the end of one iteration of a loop, back to the beginning of the next iteration of the same loop until the loop termination conditions have been met.

The following pages contain the block diagram and description of key areas. Due to size restraints the diagram is spread over 4 pages.

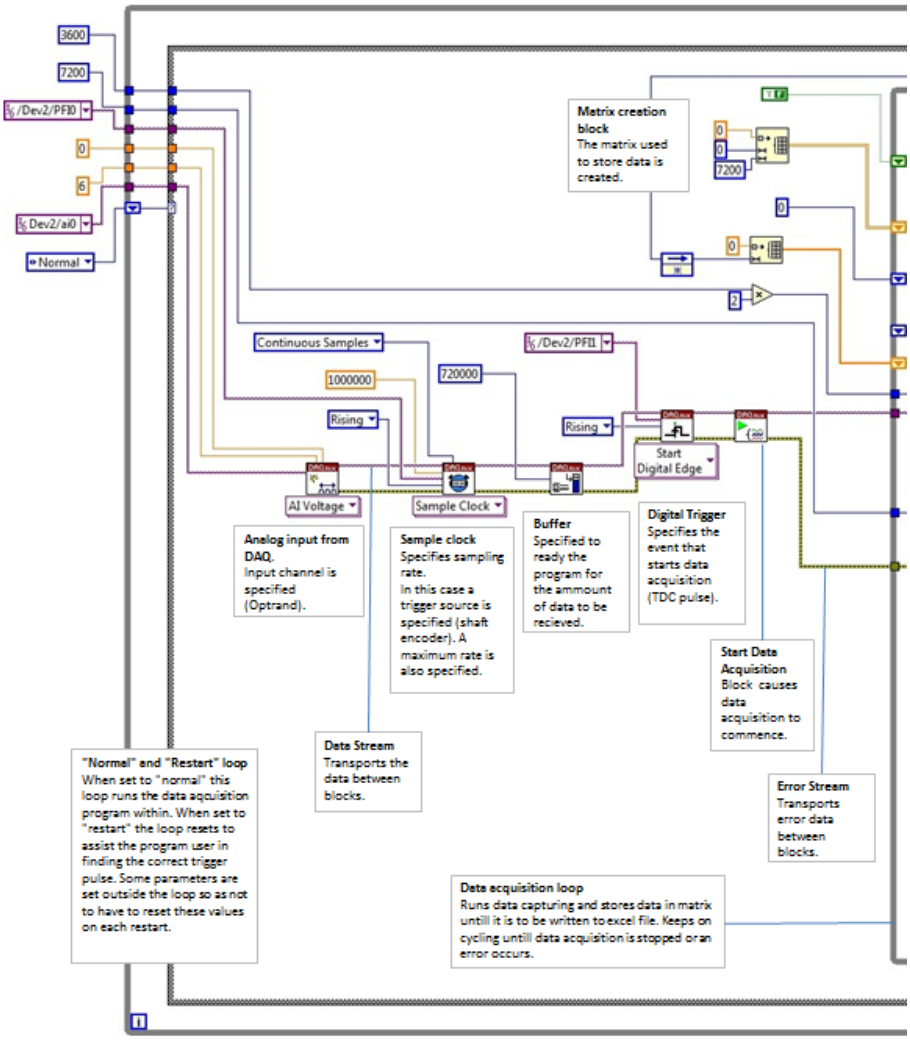

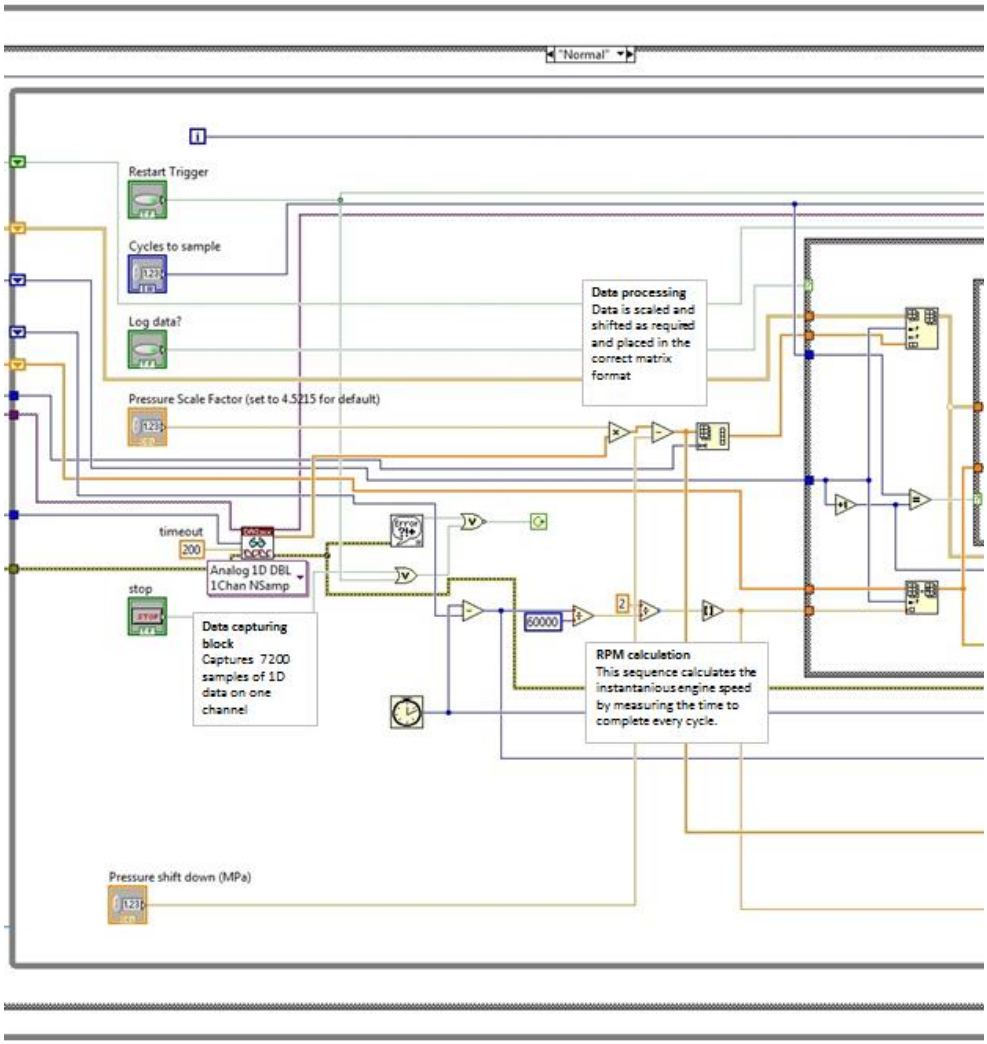

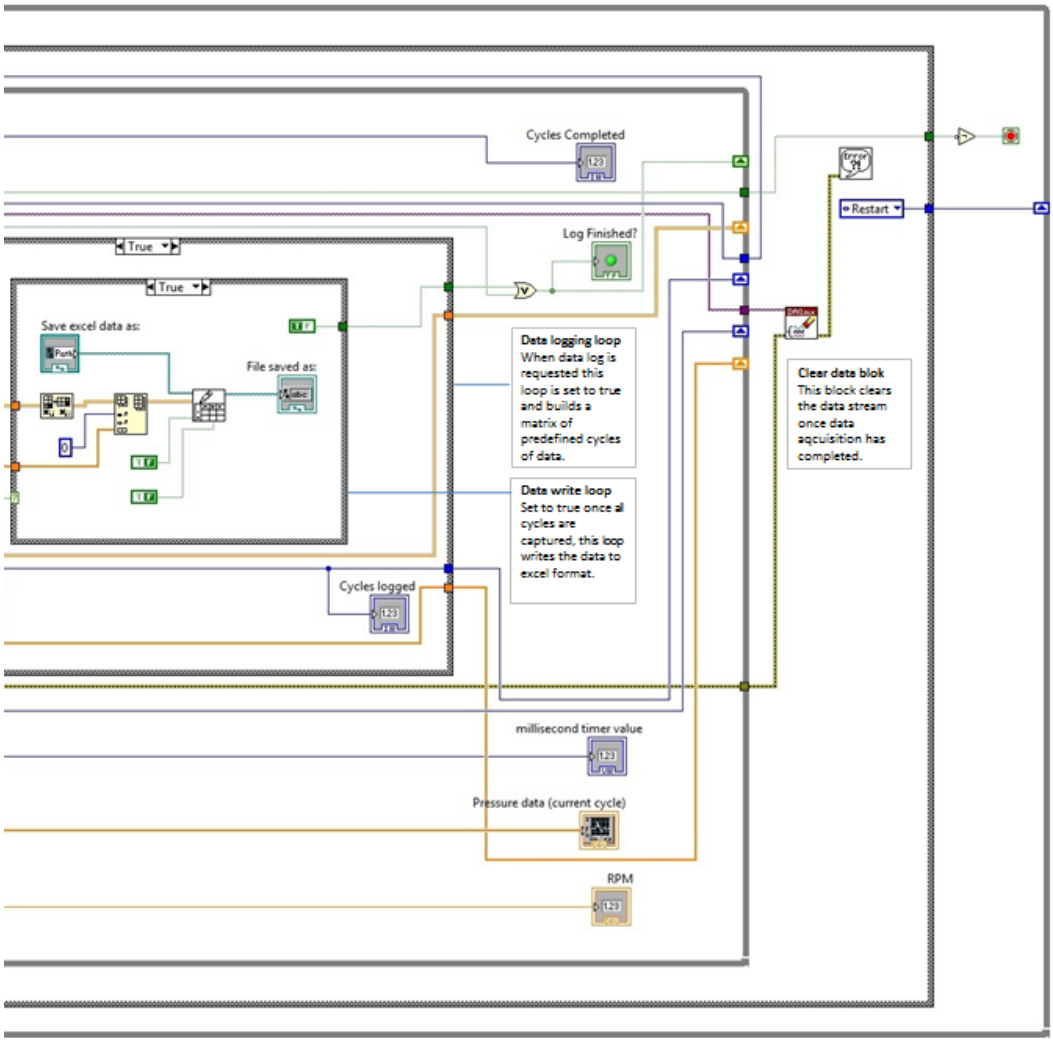

APPENDIX F – TEST SHEET

Date: ______________ Time: ______________

Fuel: ______________

Description: ____

____

____

					Pressure file:			R	
Speed:			Set	FSN:					P log:
Load:			Th	mg/m^3:					
VCDS:			lines	Blackness:					
ETA:			File	O2:					
S.st.inj.:				CO2:					
EGR:				CO:					Digitized:
Fuel Temp.:		°C		Nox					
ΔP:		mm		NO:					
Gauge Pres.:		Bar		NO2:					
Comments:									

								R	
Speed:			Set	FSN:					P log:
Load:			Th	mg/m^3:					
VCDS:			lines	Blackness:					
ETA:			File	O2:					
S.st.inj.:				CO2:					
EGR:				CO:					Digitized:
Fuel Temp.:		°C		Nox					
ΔP:		mm		NO:					
Gauge Pres.:		Bar		NO2:					
Comments:									

								R	
Speed:			Set	FSN:					P log:
Load:			Th	mg/m^3:					
VCDS:			lines	Blackness:					
ETA:			File	O2:					
S.st.inj.:				CO2:					
EGR:				CO:					Digitized:
Fuel Temp.:		°C		Nox					
ΔP:		mm		NO:					
Gauge Pres.:		Bar		NO2:					
Comments:									

								R	
Speed:			Set	FSN:					P log:
Load:			Th	mg/m^3:					
VCDS:			lines	Blackness:					
ETA:			File	O2:					
S.st.inj.:				CO2:					
EGR:				CO:					Digitized:
Fuel Temp.:		°C		Nox					
ΔP:		mm		NO:					
Gauge Pres.:		Bar		NO2:					
Comments:									

APPENDIX G – ECU VARIABLE VALIDATION

G.1. Air Mass Flow

The ECU values for air mass flow, measured in mg/strk, are compared to a Meriam flow meter that is connected to the inlet snorkel of the engine. The ECU values are converted to kg/s. A manometer is used to measure the pressure drop across the laminar flow meter. A linear fit is drawn through the points and linearity is evaluated through the R^2 value.

Mass of Airflow Validation

VCDS					Manometer			
N [RPM]	T [Nm]	MAF [mg/str]	AF [kg/s]		ΔP [mm]	ΔP [Pa]	dV [m3/s]	AF [kg/s]
1800	40	298.9	0.017934		16	156.96	0.01365046	0.016776
1800	80	382.2	0.022932		21	206.01	0.018484576	0.022718
1800	120	509.6	0.030576		26	255.06	0.023318693	0.028659
1800	160	646.8	0.038808		33	323.73	0.030086455	0.036976
3000	160	754.6	0.07546		60	588.6	0.056190684	0.069058
3000	120	710.5	0.07105		54	529.74	0.050389744	0.061929
3000	80	529.2	0.05292		43	421.83	0.039754688	0.048859
3000	40	382.2	0.03822		34	333.54	0.031053279	0.038164

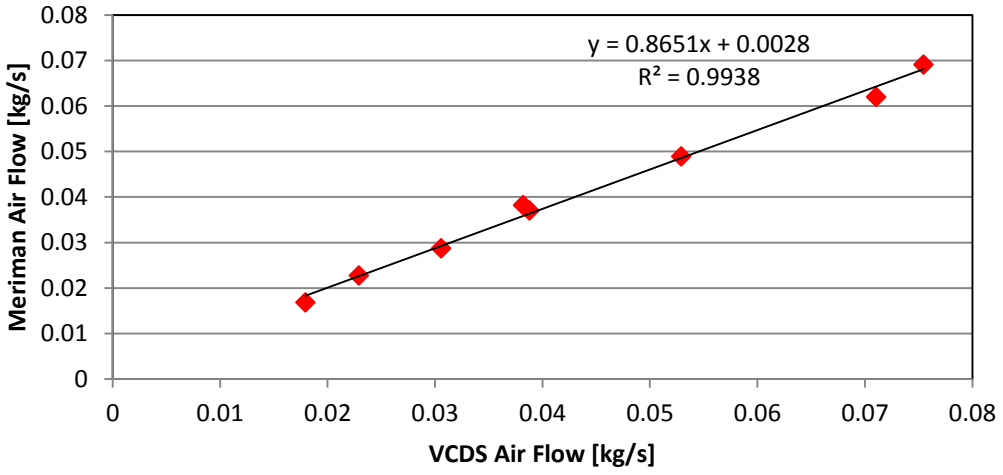

The results show good linearity and the values from the ECU can be scaled for more accurate results.

G.2. Charged Air Pressure

The boost pressure from the measured values in the ECU is compared to the charge pressure measured with a Wika calibrated pressure gauge. A linear fit is drawn through the points and linearity is evaluated through the R^2 value.

VCDS [mbar]	Wika Pressure Guage [bar]			
1060.8	0.05	=	1049.7	mbar
1193.4	0.19	=	1189.7	mbar
1468.8	0.45	=	1449.7	mbar
1723.8	0.7	=	1699.7	mbar
1795.2	0.88	=	1879.7	mbar
1693.2	0.65	=	1649.7	mbar
1397.4	0.39	=	1389.7	mbar
1244.4	0.25	=	1249.7	mbar

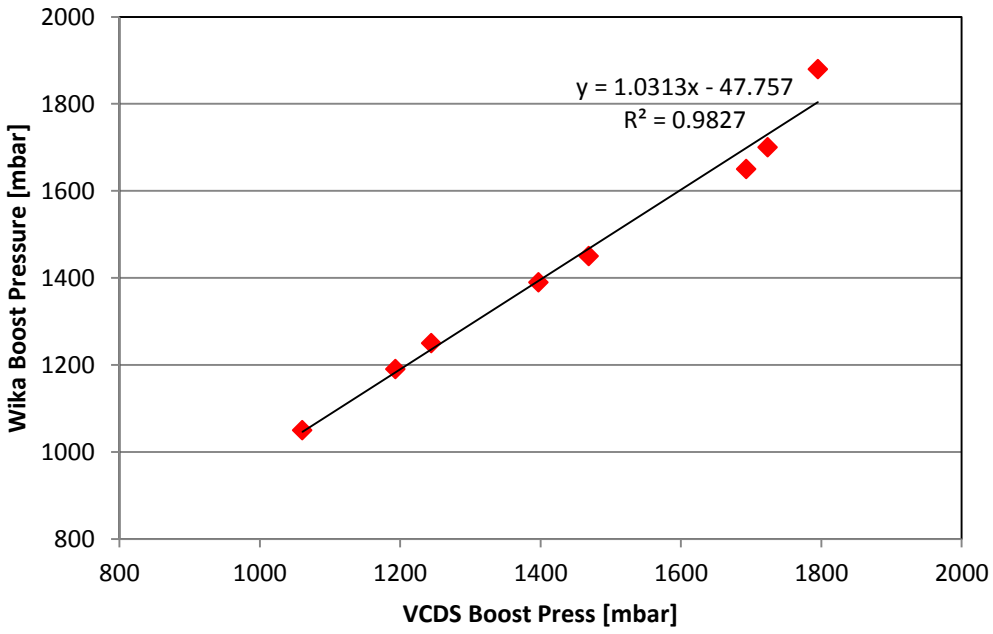

The values from the ECU have acceptable linearity with those measured by the Wika gauge.

APPENDIX H – INSTANTANEOUS HEAT RELEASE PROGRAM

All of the heat release correlations discussed in Section 2.3.3 was evaluated. The spreadsheet gives the user the option to jump between these to compare results. For the gas properties in the Annand correlation, air properties were approximated to the closest 100 °C at the mean temperature during compression and expansion. For the Woschni correlation an approximated motored curve was drawn using the known manifold temperature for the pressure at IBDC and assuming isentropic compression and expansion.

Excel Heat Release Example

3000	160	500	ppm															
Entered values	*Pressure Shift [kPa]	*Phasing [deg]	Pboost [mbar]	Engine Speed [rev/min]	*Compression ratio	*Bore [m]	*Stroke [m]	*Connecting rod length L [m]	*Swepped volume [m^3]	Encoder frequency [pulses/rev]								
	-852.9	1.39	1815.6	3000	19	0.0795	0.0955	0.144	0.001896	3600								
Calculated Values			Charge press actual [kPa]	Engine Speed N [rev/s]	Squish Volume [m^3]	Cylinder Head Area [m^2]	Radius to crank pin R [m]	L/R	Mean Piston Speed Sp [m/s]	dθ [deg]								
			182.5	50	2.63333E-05	0.00496391	0.04775	3.015706806	9.55	0.1								
		IBDC	182.5															
		CTDC	10129.4	n	1.363987222													
	FC:	3.13014009	g/s	Callahan suggests using coolant temp as Twall														
	Rg	Fuel Consumption [kg/s]	MAF ECU [mg/strk]	Twall [K]	EGR%	EGR ratio	Energy in Diesel [kJ/kg]		a	b	Pr	Stephan-Boltz σ [W/m^2K^4]	ρ [kg/m^3]	μ [kg/m.s]	Assume air @ average in Cyl temp:			
	0.287002761	0.00313014	788.9	358	51	1	43000		0.8	0.75	0.7206	5.67E-08	0.3008	4.60E-05	900	degC		
	AF	Fuel injected [kg/strk]	MAF ECU [kg/s]	MAF Meriam [kg/s]	MAF + EGR	MAF corr [kg/strk]	Mass of Charge [kg/strk]	Energy injected [J/strk]	Average in Cyl temp [K]	k [W/m.K]	Re	c	v [m^2/s]	k [W/m.K]	Cp [J/kg.K]			
	22.69794223	3.1301E-05	0.07889	0.071047739	0.107282086	0.00107282	0.001104122	1345.96024	850.9381585	0.074623925	4965.5003	3.2319E-08	1.53E-04	0.07465	1169			
	A0	A1	A2	A3	A4				[degC]		4964.671304							
	3.04473	1.34E-03	-4.88E-07	8.55E-11	-5.70E-15				577.9381585									
													Selection:	Hohenberg		S.S.inj:	-3.1	
	*Pressure Measured [Mpa]	Pressure Shifted [kPa]	dP/dθ [callahan] [kPa/0.1deg]	*Crank Angle [deg]	Crank Angle [rad]	Crank Angle shifted [deg]	Piston displacement [m]	Wall area [m^2]	Cylinder Volume [m^3]	dv/dθ [m^3/0.1deg]	In Cyl Temp [K]	γ		Selected Heat Transfer	Selected Heat Release	Energy Released	%Burn		
	1.326387172	473.487172		279.4	-1.382475301	-79.21	0.046664307	0.021582545	0.000257971		385.4567593	1.40117	2	-0.001527975	0.001527975	0	0	
	1.327686337	474.786337		279.5	-1.380729971	-79.11	0.046577056	0.021560753	0.000257538	-4.33107E-07	385.8654656	1.40110	3	-0.001552052	-0.716752226	0	0	
	1.328991343	476.091343	1.307070882	279.6	-1.378984642	-79.01	0.046489785	0.021538957	0.000257105	-4.33205E-07	386.275212	1.40104	4	-0.00157623	0.119013752	0	0	
	1.330299671	477.399671	1.309195769	279.7	-1.377239313	-78.91	0.046402495	0.021517156	0.000256671	-4.33301E-07	386.6839372	1.40097	5	-0.001600392	0.116898051	0	0	
	1.331608991	478.708991	1.30908786	279.8	-1.375493983	-78.81	0.046315186	0.021495349	0.000256238	-4.33396E-07	387.0897433	1.40091	6	-0.001624428	0.113349622	0	0	
	1.332917174	480.017174	1.306958908	279.9	-1.373748654	-78.71	0.046227858	0.021473539	0.000255804	-4.33489E-07	387.4909097	1.40084	7	-0.001648239	0.108513094	0	0	
	1.334222311	481.322311	1.303034471	280	-1.372003325	-78.61	0.046140511	0.021451723	0.000255371	-4.3358E-07	387.8859036	1.40078	8	-0.001671736	0.102540803	0	0	
	1.335522723	482.622723	1.297550532	280.1	-1.370257996	-78.51	0.046053147	0.021429904	0.000254937	-4.3367E-07	388.2733887	1.40072	9	-0.001694839	0.095590556	0	0	
	1.336816973	483.916973	1.290750054	280.2	-1.368512666	-78.41	0.045965765	0.021408079	0.000254503	-4.33758E-07	388.6522304	1.40066	10	-0.001717483	0.087823376	0	0	

APPENDIX I – FUEL PROPERTIES

I.1. Ethanol-diesel Blend Energy Content

Table 10: Ethanol-diesel energy content according to various sources.

Measure	Diesel	E5	E10	E15	Ethanol	Source
LHV(MJ/kg)	43.37	-	42.00	41.61	-	(Cole et al., 2000)
LHV(MJ/kg)	43	-	-	-	26.8	(Rakopoulos et al., 2007)
HHV(MJ/kg)	46.45	-	43.96	-	28.49	(He et al., 2003)
	-2% for each 5% of ethanol added					(Hansen et al., 2005)
LHV(MJ/kg)	42.8	-	-	-	27	(Ashok & Saravanan, 2007)
NHV(MJ/kg)	43.5	-	-	-	26.8	(Subbaiah et al., 2010)
LHV(MJ/kg)	42.5	-	-	-	26.8	(Li et al., 2005)
LHV(MJ/L)	36.6	35.8	35.1	34.3	21.3	(McCormick & Parish, 2001)
LHV(MJ/kg)	41.66	-	-	-	26.87	(Agarwal, 2007)
LHV(MJ/kg)	42.5	-	-	39.5	27	(Xing-cai et al., 2004)
NHV(MJ/kg)	42.837	-	40.443	-	25.182	(Lapuerta et al., 2008)
LHV(MJ/kg)	42.6857	-	-	-	27.42324	(Sahin et al., 2015)

I.2. Ethanol-diesel energy content calculation

The diesel blends used in this study were sent for analysis but the results, especially the energy content, were speculative and could therefore not add value to the study.

In refining the heat release calculation, more accurate LHV's for the test fuels were required. Theoretical energy content for the test fuels were therefore calculated using the most common LHV's available in literature.

Energy content was assumed to be: Diesel = 43MJ/kg ; Ethanol = 26.8 MJ/kg; and density: Diesel =830kg/m^3; Ethanol = 790 kg/m^3. These estimates were based on information from the references mentioned in Table 10.

With the test fuels blended by volume/volume %, the mass of each fuel in the blend and then finally the energy content had to be calculated.

Table 11: LHV calculation for test fuels.

Fuel	Diesel	E5	E10	E15	Ethanol	
Eth-content	0%	5%	10%	15%	100%	
Mass D in m^3	830.00	788.50	747.00	705.50	-	kg
Mass E in m^3	0	39.5	79	118.5	790	kg
Energy in m^3	35 690.00	34 964.10	34 238.20	33 512.30	21 172.00	MJ
Energy/kg	43.0000	42.2272	41.4506	40.6703	26.8000	MJ/kg
Rounded:	43.0	42.2	41.5	40.7	26.8	MJ/kg

I.3. Cetane Index Calculation

ASTM D976

$$CCI = 454.74 - 1.641416\rho + 0.00077474\rho^2 - 0.554t_{50} + 97.803log^2(t_{50}) \quad [I.1]$$

ASTM D4737

$$CCI_A = 45.2 + 0.0892(t_{10} - 215) + (0.131 + 0.901b)(t_{50} - 260) + (0.0523 - 0.420b)(t_{90} - 310) + 0.00049[(t_{10} - 215)^2 - (t_{90} - 310)^2] + 107b + 60b^2 \quad [I.2]$$

$$CCI_B = -0.3862\rho + 0.174t_{10} + 0.1215t_{50} + 0.0185t_{90} + 297.42 \quad [I.3]$$

ρ = dencity

$t_{10,50,90}$ = 10,50,90% recovery temperature corrected to standard barometric pressure.

b = exp[-0.0035(ρ-850)]-1

(Jääskeläinen, 2007)

APPENDIX J – ADDITIONAL DATA

J.1. Engine Performance Data

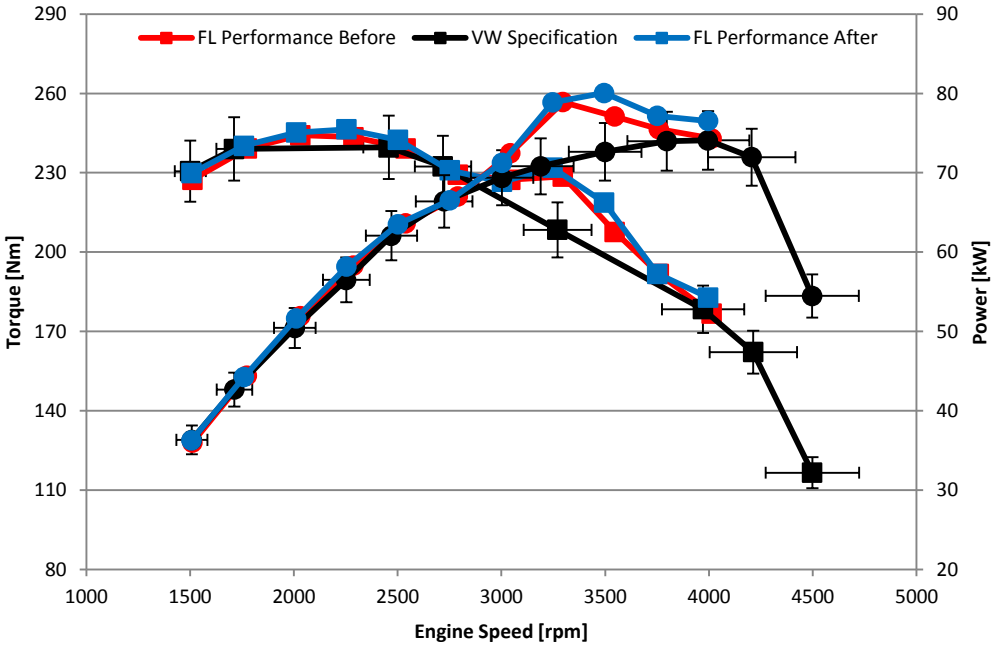

Figure 59: Full load performance curves for 1.9 L TDI ATD before and after fuel-to-fuel comparative tests compared to VW specification.

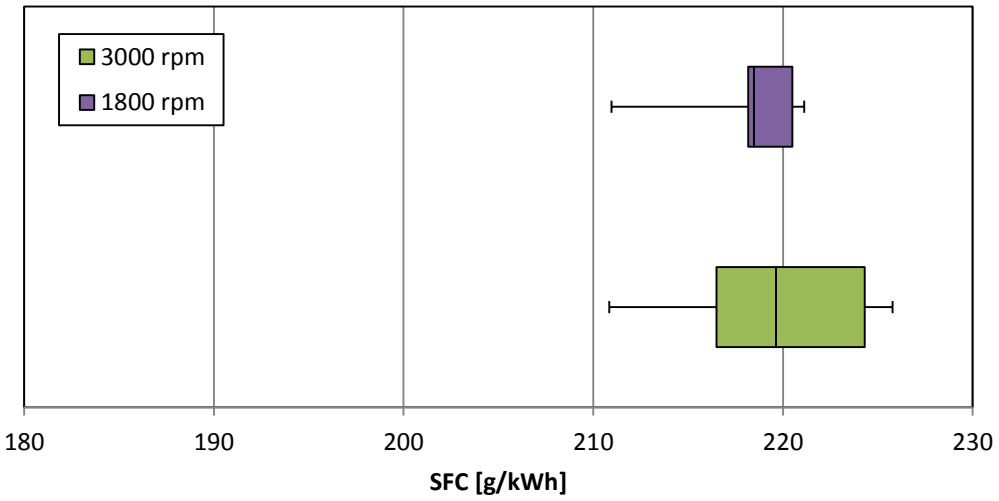

Figure 60: Box and whisker plot of bracket tests for SFC's at 160 Nm torque using 500 ppm diesel.

J.2. Exhaust Gas Recirculation Data Percentage

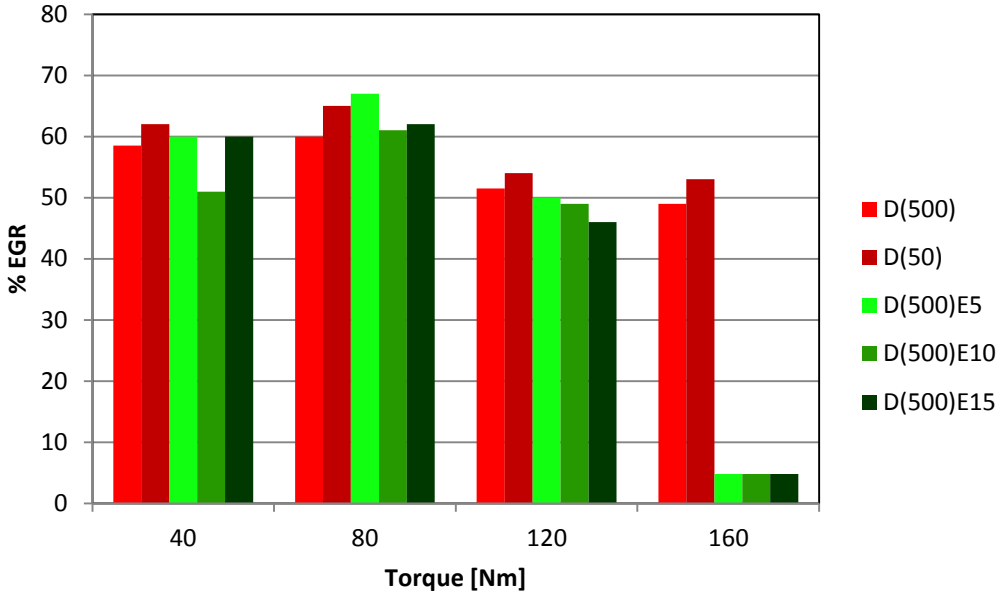

Figure 61: Percentage EGR for ethanol-diesel blends at 1 800rpm.

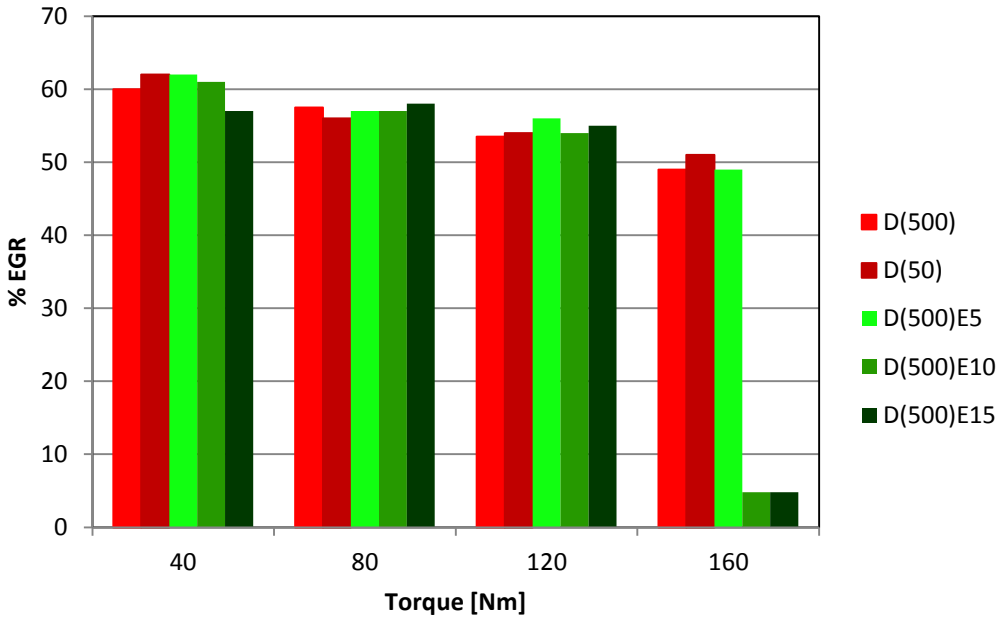

Figure 62: Percentage EGR for ethanol-diesel blends at 3 000rpm.

J.3. Pressure Data

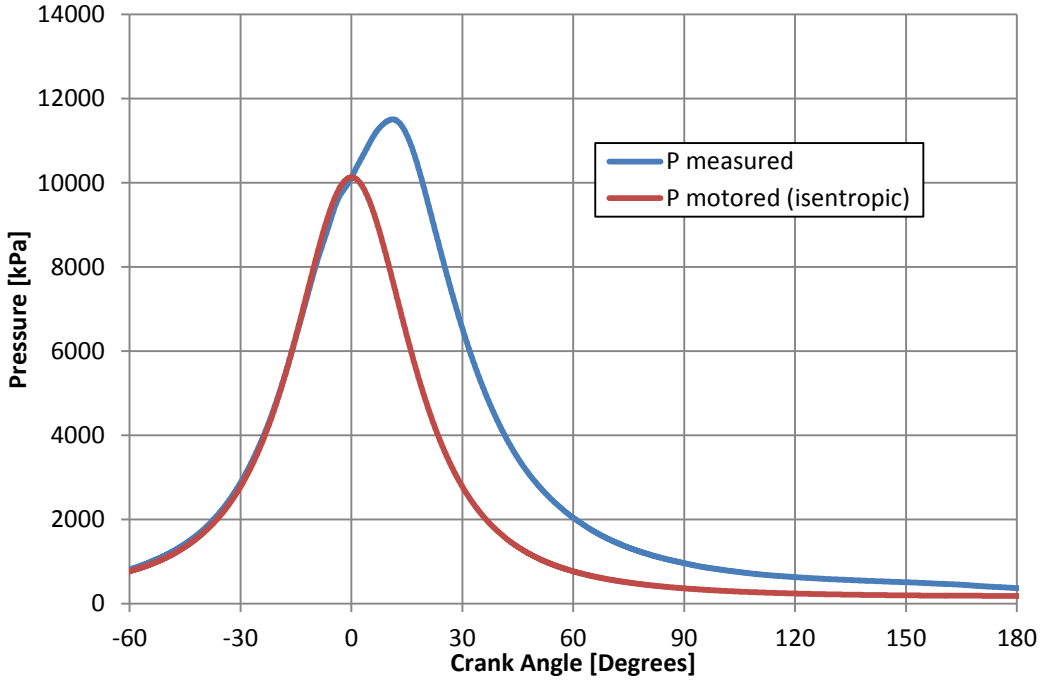

Figure 63: Pressure trace for 1.9L TDI ATD at 3 000 rpm and 160 Nm torque, compared to theoretical motored curve using measure isentropic coefficient.

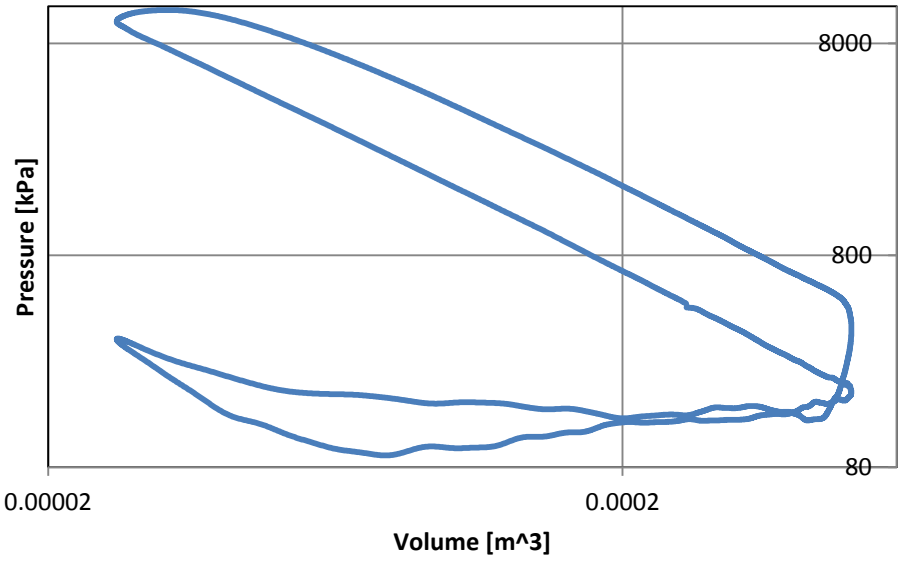

Figure 64: Logarithmic pressure-volume plot of 1.9L TDI ATD at 3 000 rpm and 160 Nm torque

APPENDIX K – ADDITIONAL FUEL MASS BALANCE INFORMATION

Calibration Procedure

The following is adapted from the Operating instructions for the AVL 730 dynamic fuel consumption measuring equipment:

1. For calibration the mode selector should be set to "CAL". The current vessel content will then be displayed in grams.
2. When the "RDY" LED is illuminated the calibration may be initiated by pressing "START" on the fuel calculator module (AVL 7030-A01). If the LED is not illuminated, the vessel contains too much fuel which will result in the ADC range being exceeded when the weight is applied.
3. During calibration operation a calibrated weight is lowered onto and removed from the vessel with a calibrating mechanism. The indicated weight should then correspond to the calibrated weight. Table 12 indicates the accuracy specifications.
4. Once started, the calibration mode cannot be stopped until it has completed.

Table 12: Calibration tolerances for AVL 730.

Weight version	Calibration Weight	Reading/Tolerance
300 g	50 g	50 g ± 0.06 g
600 g/900 g	100 g	100 g ± 0.1 g
1200 g	200 g	200 g ± 0.2 g
1800 g	200 g	200 g ± 0.3 g

If high deviations are observed adjustments to the gain and linearity should be performed as per section 6.2 in the operating instructions (AVL List GmbH, 1987).